NEW SEPARATION METHODS USING MEMBRANE AND SOLVENT EXTRACTION

SUSUMU NII

名古屋大学図書
洋 1119741

A Dissertation

for

The Degree of Engineering

Presented to

Faculty of Engineering

Nagoya University

January, 1994

CONTENTS

INTRODUCTION

Separation process is a backbone of the chemical industry. For any kinds of the chemical products, the cost of the separation and purification reaches above 50% of its total cost. There are no products without the needs for the separation from the unreacted raw material and byproduct. Many challenges have been made for lowering the energy and the cost of separation processes. As shown in the example of silicon and rare earth metals, the advance of the separation technique brings about a highly pure material, which gives a strong impact to other industries. In the development of mineral and energy resouces, separation technique itself has been played a main part and led to a present success. In future, the recovery of valuable resources which widely distributed at low concentration will be important. As the countermeasure for the environmental problems, the need of the separation of toxic compounds from highly dilute media will also increase. The application area of separation techniques is extending increasingly and it is necessary for developing sophisticated separation process; that will be a "key" technique in future advance.

For the problem of separation, interesting idea was shown by the well known Maxwell's "sorting demon"[1]. This demon has abilities of distinguishing the speed of the molecules and opening the hole as their will. Suppose that a vessel filled with a gas at a constant temperature divided into two parts with the partition having holes and that the demons sit at the every hole. The demons open the hole only at the time when the high speed molecule comes at the hole, after a while the molecules are separated into high speed and low speed ones, i.e. high temperature gas and low temperature gas. Only by such a "demon", a complete separation from disordered situation is realized. Practically, such a phenomenon does not proceed spontaneously against the second law of the thermodynamics - spontaneous change proceeds to the direction of increasing randomness, and the separation from the mixture needs an energy to compensate the loss of entropy.

From the view of thermodynamics, the minimum energy for achieving perfect separation from a dilute solution at a constant temperature is equal to the change of free energy arose from mixing.

$$W = \Delta G - T\Delta S = - \sum x_i RT \ln \gamma_i x_i \qquad (1)$$

where x_i is the mole fraction of the component i, γ_i the activity coefficient. Since the solution is dilute, the value of activity coefficient, γ_i is nearly 1. The energy needed for separating 1 molar of the component becomes $-RTlnx_i$. Therefore, the lower the concentration is, the more energy is required. It is needless to say that the energy requirement for the separation in practical situation will be many times greater than this minimum value.

Table 1 Classification of separation techniques[4,7].

system	separation techniques
gas-gas	membrane separation, gaseous diffusion
gas-liquid	distillation, absorption, evaporation, pervaporation, flotation, membrane distillation, membrane absorption
gas-solid	adsorption, sublimation
liquid-liquid	extraction, dialysis, electrodialysis, electrophoresis, reverese osmosis(RO), membrane extraction
liquid-solid	crystallization, adsorption(chromatography), ion-exchange, centrifugation, zone-melting, ultrafiltration(UF)
solid-solid	filtration, sedimentation

There are many kinds of separation processes based on various principles of the difference of physico-chemical properties. These are in size, weight and electric charge, and chemical affinity. Many separation processes utilize immiscible two-phases. **Table 1** shows a classification of separation techniques based on the phases which are used. The techniques involving phase transition such as distillation, crystallization, evaporation and sublimation are the most conventional techniques. The most widely used method is the technique based on the partitioning of the species between the phases, which is included in the operation of absorption, adsorption and extraction. These operations are defined as separation based on equilibrium, while, the representative non-equilibrium separation is membrane separation. It is based on the difference of the permeation (diffusion) rate of the species through the membrane.

After the success of developing the reverse osmosis membrane for the recovery of pure water from seawater by Loeb and Sourirajan[3] in the early 1960s, the possibility of membrane separation has been recognized as one of the major separation techniques. The advantages of membrane separation are as follows:

- Low energy consumption compared with other processes including phase transition (distillation and evaporation, etc).
- Continuous operation.
- Simple combination with other separation process.
- High scalability.
- Sophistication of performance by use of high functional membrane.
- Unnecessity of additives for separation.

Currently operated membrane processes are classified into liquid-solid(UF), liquid-liquid(RO) and gas separation as shown in Table 1. Membrane separation is a growing technology which has a potential for expanding range of variation. In most of the membrane separation processes, membrane is expected to act as a "semipermeable barrier", in which only the desired species permeate, and it behaves as a barrier for other species. Essentially, the degree of separation in membrane process is determined by a difference in the permeation rate of species. Therefore the commercial successes in membrane process have depended on the development of the membrane materials and the preparation techniques. For membrane-based gas separation, practical application was started from hydrogen recovery in ammonia plant in 1970s, and the process was developed for CO_2 and/or CH_4 separation from syngas and natural gas purification, as well known Monsanto's "prism separator"[8], then the process was developed for O_2 or N_2 separation from air.

The application of membrane is not limited as a semipermeable barrier. Another type of application of the membrane separation is in membrane distillation[4], where the membrane acts as a bound between the high and the low temperature liquids. The microporous membrane used here is also applied to microfiltration(MF) or ultrafiltration(UF). The pores are not filled with the liquid and the vapor is transferred through the membrane from the high temperature side to the low temperature side. Selectivity is not determined by the membrane itself but by the vapor-liquid equilibrium. The merit of using membrane is to attain large

contact area per volume of the contactor. This type of the application is also found in membrane absorption[6] and membrane extraction[2].

As contactor for membrane processes, hollow fiber(HF) membrane modules are widely used, which have some advantages as shown below.

- Maximum packing density per volume of contactor.
- Without membrane spacer
- Low liquid flow rate

The first point leads to a large contact area between both phases, then higher throughput is achieved in compact device. The third point is important for the process that a liquid flows on the lumen side of the HF. For example, in membrane absorption process, the reduction of the amount of absorbent brings about the lowering of the energy for regeneration of the spent absorbent.

Another approach for the membrane separation has been made from combination of solvent extraction. That is a liquid membrane. Extraction processes include both separations of the extraction step and the back-extraction. If the solvent is located between the feed and recovery phases, the desired species is transferred from the feed to recoverying solution in one operation mode, then the solvent also acts as a membrane. Since the diffusion rate through the liquid membrane is higher than in solid membranes, a high permeation flux is expected; furthermore, mobile carrier is easily available. There are three configurations of liquid membrane for applying to separation processes: the bulk liquid membrane(BLM), the supported liquid membrane (SLM) and the emulsion liquid membrane(ELM). The potential fields of liquid membrane separation are in metal ion recovery, hydrocarbon processing, waste water treatment and gas separation[5].

In membrane extraction, mobile carrier is sometimes used for attaining high selectivity due to the partitioning. The carrier has an affinity to desired species and enhances its permeation rate. For the extraction of alkali metal ions, it is well known that crown-ethers exhibit excellent partitioning. Crown-ethers are representative macrocyclic compounds synthesized as the model of an ionophore acting in the biomembrane, which forms an inclusion complex with alkali metal ions. The important step in the carrier-mediated transfer is whether the dissociation reaction of the inclusion complex proceeds in the receiving phase or not.

Practical operation of liquid extraction is usually performed in countercurrent multistage contactors such as mixer-setters. Aqueous and organic phases are repeatedly mixed and separated in the contactor, and these cascade is arranged horizontally. Thus the large floor area, pumps and agitators for each stage are necessary for higher separation. If the mixer and the settler are stacked vertically, the contactor behaves like an extraction column. Such a mixer-settler column was firstly introduced by Treybal[9], the column can realize a large number of stages and mixing with an electric motor for stirring each stage. In the column operation, the deterministic factor of the performance is throughput and the number of theoretical stages.

The objectives of the present thesis are to develop some novel operation modes of the membrane-based separation and to clarify the mass-transfer kinetics which is indispensable for the module design. The applicability is illustrated by the comparison with the conventional method. In addition, as the aid to establish the process for liquid membrane and solvent extraction, carrier chemistry and the development of a contactor are included.

In Chapter 1, a novel operation, "permabsorption", as a hybrid operation of the membrane permeation and gas absorption was proposed. The CO_2 flux in alkaline solution was expressed by the mass-transfer model based on membrane permation and gas absorption. The performance of the membrane module was comparable to that of a packed column.

In Chapter 2, the applicability of permabsorption for selective removal of SO_2 from flue gases was investigated. The effect of operating condition on the SO_2 permselectivity was examined.

In Chapter 3, studies were made on the membrane absorption of CO_2 and/or SO_2 using hydrophobic microporous membrane modules. A semi-empirical correlation was derived for the gas-phase mass-transfer coefficient on the shell side of HF modules. The CO_2 absorption rate was described by a model based on the gas diffusion through the membrane pores subsequent to gas absorption accompanied by chemical reaction. The simultaneous membrane absorption of SO_2 and CO_2 was also examined.

In Chapter 4, pervaporation of alcohols from aqueous solutions was performed by sweeping a permeate vapor with an inert gas on the

downstream side of an HF membrane module. The permeation kinetics was illustrated by the solution-diffusion model taken the vapor-liquid equilibrium into account.

In Chapter 5, a novel operation mode of a bulk liquid membrane with microporous partition was proposed. The bulk motion of the membrane liquid enhances the interchannel mass-transfer. To express the mass-tranfer kinetics, a transfer coefficient for the bulk motion of membrane liquid was introduced and then a solute transfer was simulated.

In Chapter 6, the effect of counterion on lithium extraction by 18-crown-6 as a typical neutral cyclic polyether carrier was examined; the data were interpreted in terms of Jones-Dole parameter.

In Chapter 7, a multistage mixer-settler extraction column was developed, which can achieve larger throughput at higher agitation rate. Lifter-turbine impellers were mounted on a stirring shaft and coalescers were inserted between the mixing and settling parts. The effects of operating conditions on the throughput were examined, and the superior performance was proved by measuring a pressure in the column.

In Chapter 8, the stage efficiency of the column developed in Chapter 7 was examined. The efficiency increased monotonously with agitation rate. The overall height of a transfer unit, transformed from the stage efficiency, was devided into the heights of a transfer unit of the dispersed and the continuous phases, which were correlated with the agitation rate.

REFERENCES

1) see e.g., Din., F.: *"Thermodynamic functions of gases"*, Butterworth (1962).
2) Kiani, A., R. R. Bhave, and K. K. Sirkar: *J. Memb. Sci.*, 20, 125 (1984).
3) Loeb, S. and S. Sourirajan: *Adv. Chem. Ser.*, 38, 117 (1962).
4) Mulder, M.: *"Basic principles of membrane technology"*, Kluwer Academic Publishers, Dordrecht (1991).
5) Noble, R. D. and J. D. Way: *"Liquid membranes"*, ACS Symp. Ser.Washington (1987).
6) Qi, Zhang and E. L. Cussler: *J. Memb. Sci.*, 23, 333 (1962).
7) Senoo, M. et.al.: *"Bunri kagaku handbook"*, Kyoritsu Shuppan, Tokyo (1993).
8) see e.g., Stokey, D. J., T. E. Graham and W. M. Pope: *"Natural gas processing with Prism separators"*, AIChE National Meeting, March, Atlanta (1984).
9) Treybal, *Chem. Eng. Prgr.*, 60, 77 (1964).

Chapter 1.

REMOVAL OF CO_2 BY GAS ABSORPTION ACROSS A POLYMERIC MEMBRANE*

INTRODUCTION

One of main causes in global warming is thought to be CO_2 increase in the atmosphere as a result of human and industrial activities; identifying effective countermeasures has become a world-wide problem most recently. In the present situation, where a proper countermeasure cannot be found, it would be more suitable to reduce the amount of CO_2 emitted from the combustion of fossil fuels: de-CO_2(decarbonization) of flue gases. The removal of CO_2 might be achieved industrially by gas absorption processes employing alkanolamines or carbonates as absorbents, in the same way as flue gas desulfurization processes operate.

Typical flue gas from power plants contains CO_2 in a concentration range of 10-15%. Thus the efficient CO_2 removal by gas absorption under ambient pressure requires a source of alkalinity to neutralize it. This implies that energy for the regeneration of the absorbent is deterministic in realization of wet decarbonization processes, and therefore it is advisable to operate an absorber and stripper at a low circulation rate of the absorbent liquid.

In conventional gas-liquid contactors, the high flow rate tends to increase not only the overall mass-transfer coefficient but often the contact area as well. High throughput is desirable but often limited, as in packed columns, because of flooding. The most effective way to reduce the size of the contactor is to provide a very large interfacial area between the phases. Hollow fiber(HF) modules have a large surface area per volume advantage, and they have been widely used in gas permeators or separators.

In gas separation using membranes, the permeate(downstream) side must be regulated under a reduced pressure to attain a concentration difference across the membrane. If an absorbent liquid flows on the permeate side,

---

* This chapter is appeared in J. Chem. Eng. Japan, **25**, No. 1, 67-72(1992).

then the gaseous species to be permeated dissolves into the liquid, subsequent to a reaction with the absorbent, whereby the largest driving force to mass transfer across the membrane can be attained.
In addition, a sparingly soluble gas cannot permeate through the membrane even though it has high permeability. Then we can expect that such hybrid-operation mode of gas permeation and gas absorption with a chemical reaction makes it possible to separate a desired gas from a gaseous mixture with excellent selectivity. Thus we call this process "permabsorption".

This view will be demonstrated in the present study with the object of confirming its applicability to the CO_2 removal from flue gases at moderate temperature.

1 THEORY

Figure 1.1 shows plausible concentration profiles of a permeant, A, for a polymeric membrane situated between gas and liquid flows. The rate of permeation of A, N_A, across the membrane at a steady state can be expressed as

$$N_A = k_G(p_A - p_{A1}) = k_S(\overline{C_{A1}} - \overline{C_{A2}}) = k_L(C_{A2} - C_A)$$
$$= (P_A/\delta)(p_{A1} - p_{A2}) = K_G(p_A - p_A^*) \qquad (1.1)$$

where k_G and k_L are the mass-transfer coefficients for the gas and liquid boundary films, respectively, k_S the membrane-transfer coefficient, p_A the partial pressure of A in the gas phase, and $\overline{C_A}$ the concentration of A in the membrane phase. The subscripts 1 and 2 represent each membrane surface contacting with gas and liquid flows, respectively. P_A is the permeability of the membrane and δ is the membrane thickness. p_{A2} is a hypothetical partial pressure in equilibrium with C_{A2} as well as $\overline{C_{A2}}$. The partial pressure of A in equilibrium with the liquid concentration is given in terms of the Henry's constant

$$p_A^* = HC_A \qquad (1.2)$$

From the additive rule for mass-transfer resistances, an overall permeation coefficient based on the gas phase, K_G, in Eq.(1) can be given as:

$$1/K_G = 1/k_G + \delta/P_A + H/k_L \qquad (1.3)$$

The value of K_G can be evaluated from the individual film coefficient.

We here consider the permabsorption of CO_2 by use of a multiple HFs module, where gas and liquid flows are on the shell and lumen sides,

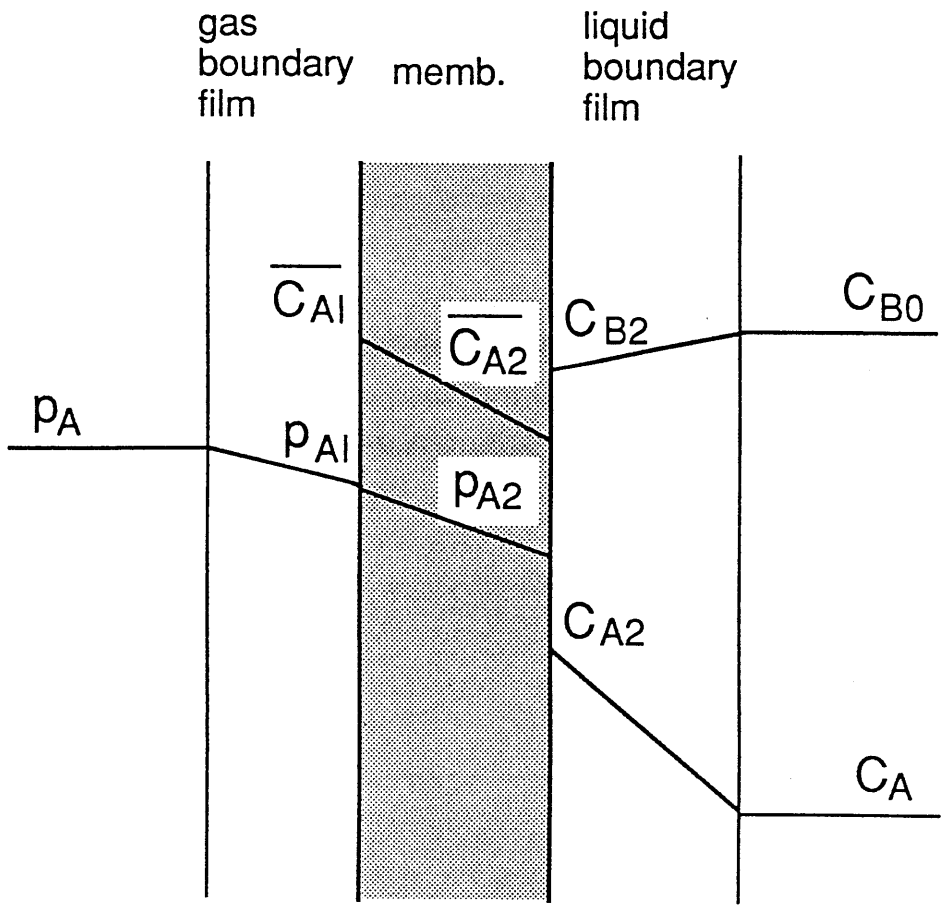

Fig.1.1 Schematic concentration profiles in gas, membrane, and liquid phases for permabsorption of species A.

Table 1.1 Gas permeability of PDMS-HF membrane at 298K.

Permeability	[cm^3 (STP)·cm/ (cm^2·s·cmHg)]	Literature value [9]
CO_2	2.27×10^{-7}	3.24×10^{-7}
O_2	3.49×10^{-8}	6.05×10^{-8}
N_2	—	3.00×10^{-8}

respectively. According to Takeuchi *et al*[13], the following equation can be applied to the prediction of the mass-transfer coefficient for laminar flow on the shell side.

$$Sh = 0.85\ (d_S/d_W)^{0.45}\ (d_e/L)^{0.25}\ Re^{1/3}\ Sc^{1/3} \qquad (1.4)$$

where d_S is the inside diameter of the shell tube, d_W wetted perimeter, d_e the hydraulic equivalent diameter as the characteristic length of the HF module, and L the HF length.

For laminar flow inside solid tube, the mass-transfer coefficient can be expressed by the Leveque solution[8]

$$k_L\, d_i\, /D_A = 1.62\{(d_i\, /L)\ Re\ Sc\}^{1/3} \qquad (1.5)$$

where d_i is the inside diameter of the HF, and D_A is the diffusion coefficient of CO_2 in the liquid phase.

When an aqueous solution of NaOH is used as the absorbent liquid, CO_2 reacts with hydroxyl ion within the liquid film as follows:

$$CO_2 + OH^- \rightleftarrows HCO_3^- \qquad (1.6)$$

$$HCO_3^- + OH^- \rightleftarrows CO_3^{2-} \qquad (1.7)$$

where reaction(1.6) is of second order in the forward direction. Reaction(1.7) is much faster than reaction(1.6); therefore, the carbonization reaction is of no significance in determining the rate of CO_2 transfer. The permeation rate is given by

$$N_A = \beta\, k_L\, C_{A2} \qquad (1.8)$$

provided that the CO_2 concentration in the liquid bulk, C_A, is negligible: $p_A^* = 0$. In Eq.(1.8), β is the enhancement factor due to the chemical reaction, which can be evaluated from the classical solution of gas absorption accompanied by a second-order chemical reaction;[7]

$$\beta = \frac{\gamma\sqrt{1 - [(\beta - 1)/r\,q]}}{\tanh \gamma\sqrt{1 - [(\beta - 1)/r\,q]}} \qquad (1.9)$$

where $r = D_B/D_A$, $q = C_{B0}/(\gamma C_{A2})$, and $\gamma = \sqrt{k\, C_{B0} D_A}\ /(k_L.D_B)$ is the diffusion coefficient of OH^- in the liquid phase, C_{B0} the OH^- concentration in the liquid bulk, and k the rate constant for reaction(6). If there is a reaction between the dissolved gas and a reactant in the liquid, the k_L is substituted to βk_L; where β is the enhencement factor. At high NaOH concentration, β approaches γ and Eq.(3) reduces to

$$1/K_G = \delta/P_A + H/\sqrt{k\, C_{B0} D_A} \qquad (1.10)$$

where the gas film resistance is *a priori* negligible compared with the membrane resistance. Then it can be expected that the variation of N_A

with the liquid flow rate is of no significance, and this condition can be used to determine the permeability for CO_2.

2 EXPERIMENTAL

Polydimethylsiloxane(PDMS) is a material of special interest for gas separation because it has a very high gas permeability value compared with other polymers. PDMS-HF membranes used in this study were supplied from Nagayanagi Co. Ltd., having an inside diameter of 200μm and a wall thickness of 60μm. Membrane module consisted of one hundred HFs, which were fixed with epoxy resin at the both ends of a teflon tube (1.7cm I.D. and 30cm long).

A schematic diagram of the experimental apparatus is shown in **Fig.1.2**. The completed module was installed vertically in a constant-temperature air bath whose temperature ranged from 298K to 338K. Gas mixture of CO_2 and N_2 supplied from respective cylinders was introduced on the shell side at the top of the module, through a preheater. An aqueous solution of NaOH or K_2CO_3 was supplied on the lumen side at the bottom of the module via a peristaltic pump from a reservoir in a constant-temperature water bath.

The concentration of CO_2 in the gas phase was determined for the influent and effluent streams from the module on an infrared gas analyzer (Fuji Electric Co. Ltd. ZFU-IDM23). The liquid concentration of aqueous solution was determined by titration; the mass balance of CO_2 between the two streams was then checked. The permeation rate across the membrane was calculated in terms of concentration difference in the gas phase. In all experimental runs, the temperatures of both phases was measured with thermocouples mounted at the top and the bottom of the module.

To obtain the gas permeability of the HF membrane used in this study, a permabsorption test was conducted for pure carbon dioxide and oxygen using a single PDMS-HF module, whereby aqueous solution of 1*M* NaOH or pyrogallol as the absorbent for CO_2 or O_2, respectively, was supplied on the lumen side of the HF. After having reached a steady state, the amount of gas permeated through the membrane was determined volumetrically using a soap-film meter.

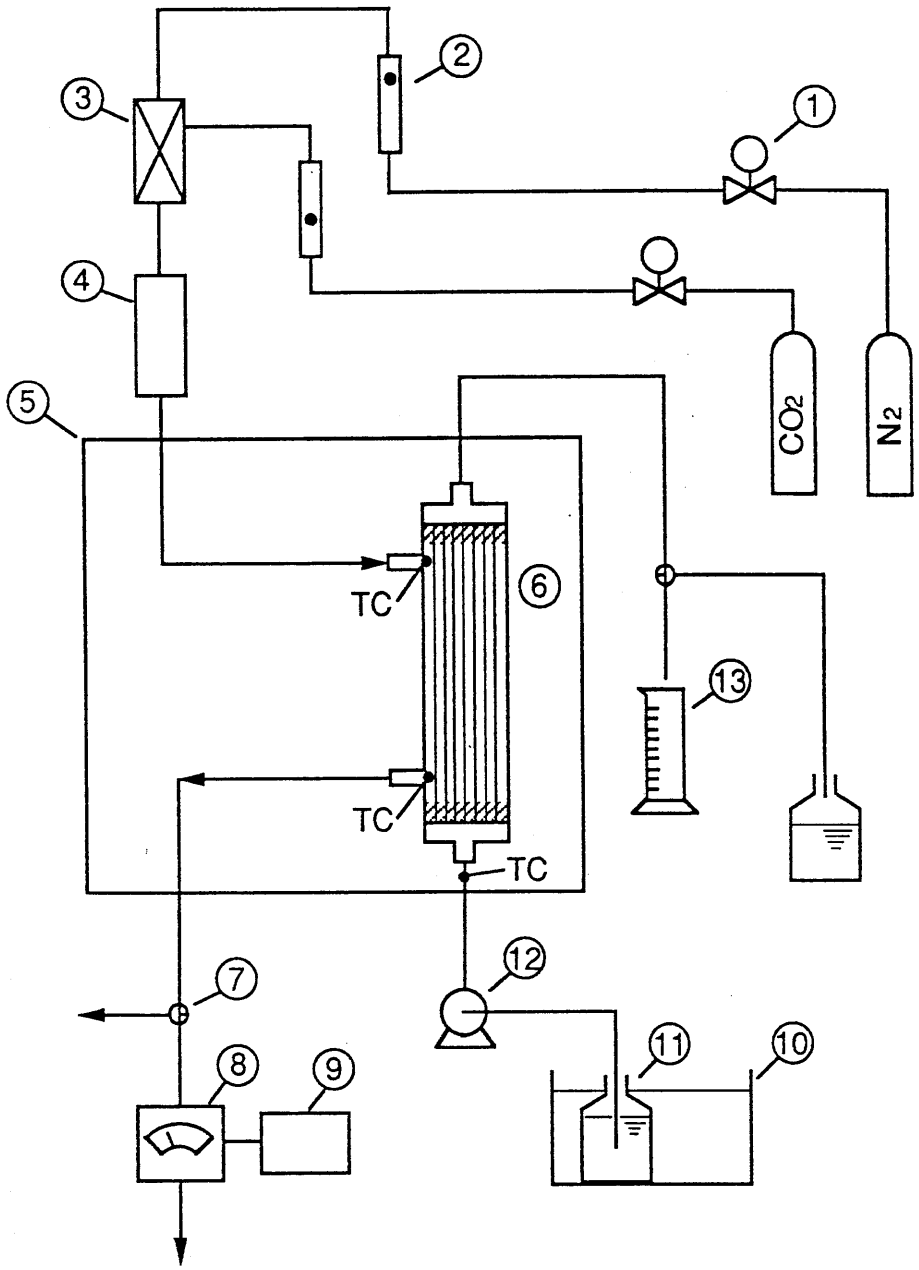

1 FLOW CONTROL VALVE
2 FLOW METER
3 GAS MIXER
4 PREHEATER
5 CONST. TEMP. AIR BATH
6 MODULE
7 VALVE
8 ANALYZER
9 RECORDER
10 THERMO CONTROLLED BATH
11 RESERVOIR
12 PERISTALTIC PUMP
13 MEASUREING CYLINDER
TC THERMOCOUPLE

Fig.1.2 Schematic diagram of experimental apparatus.

3 RESULTS AND DISCUSSION

3.1 Gas permeability

The permeability of the PDMS-HF membrane for CO_2 and O_2 was calculated from

$$P_A = V\,(273/T)\,\delta/(A\,t\,p_A) \tag{1.11}$$

where V is the volume of gas permeated through the membrane, T the temperature, A the membrane area and t the contact time.

The permeabilities of PDMS membrane obtained for CO_2 and O_2 are shown in **Table 1.1**, where the diffusional resistance through the liquid boundary film was neglected. In the case of the CO_2 permabsorption, the value of $H / \sqrt{k\,C_{B0}D_A}$ in Eq.(1.10) is $3.3\text{x}10^2$, whereas the value of $1/K_G$ is $2.64\text{x}10^4$; therefore $1/K_G \cong \delta/P_A$. There is no available data on k for the reaction of O_2 with pyrogallol; it is considered that the ratio of the liquid phase resistance to the total resistance is within a few percent. The present results are comparable to literature values[9] obtained in conventional gas permeators under reduced pressure on the permeate side. Such a reasonable agreement leads to the expectation that permabsorption is applicable to the measurement of gas permeability of homogeneous HF membranes in a simple-operation mode.

For the recovery of CO_2 from exhaust gas, especially from combustion gas, the selectivity of CO_2 to N_2 as the major component is crucial. In the present permabsorption experiments with pure gases, no appreciable permeation of N_2 through the membrane was observed. This implies that the permselectivity of CO_2 to N_2 is extremely high. Therefore, permabsorption using PDMS membrane has great potential for selective recovery of CO_2 from flue gases.

3.2 Effect of NaOH concentration on overall permeation coefficient

In the permabsorption of CO_2 by using alkaline solution, it is expected that the concentration of NaOH in the absorbent liquid, C_{B0} falls remarkably owing to small liquid flow rate, and its decrease results in smaller values of K_G. **Figure 1.3** shows the effect of liquid velocity, u_L, inside the HF on the apparent value of K_G on the assumption that $p_A^* = 0$. For C_{B0} = 1mol/dm^3, the value of K_G was independent of u_L, being close to the dashed line, which was calculated on the assumption that only membrane resistance controls the permeation rate for CO_2, as

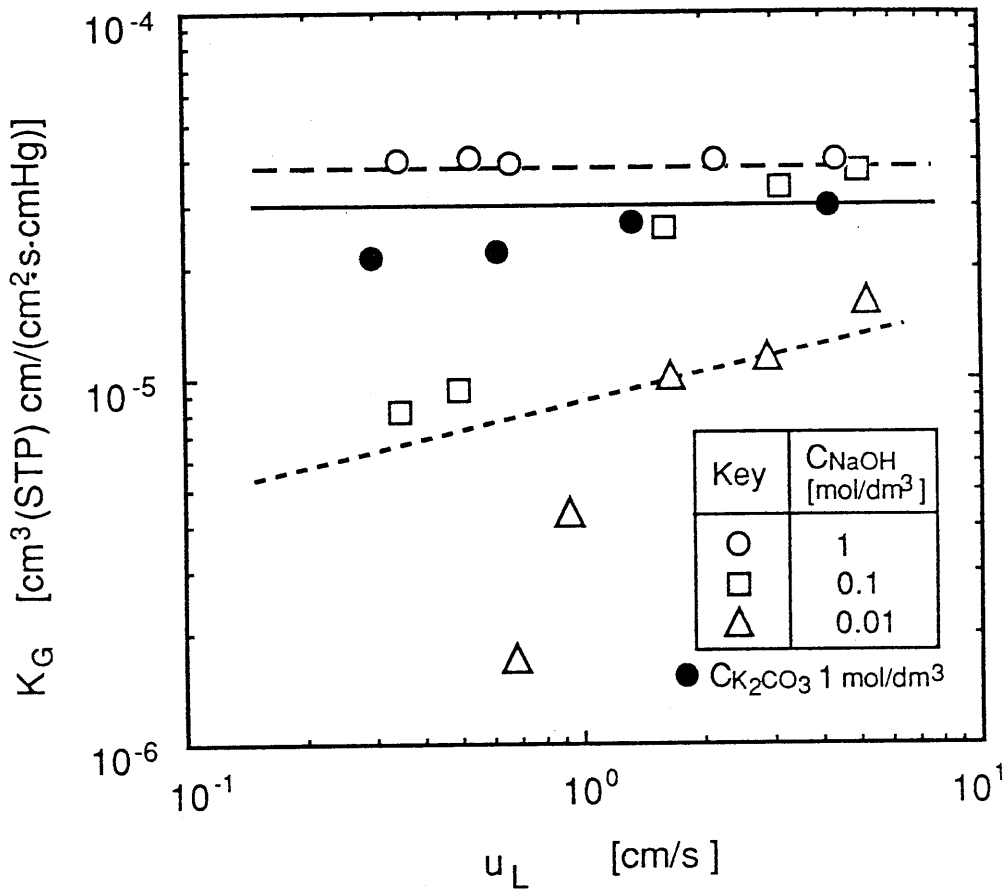

Fig.1.3 Effect of liquid velocity on overall permeation coefficient. Dashed, solid, and dotted lines are the calculated values for membrane diffusion-controlling, 1mol/dm^3 K_2CO_3, and water, respectively.

discussed in the above section. However, the K_G values for aqueous solutions having smaller C_{B0} decreased drastically with u_L. It is to be noted that the NaOH in the liquid through the HF tube was depleted by the reaction with CO_2 for smaller values of C_{B0} and u_L. This leads to lowering of β given by Eq.(1.9). Furthermore, when considering the depletion of NaOH, the back pressure, p_A*, in the liquid bulk would be appreciable; thus, the value of K_G can be regarded as apparent.

The results for 1M K_2CO_3 solution are also shown in Fig.1.3. The value of K_G is smaller than that for 1M NaOH because of the diffusional resistance* through the liquid boundary layer due to the low alkalinity, i.e. the smaller value of β.

The permeation rates of CO_2, N_A, obtained for various concentrations of NaOH are compared with the theoretical values in **Fig.1.4**, where the value of N_A is plotted against p_{CO2} together with the calculated line. The observed values for 1M NaOH locate on the dashed line that was obtained on the assumption that the permeation rate is controlled solely by the membrane resistance, as mentioned above.

The calculation of permabsorption rate in the second-order reaction regime was made as follows. Since the diffusional resistance through the gas boundary film is negligible, (k_G = 2.5x10^{-2}cm^3(STP)/(cm^2• s•cmHg) for u_G = 15.2cm/s from Eq.(1.4)), $p_{A1} = p_A$. Assuming an appropriate value of N_A in Eq.(1.1), we can obtain p_{A2} and then C_{A2} is determined from Eq.(1.2)[11]. The value of N_A calculated from Eqs.(1.8) and (1.9) along with the C_{A2} value is compared with the assumed value. This procedure is repeated until giving the tolerance within an allowable error. For permabsorption by water, on the other hand, the CO_2 concentration in the liquid bulk was taken into account.

The results thus obtained(solid lines) are in good agreement with the observed values, as can be seen in Fig.1.4. In conclusion, the permabsorption process using the HF membrane can be interpreted by a simple model based on the membrane permeation with gas absorption.

---

*) The mass transfer resistance of each phase is as follows: $1/k_G$ = 40, δ/P_A = 2.66x10^4, and $H/(\beta k_L)$ = 3.87x10^3

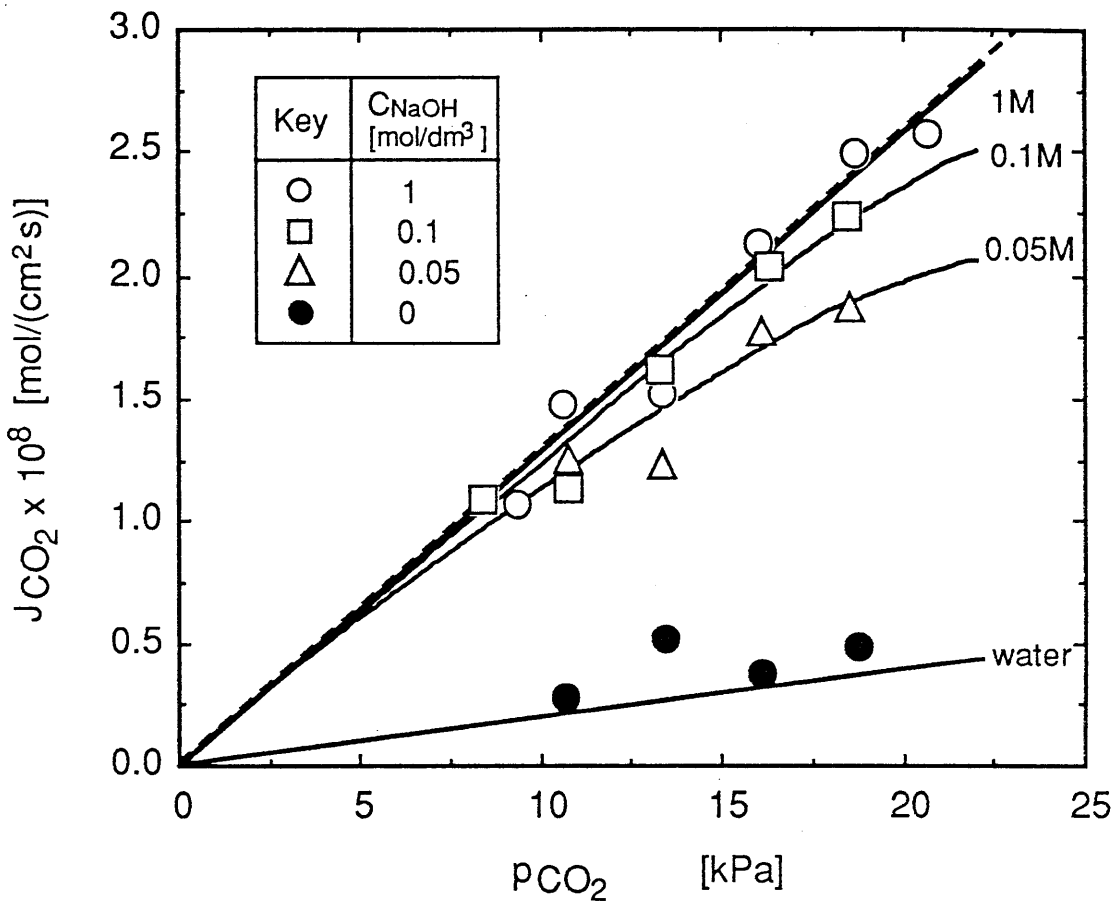

Fig.1.4 Effect of CO_2 partial pressure on permeation flux. (T=299K and u_L=5.1cm/s). Solid lines represent calculated values and dashed line is that for membrane-diffusion controlling.

3.3 Permabsorption of CO_2 by use of carbonate solutions

In acid gas treating, aqueous solutions of various alkanolamines and carbonates have been used extensively for the removal of CO_2[6]. Though having excellent capability of CO_2 removal, the amine solution requires a large amount of energy for the regeneration of the rich solution, in contrast to carbonate solution. In the case of flue gas decarbonization, it may be sufficient to remove about 70% of the CO_2 because it is non-toxic; thus, alkali-carbonate solution is preferable to alkanolamines. The absorption of CO_2 in carbonate solutions has been examined extensively,[2,3,4,12] and the chemistry of the process is well understood. As discussed in the above section, when CO_2 permeates across the membrane into carbonate solution, carbonate ion is partially converted to bicarbonate, and the overall chemical reaction is expressed as:

$$CO_3^{2-} + CO_2 + H_2O \rightleftarrows 2HCO_3^- \qquad (1.12)$$

In reaction(1.12), the rate-controlling step is the elementary reaction(1.6); the hydroxyl ion concentration can then be determined in terms of equilibrium constant, K

$$[OH^-] = K\,[CO_3^{2-}] / [HCO_3^-] \qquad (1.13)$$

for which the equilibrium data are available elsewhere.[3]

The effect of the concentration ratio of carbonate to bicarbonate ions in the effluent liquid on the permeation rate of CO_2 is shown in **Fig.1.5**, together with calculated lines from Eq.(1.1) on the basis of a film-theory model presented by Astarita and Savage[1]; in addition, the equilibrium partial pressure of CO_2 was estimated from[5]

$$p_A^* = (4H / K_l)\, m X^2 /(1-X) \qquad (1.14)$$

where K_l is the equilibrium constant for reaction(1.12), m the molarity of the carbonate solution, mol/cm^3, and X the fractional conversion of carbonate to bicarbonate ($[HCO_3^-] / [K^+]$).

The reasonable agreement between the theoretical values and the observations in Fig.1.5 suggests that reaction(1.12) in the liquid boundary film takes place under fast reaction conditions. However, when the carbonate-to-bicarbonate ratio is less than 1, the permeation rate decreases significantly, even for 2M K_2CO_3. Such behavior was due to the higher back-pressure resulting from the increase of bicarbonate in the liquid. In a practical view of flue gas decarbonization, this result leads to a conclusion that the absorbent liquid must be regenerated at a carbonate conversion of 0.33 under the present conditions.

3.4 Effect of temperature on overall permeation coefficient

For flue gas decarbonization, we are considering that removing CO_2 from the gas after desulfurizing by gas absorption (wet desulfurization) is really advantageous; thus the process must have a suitable transport efficiency at moderate temperature. It is well known that polymeric membranes have larger gas permeability at higher temperature. PDMS is especially characteristic of heat-resistance at temperature below 423K.

We here examined the performance of a permabsorption device over the temperature range 298K to 328K. The overall coefficients for 0.5*M* NaOH are plotted in **Fig.1.6** against the reciprocal temperature. The result shows a constant value independent of the temperature, corresponding to the membrane diffusion-controlling at 298K.(see Fig.1.3). This may be due to the trade-off of diffusivity and solubility in PDMS with temperature rise.

3.5 Comparison of permabsorption and gas absorption for CO_2 removal

From a practical viewpoint of gas treating, an important point is to show how permabsorption by use of the HF module is advantageous in the removal of CO_2 compared with gas absorption. We here compared the performance of a PDMS-HFs module with that of a packed column[10] as a representative conventional absorber.

Table 1.2 summarizes the results together with the design and operating parameters. The comparison was made between module and column of equal volume, where the module was composed of 15,000 PDMS-HFs packed in triangular arrangement with a pitch width of 0.78mm. The hollow fibers are the same as those used in this study. As Table 1.2 shows, an advantage of permabsorption is observed in liquid flow rate: the required rate is smaller than that for the packed column by one order of magnitude. This is due to the large interfacial area in the hollow fiber module. It is to be noted that the lower liquid flow rate makes it possible to reduce the energy needed for solution circulation through the regenerator as well as for the heat of regeneration of the rich solution. Unfortunately, the value of K_G in the permabsorption process is lower than that in the packed column operation owing to the polymeric membrane itself; however, higher performance can be realized by use of PDMS-HFs of lesser thickness. Furthermore, the membrane module is

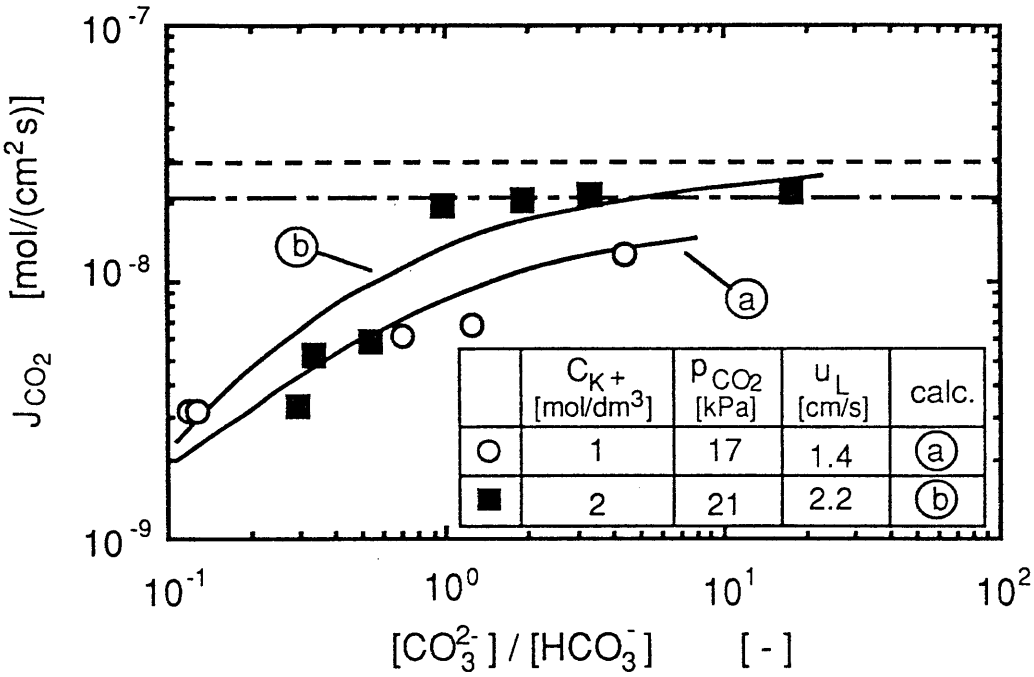

Fig.1.5 Effect of the carbonate-to-bicarboneate ratio for carbonate solution. Solid lines are calculated values for carbonate soltions. Dashed and dash-dotted lines represent membrane diffusion-controlling for p_{CO_2}=17 and 21kPa, respectively.

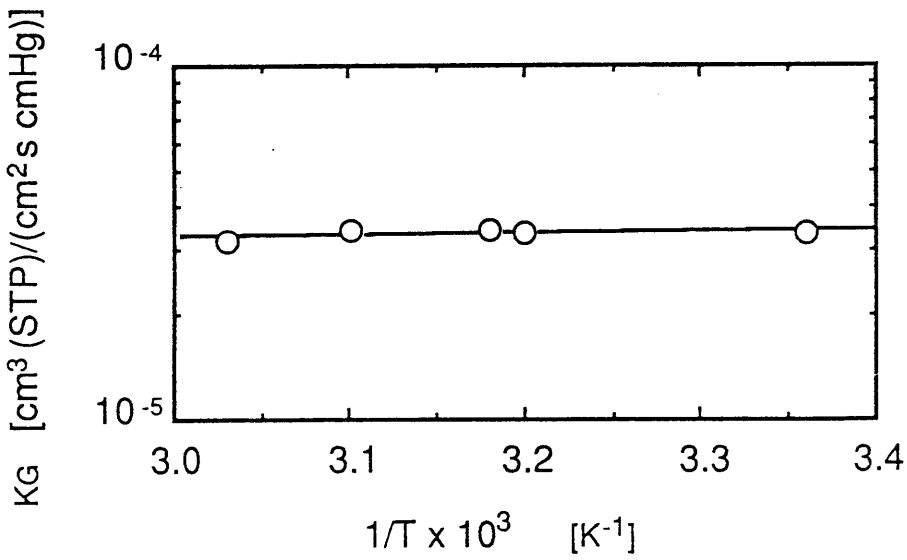

Fig.1.6 Effect of temperature on overall permeation coefficient for 0.5mol/dm^3 NaOH. (p_A=17kPa and u_L=5.1cm/s).

Table 1.2 Comparison of performance of PDMS-HF membrane module and packed column.

	PDMS-HFs membrane module	Packed column [10]
Column diameter [cm]	10	10
Packing	15000 PDMS-HF	12mm Raschig Ring
ε [–]	0.97	0.72
Gas velocity [g/(cm^2·s)]	0.192	0.025
Liquid velocity [g/(cm^2·s)]	1.0	0.278
Q_L [cm^3/s]	4.71	21.8
a [cm^{-1}]	20	1.20
K_G [cm^3 (STP)/(cm^2·s· cmHg)]	3.80×10^{-5}	6.80×10^{-4}
K_Ga [cm^3 (STP)/(cm^3·s· cmHg)]	7.60×10^{-4}	8.19×10^{-4}

free from flooding, unlike the direct contacting between gas and liquid phases in packed columns; therefore, the permabsorption process is suitable for treating a large amount of acid gases, including flue gas and gas from coal gasification.

CONCLUSIONS

In this article we have proposed a hybrid operation mode of gas permeation across a non-porous membrane and gas absorption, which is termed permabsorption. The applicability of polydimethylsiloxane hollow-fiber membrane was examined for the removal of CO_2 from gas mixture of N_2 and CO_2, the following conclusions were obtained.

Permeability of the membrane for pure gases was obtained by means of permabsorption in a simple device.

Excellent permselectivity can be attained by selecting an absorbent liquid suitable for gaseous species.

In the permabsorption of CO_2 using alkaline solutions, the rate of mass transfer across the membrane can be expressed by a model based on membrane permeation with gas absorption accompanied by chemical reaction; the permeation rate was controlled mainly by the diffusional resistance in the membrane.

In practical situations of CO_2 removal from flue gas, the performance of the multiple-fiber membrane module was compared with that of a packed column. It was found that the liquid flow rate required to achieve a desired removal of CO_2 is remarkably low. In addition, the permabsorption method has the advantage of operability at high gas-flow rate because of the indirect contact between gas and liquid flows.

NOMENCLATURE

A	contact area	[cm^2]
a	interfacial area per unit volume of contactor	[cm^{-1}]
C	concentration	[mol/cm^3]
$\overline{C}$	concentration in the membrane	[mol/cm^3]
D	diffusion coefficient	[cm^2/s]
d_e	hydraulic equivalent diameter	[cm]

d_i	inside diameter of hollow fiber	[cm]
d_S	inside diameter of shell tube	[cm]
d_W	wetted perimeter	[cm]
H	Henry's constant	[cmHg•cm^3/mol]
K	equilibrium constant for reaction(1.12)	[-]
K_G	overall permeation coefficient or mass-transfer coefficient	[cm^3(STP)/(cm^2•s•cmHg)] or [mol/(cm^2•s•kPa)]
k	reaction rate constant	[cm^3/mol•s]
k_G	gas film mass-transfer coefficient	[cm^3(STP)/(cm^2•s•Δp)]
k_S	mass-transfer coefficient in the membrane phase	[cm/s]
k_L	liquid film mass-transfer coefficient	[cm/s]
N_A	flux of component A	[mol/(cm^2•s)] or [cm^3(STP)/(cm^2•s)]
P	gas permeability	[cm^3(STP) cm/(cm^2•s•cmHg)]
p	partial pressure	[kPa] or [cmHg]
Q	volumetric flow rate	[cm^3/s]
t	contact time	[s]
T	temperature	[K]
u_L	liquid velocity per unit cross sectional area of lumen of HF	[cm/s]
V	volume of gas permeated through the membrane	[cm^3]

Subscripts

A	reactant in the gas phase (permeant)
B	reactant in the liquid phase
1	membrane surface contacting with gas
2	membrane surface contacting with liquid

Greeks

β	menhancement factor	[-]
δ	membrane thickness	[cm]
ε	voidage	[-]
ν	stoichiometric coefficient	[-]

REFERENCES

1) Astarita. G, and Savage, D. W.: *Chem. Eng. Sci.*, 35, No.3, 649 (1980).
2) Danckwerts, P. V.:*"Gas-Liquid Reactions"*, McGraw-Hill Inc., New York, NY (1970).
3) Danckwerts, P. V.and Sharma, M. M.: *The Chem. Eng.*, CE244-CE280, October (1966).
4) Hikita, H, Asai, S. and Takatsuka, T.: Chem. Eng. J., 11, 131 (1976).
5) Joshi, S. V, Astarita G. and Savage, D. W.: *AIChE Symp. Series* 77, 202, 63 (1981).
6) Kohl, A. L, and Riesenfeld, F. C.:*"Gas Purification"*, 4th ed.,Gulf Publishing Co., Houston, TX (1985).
7) van Krevelen D. W, and Hoftyzer, P. J.: *Rec. Trav. Chim.*, 67, 563, 587 (1948).
8) Leveque, M. A.: *Ann. Mines Rec. Mem. L'Explotas. Mines* 13, 201 (1928).
9) Nakagawa, T:*"Bunrimaku"*, p96, Sangyo-Tosho, Tokyo (1987).
10) Onda, K, Sada, E. and Takeuchi, H.: *J. Chem. Eng. Japan*, 1, 62 (1968).
11) Onda, K, Sada, E. Kobayashi, T. and Kito, S.: *J. Chem. Eng. Japan*, 3, 18 (1970).
12) Savage, D. W.:*"Recent Development in Separation Science Vol.7"*, p73, CRC Press (1982).
13) Takeuchi, H., Takahashi, K. and Nakano, M. : *Ind. Eng. Chem. Res.*, 29, 1471 (1990).

Chapter 2.

SELECTIVE REMOVAL OF SO_2 WITH RESPECT TO CO_2 FROM FLUE GAS STREAM BY PERMABSORPTION METHOD*

INTRODUCTION

In the previous chapter, the possibility of CO_2 permabsorption was clarified for flue gases after desuphurization process. The present chapter is focused on examining the applicability of the permabsorption method for the selective removal of SO_2 from flue gases after scrubbing, which contains CO_2 as well as SO_2.

Some conventional wet desulphurization processses are operated by using slurries as the absorbent. In permabsorption, it is difficult to apply slurry absorbents because of the problem of HF clogging. Thus aqueous soution of sodium sulphite was selected as the absorbent . The effect of operating conditions on the selectivity were investigated by using the same membrane modules in the previous chapter.

1 THEORETICAL BASIS FOR EXPERIMENTAL MEASUREMENTS

In the permabsorption process using an HF module, gas and liquid flows were on the shell and lumen sides of the HF, respectively. In the case of supplying a reactive absorption liquid. The flux of A across the membrane can be expressed as

$$J_A = k_G(p_A-p_{A1}) = k_S(\overline{C_{A1}}-\overline{C_{A2}}) = \beta k_L(C_{A2}-C_A)$$
$$= (P_A/\delta)(p_{A1}-p_{A2}) = K_G(p_A-p_A^*) \qquad (2.1)$$

where k_G and k_L are the mass-transfer coefficients for the gas and liquid films respectively, k_S the membrane transfer coefficient, p_A the partial pressure of A in the gas phase, and $\overline{C_A}$ the concentration of A in the membrane phase. The subscripts 1 and 2 represent each membrane surface in contact with the gas and liquid flows, respectively. P_A is the membrane permeability of A, δ being the membrane thickness. p_{A2} is a

---

* Articles related to this chapter are appeared inTrans. IChemE, Part B Proc. Safety and Env. Prot., **72**, No. B2 (1994).

hypothetical partial pressure in equilibrium with C_{A2} as well as $\overline{C_{A2}}$ The partial pressure of A in equilibrium with the concentration in the liquid phase is given by Henry's law.

The overall mass-transfer coefficient, K_G, based on the gas phase is given as

$$1/K_G = 1/k_G + \delta/P_A + H/\beta k_L \quad (2.2)$$

$$= 1/K + H/\beta k_L \quad (2.2')$$

where $1/K$ is the combined resistance of the gas-film and membrane. The permeability of the membrane for the permeant can be observed as shown in the previous Chapter.

For simultaneous absorption of SO_2 and CO_2 in aqueous Na_2SO_3 solution, the following reactions are likely to be significant:

$$SO_2 + SO_3^{2-} + H_2O \rightleftarrows 2HSO_3^- \quad (2.3)$$

$$CO_2 + SO_3^{2-} + H_2O \rightleftarrows HSO_3^- + HCO_3^- \quad (2.4)$$

$$SO_2 + HCO_3^- \rightleftarrows HSO_3^- + CO_2 \quad (2.5)$$

where the values[1] of equilibrium constants K_1, K_2, and K_3 of Reactions(2.3), (2.4), and (2.5) are 2.76×10^5, 7.12, and 3.08×10^4 in infinite dilution at 298K, respectively. Reaction(2.3) proceeds much faster than the others: the reaction rate constant, k_r, for Reaction(2.3) is of the order of 10^5 $m^3/(mol\cdot s)$, being widely defferent from that for Reaction(1.4)($2.39\times10^{-2} m^3/(mol\cdot s)$)[1]. In the simultaneous permabsorption process, SO_2 dissolved in the liquid reacts instantaneously with a sulphite ion, and then depletes in the liquid boundary film, provided that $C_B > C_{A2}$. The enhancement factor for SO_2 is calculated from the solution based on the film theory in the instantaneous irreversible reaction regime:

$$\beta = 1 + rq \quad (2.6)$$

where the diffusivity ratio, r, was assumed to be 0.56[6]. For CO_2, on the other hand, the contribution of the enhancement factor due to Reaction(2.4) is of no significance as compared with the SO_2 absorption.

2 EXPERIMENTAL

The membrane and membrane module is the same as in Chapter 1. Details of membrane and membrane modules are shown in the section 1.2. and Table 1.1. A schematic diagram of the experimental apparatus is shown in **Fig.2.1** The completed module was installed vertically. A gas mixture consisting of N_2, CO_2 and/or SO_2 was introduced on the shell

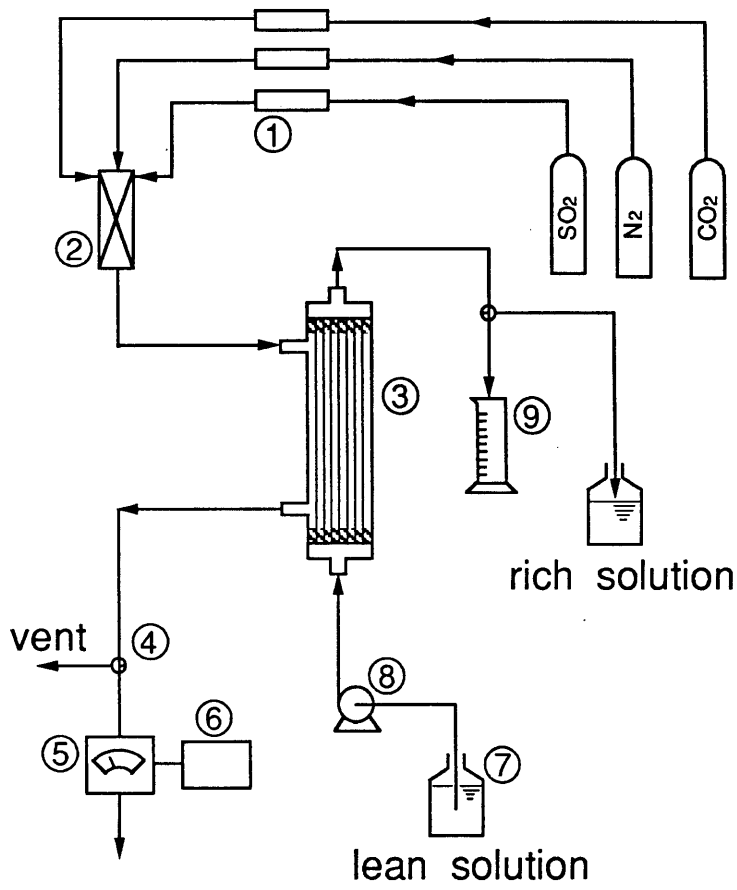

1 flow controller
2 gas mixer
3 HF module
4 three-way cock
5 analyzer
6 recorder
7 reservoir
8 pump
9 measuring cylinder

Fig.2.1 Schematic diagram of experimental apparatus.

Table 2.1 Gas permeability of PDMS-HF membrane at 299K.

Gas	Permeability [mol/(cm• s•Pa)]	
	Observed	Literature value
CO_2	1.35×10^{-8}	1.8×10^{-8} *
O_2	2.07×10^{-9}	2.8×10^{-9} *
SO_2	5.82×10^{-8}	-
N_2	non detect.	1.3×10^{-9} **

* Hwang et al.[2] , ** Stern et al.[5]

side at the top of the module. An aqueous solution of NaOH, K_2CO_3, or Na_2SO_3 was supplied from a reservoir on the lumen side at the bottom of the module via a peristaltic pump. After having reached a steady-state, concentrations of CO_2 and of SO_2 in the gas phase were determined for the influent and effluent streams from the module using each infrared gas analyzer. The transport rate of A across the membrane, J_A, was calculated in terms of the concentration difference in the gas phase at the top and bottom of the module. In all the experimental runs, the temperature was kept at 299±1K, and the total pressure at that of the atmosphere

2.3 RESULTS AND DISCUSSION

2.3.1 Gas permeability of PDMS-HF membrane

The permeabilities of the PDMS-HF membrane for CO_2 and O_2 were examined in the previous paper. For SO_2, the permeability was determined from the slope on a plot of J_{SO_2} versus the partial pressure(see Fig.2.2) under conditions allowing the permeation to be in membrane controlling mode, i.e. $1/K_G = 1/K$ in Eq.(2.2').

The results obtained for CO_2[3], SO_2 and O_2[3] are given in **Table 2.1**; these values are comparable to literature values[2,5] obtained by reducing pressure on the permeate side in conventional gas permeators. Such agreement leads to the expectation that the present permabsorption method is suitable for measuring gas permeability of nonporous HF membranes in a simple operational mode.

For the selective separation of SO_2 or CO_2 from exhausted gas, the permeation of N_2 through the membrane should be kept as low as possible. In the present experiments, no appreciable permeation of N_2 across the membrane was observed. Therefore, the experiment suggests that the permabsorption process using PDMS-HF membrane has the potential for highly selective removal of SO_2 or CO_2 to N_2 in flue gases, even though a permselectivity defined as P_{SO_2}/P_{CO_2} has a value of *ca.*4.5(see Table 1).

2.3.2 Permselectivity of SO_2 with respect to CO_2

To examine the applicability of permabsorption to flue gas desulphurization, simultaneous permabsorption of SO_2 and CO_2 from a gaseous feed (10vol% CO_2 and 0.5vol% SO_2 balanced with N_2) was

conducted with varying u_L. In wet flue gas treating, it is advisable to absorb SO_2 from the gas stream prior to the CO_2 removal. The present result showed that with decreasing liquid velocity the CO_2 flux decreases remarkably as shown in Fig.1.3., whereas the SO_2 flux was not so much influenced by u_L, because the amount of sulphite ion in the liquid was sufficient in relation to the SO_2 permeated through the membrane. Thus we can expect that the selective removal of SO_2 in preference to CO_2 is attained under conditions such that the liquid flow rate is low, viz. the sulphite concentration near the membrane-liquid interface is low.

Figure 2.2 shows the effect of the partial pressure of SO_2 on both SO_2 and CO_2 fluxes in the simultaneous permabsorption for 0.01*M* Na_2SO_3 at u_L of 2cm/s. The solid lines represent the theoretical values based on the model with one reaction plane within the liquid boundary film, at which only Reaction(2.3) takes place instantaneously.

If there is a sufficient quantity of the reactant in the liquid bulk, then the absorbed SO_2 would react instantaneously and deplete within the liquid film, and a reaction plane is thus formed. In this situation we assumed that the transfer of CO_2 through the liquid film is caused only by molecular diffusion, as the effect of Reaction(2.4) is negligible. Thus, Reactions(2.4) and (2.5) proceed in the liquid bulk under equilibrium conditions. In the calculation, the concentration of sulphite ion was evaluated at successive points through the module, because a remarkable concentration fall was observed in the effluent liquid; the enhancement factor for SO_2 was given by Eq.(2.6). Concentration of CO_2 in the liquid bulk was obtained using the equilibrium constants K_1, K_2 and K_3 for reactions (2.3), (2.4), (2.5). In each segment of the module, the local values of CO_2 and SO_2 fluxes were calculated by an iterative method; the over-module fluxes were obtained by integrating the values from the bottom to top of the module. The solid lines in Fig.2.2 represent a plot of the average fluxes over module for SO_2 and CO_2 against the SO_2 partial pressure averaged from the inlet to outlet of the module. The diffusion coefficient and solubility used for the calculations were as follows[6]: $D_{SO_2}= 1.95\times10^{-5}$, $D_{CO_2}=1.95\times10^{-5}$, $H_{SO_2}=69.4$, and $H_{CO_2}=2.52\times10^3$ (see nomenclature for units).

The permeation behavior of the two gases can be interpreted reasonably by use of the model with one reaction plane, indicating that the absorption of CO_2 is suppressed in the presence of SO_2.

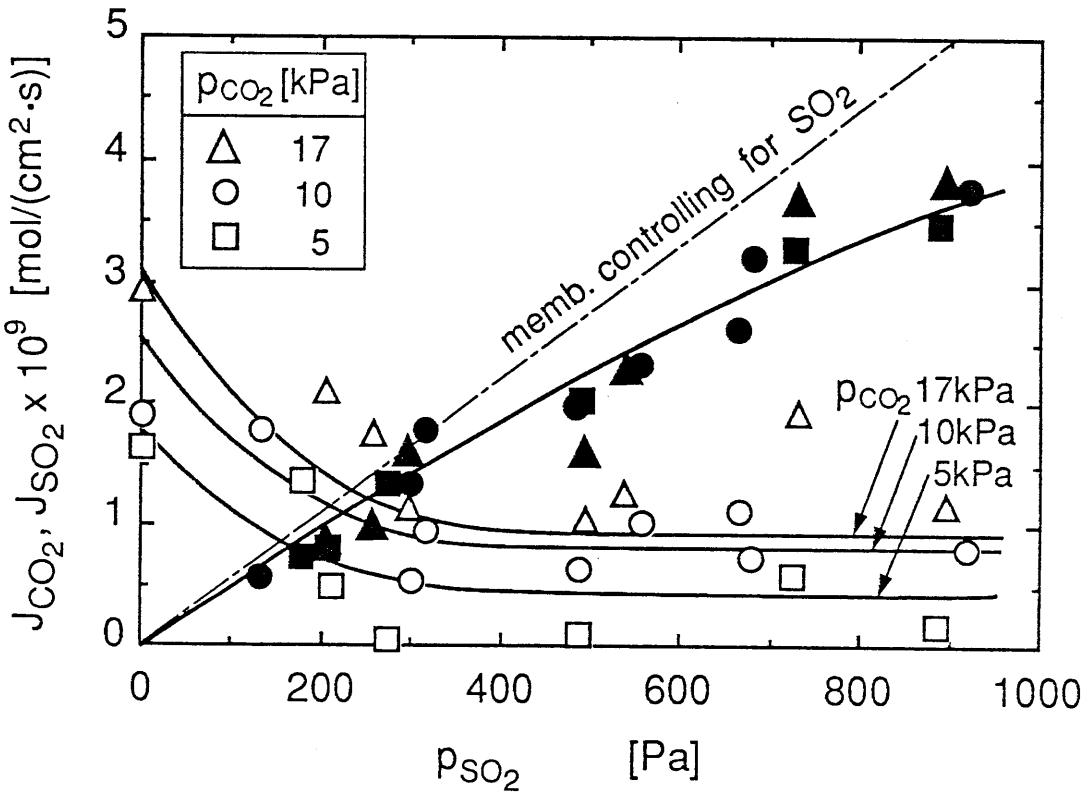

Fig.2.2 Effects of partial pressures of SO_2 and CO_2 on the respective fluxes in 0.01*M* Na_2SO_3. Solid lines are calculated values. Dash-dotted line refers to membrane diffusion controlling mode for SO_2. Open symbols are for CO_2, and closed symbols are for SO_2.

Here we define the permselectivity of SO_2 in preference to CO_2 as

$$\sigma(SO_2/CO_2) = [J_{SO2}/p_{SO2}] / [J_{CO2}/p_{CO2}] \quad (2.7)$$

In **Fig.2.3** the σ values are plotted against the SO_2 partial pressure for p_{CO2} values of 5, 10 and 17kPa. The SO_2 permselectivity varied in a complicated manner with p_{SO2}, depending also on p_{CO2}. Such complicated behavior may be attributed to differences in the membrane resistance to permeation for each gas, as well as in the reaction kinetics of each gas in the liquid. There are substantial differences between the results obtained from the experimental data(see Fig.2.2) and those obtained from the theory, especially for p_{CO2} = 5kPa; such deviation arose from the deviation between observed and calculated values of J_{CO2}. This is probably attributable to tlarge but unquantified experimental variations of p_{CO2}. These may be due to the multi-HF module itself, for example, because of variations in the configuration of the HF bundle in its elastic response to fluctuations in the gas and liquid flow conditions in the module.

Qualitatively, the σ behavior shown in Fig.2.3 can be explained as follows: if there was no membrane between the gas and liquid phases and also the gas-phase resistance was of no significance, the value of σ should decrease monotonically with an increase in p_{SO2} because of the decrease in the enhancement factor. However, the permabsorption of SO_2 is in membrane-diffusion controlling mode at lower p_{SO2}; also, the rate of Reaction(2.5) is very slow. This leads to lowering of the σ value. Consequently, the permselectivity of SO_2 at a constant p_{CO2} reaches a maximum and then gently declines in the p_{SO2} range studied as shown in Fig.2.3. It is to be noted that further increase in p_{SO2} beyond the range investigated here would be expected, on theoretical grounds, to bring about a subsequent rise in σ owing to the contribution of Reaction(2.5) to the stripping of CO_2 together with the influence of the enhancement factor for SO_2.

CONCLUSIONS

The permabsorption method using polydimethylsiloxane hollow-fibre membrane was examined for the selective removal of SO_2 from gas streams containing N_2, CO_2 and SO_2. It was found that an excellent permselectivity can be obtained in the HF module by selecting an

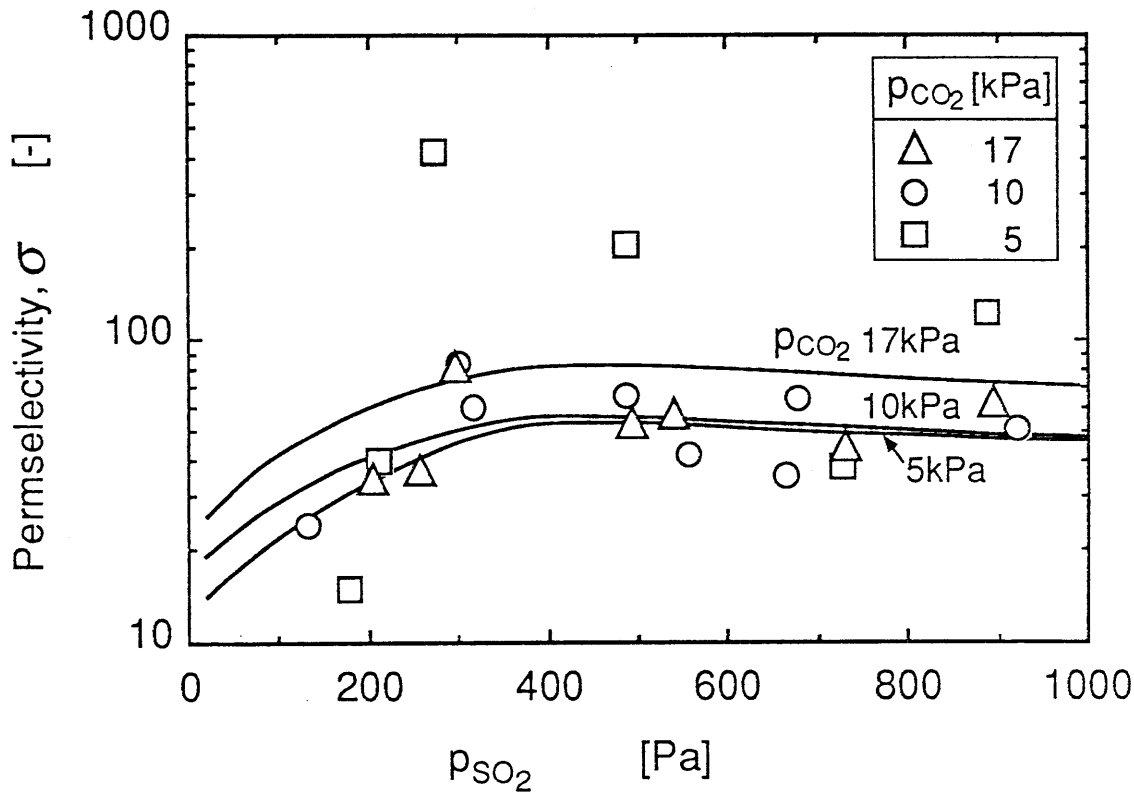

Fig.2.3 Effect of partial pressure of SO_2 on the permselectivity of SO_2 in preference to CO_2 for 0.01*M* Na_2SO_3.

absorbent liquid suitable for the gaseous species to be removed, and by controlling operating conditions.

NOMENCLATURE

C	concentration in liquid phase	[mol/cm^3]
$\overline{C}$	concentration in membrane phase	[mol/cm^3]
D	diffusion coefficient	[cm^2/s]
J	permeation flux	[mol/(cm^2•s)]
H	Henry's constant	[Pa•cm^3/mol]
K_G	overall mass-transfer coefficient, overall permeation coefficient,	[mol/(cm^2•s•Pa)]
k_r	reaction rate constant	[m^3/(mol•s)]
k_G	gas film mass-transfer coefficient	[mol/(cm^2•s•Pa)]
k_S	membrane-transfer coefficient	[mol/(cm^2•s•Pa)]
k_L	liquid film mass-transfer coefficient	[cm/s]
P	permeability of the membrane	[mol/(cm•s•Pa)]
p	partial pressure of CO_2 or SO_2	[Pa]
q	concentration ratio of C_B to C_{A2}	[-]
r	diffusivity ratio of B to A	[-]
u_L	liquid velocity per cross sectional area of HF	[cm/s]

Subscripts

0	aqueous feed
1	membrane surface contacting with gas (outer surface of HF)
2	membrane surface contacting with liquid (inner surface of HF)
A	CO_2 or SO_2
B	reactant in the liquid phase

Greeks

β	enhancement factor	[-]
δ	membrane thickness	[cm]
σ	permselectivity of SO_2 to CO_2	[-]

REFERENCES

1) Hikita, H. and Konishi, Y.: *Chem. Eng. J.*, 27, 167 (1983).

2) Hwang, S. T., and Kammermeyer, K.: *"Membranes in Separations"* (Wiley-Interscience, New York) (1975).

3) Nii, S., Takeuchi, H. and Takahashi, K.: *J. Chem. Eng. Japan*, 25, No.1, 67 (1992).

4) Onda, K., Sada, E. and Takeuchi, H.: *J. Chem. Eng. Japan*, 1, 62 (1968).

6) Takeuchi, H., Maeda Y. and Ito, K.: *Kagaku Kogaku Ronbunshu*, 1, No.3 257 (1975).

5) Stern, S. A., Onorato F. J. and Libove, C.: *AIChE J*, 23, 567 (1977).

Chapter 3.

REMOVAL OF CO_2 AND/OR SO_2 FROM FLUE GAS STREAM BY MEMBRANE ABSORPTION METHOD*

INTRODUCTION

The emission of sulfur dioxide and carbon dioxide resulting from the combustion of fossil fuels is regarded as a cause of deforestation by acid rain as well as global warming. In 1992 the United Nation Conference on Environment and Development, held in Rio de Janeiro, established the goal of keeping the emission of CO_2 and other greenhouse gases below the level at 1990 by the year 2000. To cope with the problem of great urgency, it is advisable to reduce the CO_2 as well as the SO_2 being emitted from large-scale stationary sources.

The removal of the CO_2, in principle, can be achieved in the same way as in gas sweetening processes. However, the amount of flue gas being emitted from a thermal power plant reaches a few million Nm^3 per hour, to treat such a large amount of gas in a conventional gas-liquid contactor, a large cross-sectional area of the column is needed to prevent flooding, resulting in too much absorbent liquid. This causes an increase in regenerator duty and operating costs. Of practical interest is the development of energy saving processes for acid gas removal from flue gases. The most effective way of providing a large surface area of contact between phases and improving the operability at low liquid flow rate is by using a hollow-fiber(HF) module with a high packing density.

Gas mixtures can be separated with porous and nonporous membranes. Qi and Cussler[12] have studied gas absorption using a hydrophobic microporous hollow-fiber membrane module, where the microporous membrane acted as a bound between the gas and liquid phases. They demonstrated the advantage of operability at high gas-flow rates without flooding because of the indirect contact between the gas and liquid streams.

---

* This chapter is appeared in Gas Separation and Purification, (1994).

For the purpose of bulk removal of CO_2 from flue gas, we have proposed permabsorption, using a non-porous polymeric HF module[10]. This method has all the advantages mentioned above; an absorption rate comparable to the performance of conventional packed columns can be achieved at a low liquid flow rate. Furthermore, selectivity for the separation of a gaseous species from a gas mixture can be enhanced by the membrane itself. In permabsorption using poly(di-methylsiloxane) HFs, however, there was a problem in significant mass-transfer resistance through the solid membrane. In the present study, the applicability of membrane absorption to the removal of SO_2 and CO_2 was examined with a view to developing an energy saving process for CO_2 and/or SO_2 removal from flue gases by using a hydrophobic microporous HF membrane.

3.1 EXPERIMENTAL

Microporous Teflon HF, supplied by Japan Gore Tex Co., Ltd., was used as a bound membrane, with an outside diameter of 0.18cm , an inside diameter of 0.1cm, a maximum pore diameter of 2μm and porosity of 0.5. The membrane module consisted of a glass tube and the HFs, which were fixed with epoxy resin at both ends of the tube. For multiple HF module, these HFs were arranged with a triangular pitch width of 0.3cm. Three modules consisting of the different number of HFs were used in this study; the specifications of the modules are given in **Table 3.1.**

A schematic drawing of the experimental setup is shown in **Figure 3.1.** A completed module was installed vertically. Absorbent liquid was supplied at the bottom of the module and flowed on the lumen side of the HF. Gaseous feed entered at the top of the module, and flowed on the shell side. At the end of the module, both the gas and liquid streams were kept at the atmospheric pressure. Concentration of the solute gas diluted with N_2 ranged from 0 to 20kPa for CO_2, and from 0 to 500Pa for SO_2. The concentrations of CO_2 and SO_2 in the influent and effluent gas streams were measured on each infrared gas analyzer.

As the absorbent liquid, aqueous solutions of the following chemicals of reagent grade were used: NaOH, K_2CO_3, Na_2SO_3, monoethanol amine(MEA), diethanol amine(DEA), diisopropanol amine(DIPA), N-methyldiethanol amine(MDEA), 2-amino-2-methyl-1-propanol(AMP).

To check a mass balance between the gas and liquid phases the basicity of the influent and effluent liquids was determined by titration .

3.2 RESULTS AND DISCUSSION

3.2.1 Mass-transfer characteristics of multiple HF module

In the present situation, a gas stream containing a solute as the permeant is in contact with an absorbent liquid flowing on the lumen side of the HF through the membrane pores. In the case of a hydrophobic membrane, the gas-liquid interface is just on the inner surface of the HF because the aqueous solution is not imbibed within the pores under the present conditions of laminar flow. Thus we can apply the film theory for the transfer of the gaseous solute across the membrane. The permeant in the gaseous stream diffuses through the gas boundary film outside the HF and the membrane pore and is absorbed at the gas-liquid interface inside the HF. Subsequently, the solute dissolved in the liquid phase diffuses through the liquid boundary film or reacts with a reactant in the film and liquid bulk. A plausible concentration profile of the solute in the steady state without chemical reaction is shown in **Fig.3.2.**

The flux for the permeant gas is expressed as

$$J=k_G(p-p_1)=k_M\varepsilon(p_1-p_2)=k_L(C_2-C) \quad (3.1)$$

where k_G and k_L are the mass-transfer coefficient for the gas and liquid boundary films, respectively, and k_M is the membrane transfer coefficient given by

$$k_M=D_G/\delta RT\tau \quad (3.2)$$

where D_G is the diffusion coefficient in the gas phase, δ the membrane thickness and τ the tortuosity. Assuming Henry's law, $p=HC$, the molar flux is represented in terms of the partial pressure as

$$J=K_G(p-p^*) \quad (3.3)$$

where K_G is the overall gas phase mass-transfer coefficient, being expressed as the sum of the three transfer resistances:

$$1/K_G=1/k_G+\delta RT\tau/D_G\varepsilon+H/k_L \quad (3.4)$$

provided that $A_{av}=A_o=A_i$.

For laminar liquid flow on the lumen side, value of k_L can be evaluated from the Leveque solution[9] as suggested by Yang and Cussler[16]:

$$k_Ld_i/D_A=1.62[(d_i/L)Re\cdot Sc]^{0.33} \quad (3.5)$$

Table 3.1 Specifications of membrane modules.

module	number of HF	effective area [cm^2]	effective HF length [cm]	I.D. of shell tube [cm]
A	14	134.2	30.5	1.7
B	5	35.7	22.7	1.25
C	1	6.7	21.3	0.8

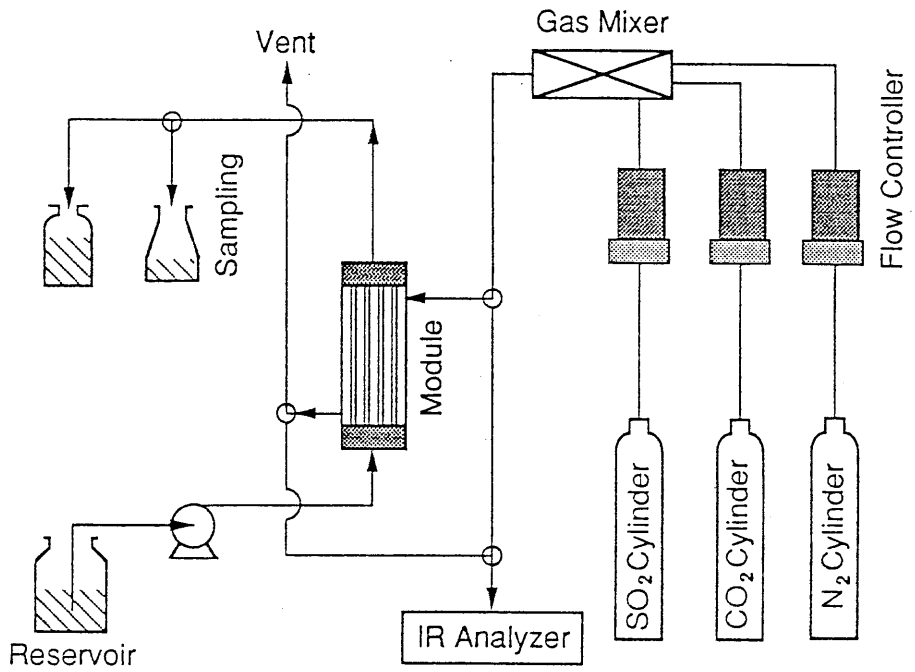

Fig.3.1 Schematic diagram of experimental apparatus.

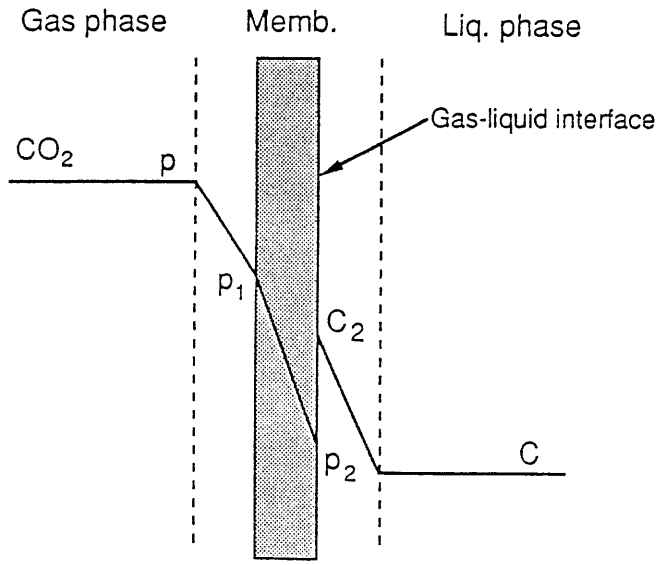

Fig.3.2 Plausible concentration profile in membrane absorption with hydrophobic porous membrane.

3.2.2 Determination of gas phase mass-transfer coefficient and mass-transfer coefficient in membrane

Values of k_G and k_M were determined by means of SO_2 absorption in aqueous alkaline solution for the three modules with different numbers of HFs and diameters of the shell tube. Gaseous feed containing 0.2%SO_2 (in nitrogen) was brought into contact with 1.2*M* NaOH as the absorbent. The SO_2 reacts instantaneously with hydroxide ion at the gas-liquid interface inside the HF; thus, the overall coefficient K_G is written as

$$1/K_G=1/k_G+1/k_M\varepsilon \qquad (3.6)$$

From the Eq.(1.4) in Chapter 1, k_G is presumed to correlate with $u_G^{1/3}$. Thus, K_G is supposed to increase proportinal to $u_G^{1/3}$.

Figure 3.3 shows the Wilson plot of $1/K_G$ vs. $1/u_G^{1/3}$. For each of the three modules A, B and C, the data points are located on a straight line with the same intercept of $1/k_M$; thus, the value of k_M is found to be 5.34×10^{-10} [mol/(cm^2•s•Pa)] for all three modules. It should be noted that this value is equal to that predicted from Eq.(2) with the membrane tortuosity $\tau=2$ and $D_G=0.108$cm^2/s. The value of k_G was obtained from the value of K_G by Eq. (3.6) using the value of k_M. **Figure 3.4** shows the dependence of k_G on the Reynolds number, suggesting that the values of k_G are correlated with $u_G^{1/3}$.

With an assumption that the Sherwood number, *Sh* varies with the $(d_e/L)^{0.25}$ according to Takeuchi *et al.* [14], the values of $Sh/(Re^{1/3}Sc^{1/3}(d_e/L)^{1/4})$ are plotted in **Fig.3.5** against $n(d_o/d_s)^2$, where the solid line represents

$$Sh=0.41(1/n)(d_s/d_o)^2(d_e/L)^{1/4}Re^{1/3}Sc^{1/3} \qquad (3.7)$$

For the shell-side mass-transfer in multiple HF modules, Prasad and Sirkar[11] have reported a correlation:

$$Sh=5.8[d_e\bullet(1-\phi)/L]Re^{0.6}Sc^{0.33} \qquad (3.8)$$

where ϕ is the packing fraction of the module. The comparison between Eq.(3.7) and Eq.(3.8) is shown in **Fig.3.6** in terms of the effects of outside diameter of the HF, the gas velocity and the module length for the shell tube 3cm in diameter, where the packing fraction was less than 0.2 and the diameter ratio, d_o/d_s, varied from 0.01 to 0.2. In the case of lower gas velocity and of smaller d_o, a reasonable agreement can be found between Eqs.(3.7) and (3.8). With increasing gas velocity and HF diameter, Eq.(3.7) gives smaller k_C than Eq.(3.8) by about 50%. In the two equations the different dependencies of *Sh* on the *Re* number and on

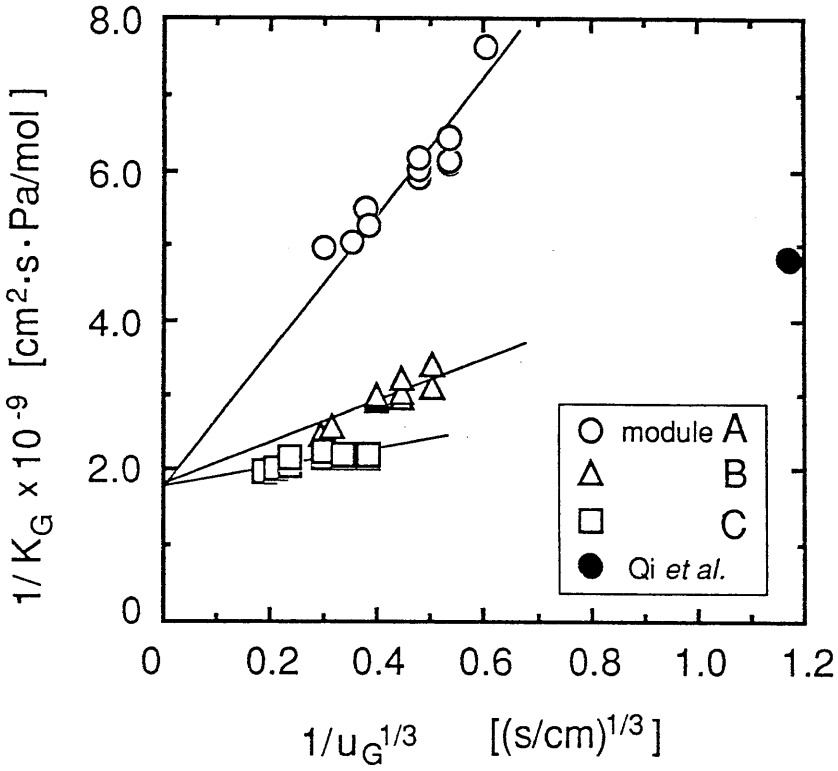

Fig.3.3 Wilson plot for single and multiple HF membrane modules. p_{SO_2}:200Pa, absorbent: 1.2*M* NaOH, temp.: 303K.

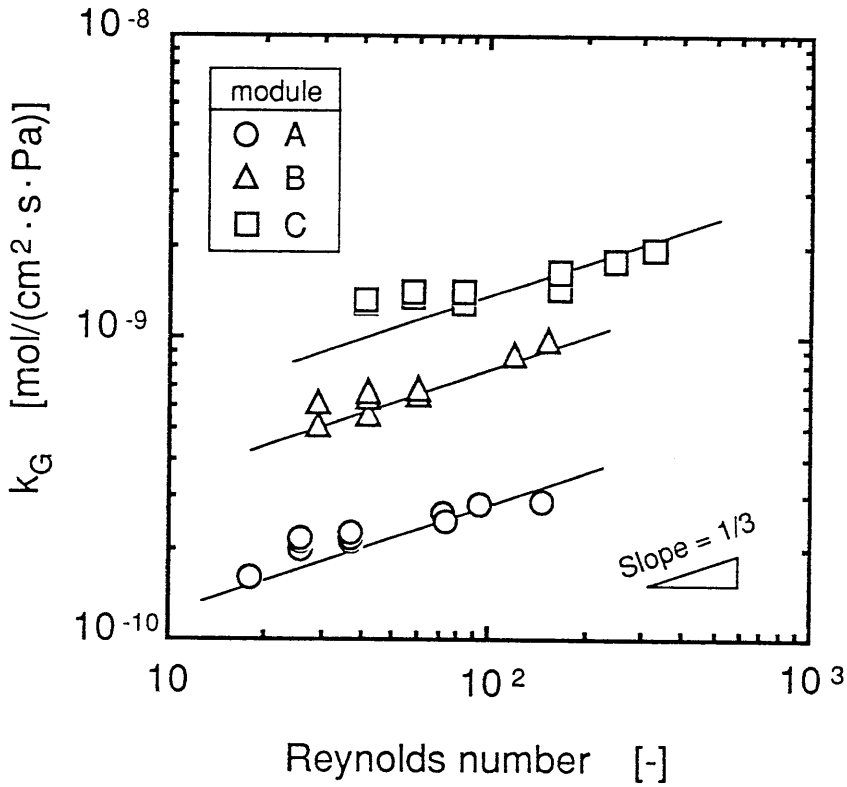

Fig.3.4 Effect of Reynolds number on gas-film mass-transfer coefficient. p_{SO_2}: 200Pa, absorbent: 1.2*M* NaOH, temp.: 303K.

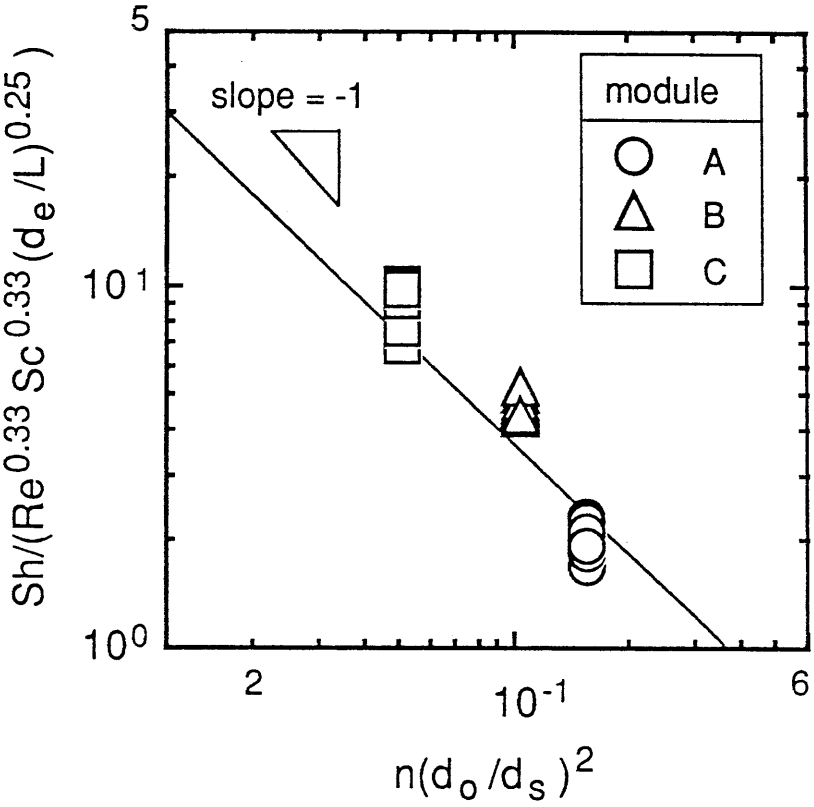

Fig.3.5 Correlation of k_G with $n(d_o/d_s)^2$.

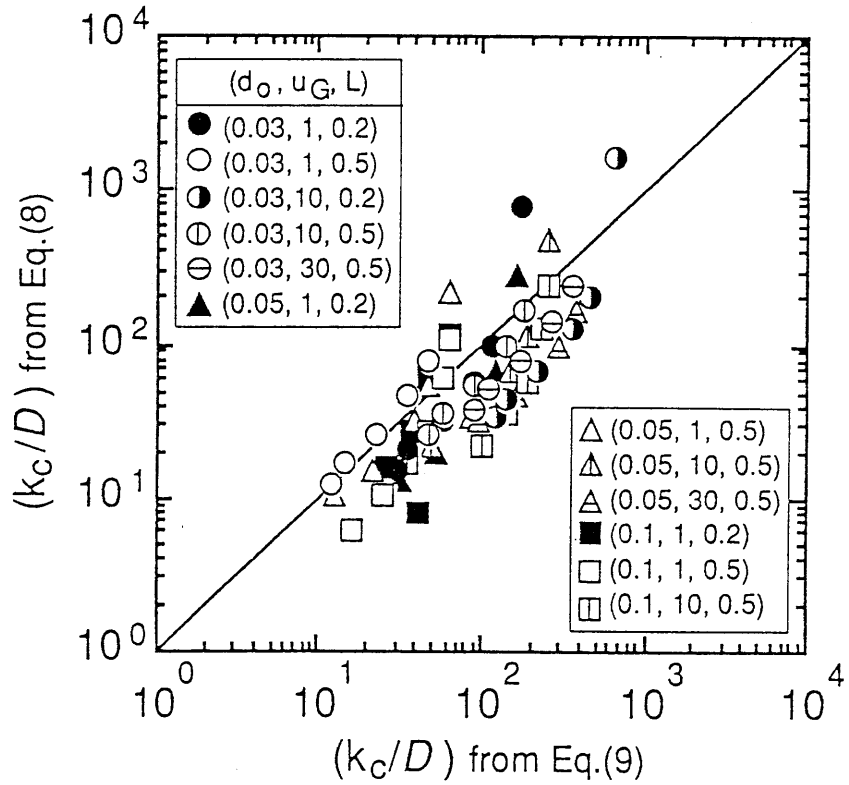

Fig.3.6 Comparison between Eq.(8) and Eq.(9).

the hydraulic diameter are probably arise from the difference between the conditions for which they were obtained: Eq.(3.7) was derived for the gas phase in the modules with d_O/d_S up to 0.024, whereas Eq.(3.8) for liquid phase in the d_O/d_S range of 0.12 to 0.25.

3.2.3 Membrane absorption using aqueous NaOH solution

Typical results for the absorption rates of CO_2 in aqueous solution with different NaOH concentrations are shown in **Fig.3.7** as a plot of the flux, J, versus p_{CO2}, together with the theoretical lines based on the gas absorption accompanied by the second-order chemical reaction between CO_2 and OH^-. Since the CO_2 concentration in the liquid bulk, C, is negligible in case of the presence of OH^- in the effluent liquid, the absorption rate is given by

$$J=\beta k_L C_2 \qquad (3.9)$$

where β is the enhancement factor which can be evaluated from an equation given in Chapter 1. Thus the CO_2 permeation flux through the membrane was calculated from Eq.(3.9) with the correlations of k_G and k_M, derived in the above section.

The observed values are in good agreement with the calculated ones. This suggests that the behavior of the membrane absorption can be interpreted by a classical model for chemical absorption with the individual mass-transfer coefficients from Eq.(3.2) and (3.7).

3.2.4 CO_2 removal using alkanolamine solutions

The absorption of acid gases has been carried out extensively with aqueous solutions of alkanolamines and carbonates as the absorbent[1,2,7]. For a deep removal of CO_2 from gas stream, alkanolamines have the advantage of a high absorption rate and capacity in contrast to carbonates. The CO_2 absorption by an amine solution is accompanied by a fast reaction leading to the formation of its amine carbamate. For primary and secondary amines, the following reaction occurs

$$CO_2+2RNH_2 \rightleftarrows RNHCOO^- + RNH_3^+ \qquad (3.10)$$

This reaction is followed by a slow reaction

$$RNHCOO^- + H_2O \rightleftarrows RNH_2 + HCO_3^- \qquad (3.11)$$

For the Reaction(3.10), values of the second-order rate constant and amine basicity are available elsewhere[5,13].

The CO_2 absorption rates obtained by aqueous solutions of DEA, DIPA, and MDEA are plotted in **Fig.3.8** against p_{CO_2}, where the solid lines represent the calculated values based on the second-order reaction(3.10). In the calculation, the liquid phase diffusivity of DEA was cited from the literature[5], those of DIPA and MDEA were estimated from the equation of Wilke and Chang[15]. The diffusivities of CO_2 in the amine solutions were also estimated from the equation[15]. For simplicity, Henry's low constants for CO_2 in the amine solutions used in the present study were approximated by the value for water. As Fig.3.8 shows, the absorption rates decrease in the sequence of amine basicity and therefore the reaction rates decrease in the same sequence.

Figure 3.9 shows the results for MEA solutions together with the respective calculated lines. The CO_2 flux for MEA is much higher than those for other amines because of the high reaction rate and basicity. The calculated values were obtained in the same second-order reaction regime as in the reaction of CO_2 with OH^-, then being in a reasonable agreement with the observed values. This indicates that the membrane absorption using a hydrophobic microporous HF module is not only efficient for the removal of acid gas from flue gas, but also suitable for investigating gas absorption accompanied by chemical reaction.

3.2.5 Effect of amine addition using K_2CO_3 solution

Although giving rise to an enhancement in the CO_2 absorption rate, aqueous alkanolamine solution has a drawback of a much higher energy requirement for regeneration of the CO_2 rich solution compared with carbonate solution. It is well-known that the addition of a small amount of amine to aqueous carbonate solution can not only enhance the rate of CO_2 absorption but also improve the regeneration efficiency. Such an enhancement in the presence of zwitterion can be interpreted by 'shuttle mechanism' [3,4]. For the absorption of CO_2 in an amine-mixed carbonate solution, the fast reacting amine may combine with CO_2 near the gas-liquid interface and release it again in the bulk of the liquid; the free amine diffuses back to the interface to react with CO_2.

The shuttle mechanism in CO_2 absorption was examined by adding various amines to potassium carbonate solution. **Figure 3.10** shows the effect of the addition of MEA, DEA, AMP and MDEA on the CO_2 absorption by aqueous K_2CO_3 solution, where the solid lines were

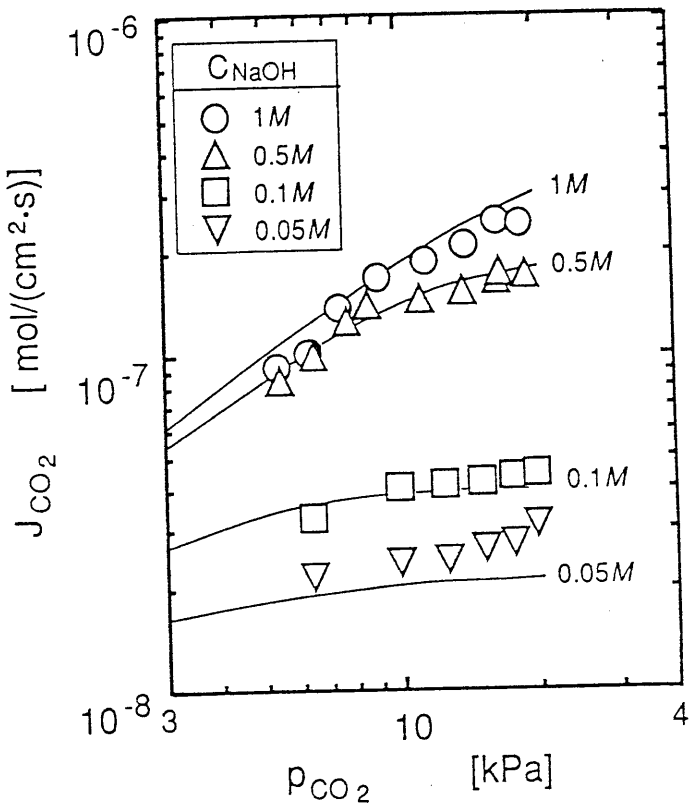

Fig.3.7 Effect of CO_2 partial pressure on absorption flux. Solid lines represent calculated values. u_G: 10cm/s, u_L: 2.0cm/s, temp.: 294K.

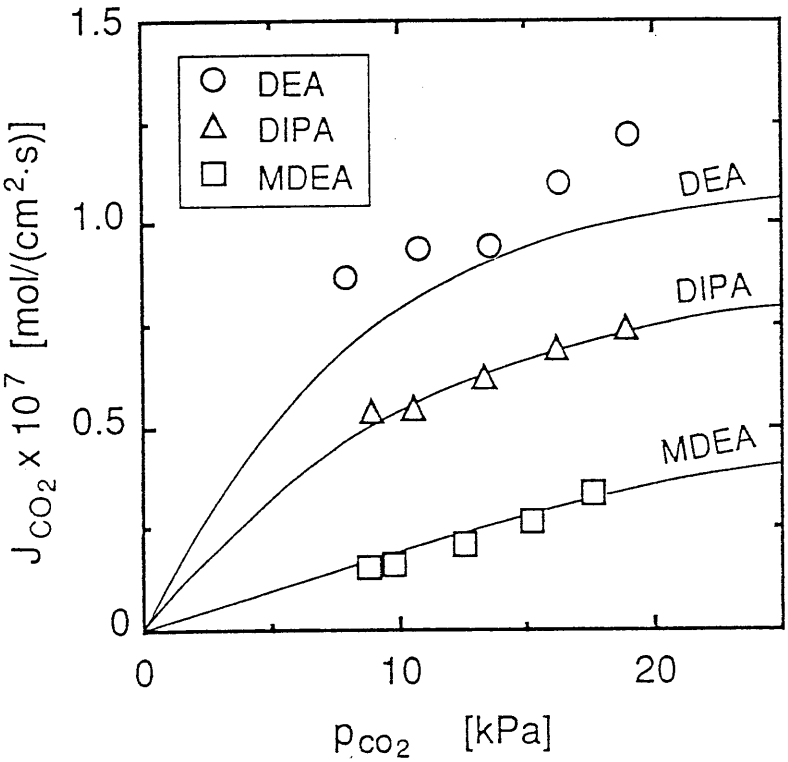

Fig.3.8 CO_2 membrane absorption in 10wt% alkanolamine aqueous solution. Solid lines represent calculated values based on second order reaction. u_G:10cm/s, u_L: 1.1cm/s, temp.: 294K, module: A.

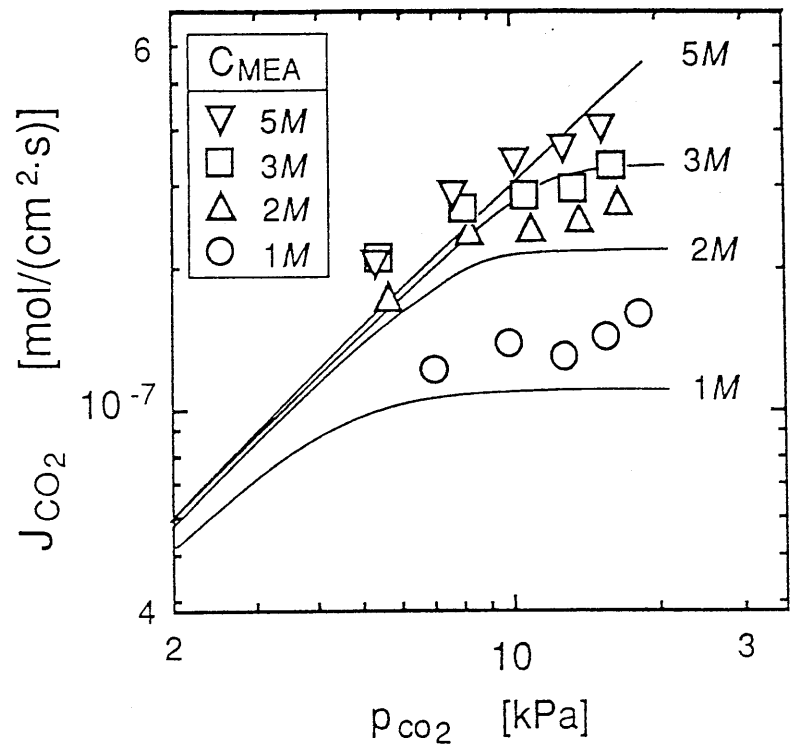

Fig.3.9 CO_2 membrane absorption in monoethanolamine aqueous solution. Solid lines represent calculated values. u_G: 10cm/s, u_L: 1.1cm/s, temp.: 293K, module: A.

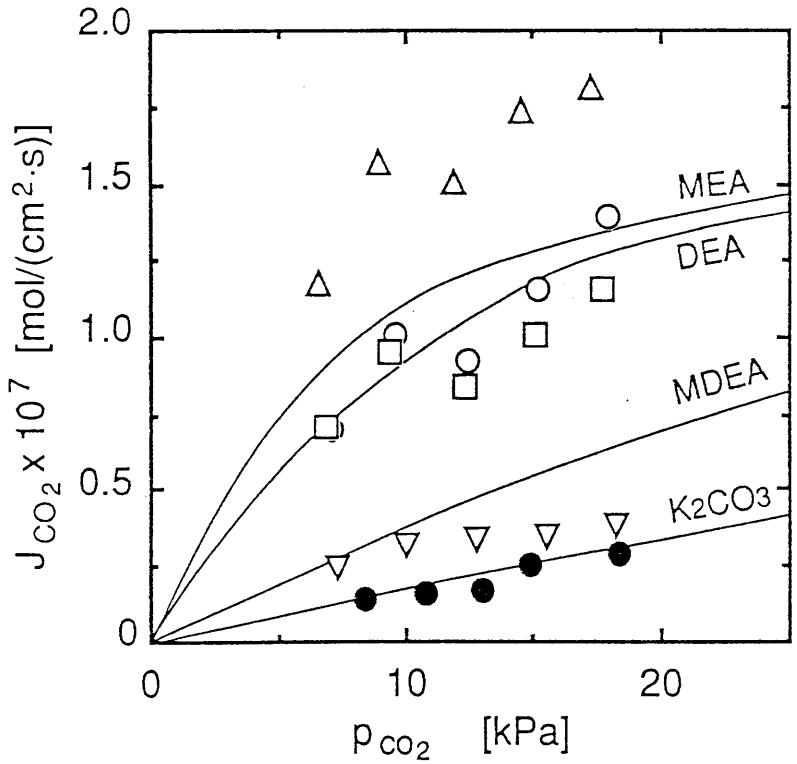

Fig.3.10 Effect of alkanolamine addition to potassium carbonate solution(2*M*) on CO_2 absorption fluxes. Solid lines represent calculated values. u_G: 10cm/s, u_L: 1.1cm/s, temp.: 294K, module: A.
(△: MEA, ○: DEA, □: AMP, ▽: MDEA, ●: without amine)

obtained as the sum of both calculated fluxes for $2M$ K_2CO_3 and for each $1M$ amine solution. For the mixed K_2CO_3-AMP solutions, the enhancement factor could not be calculated because of the complicated reaction mechanism involving CO_2 hydration which should be taken into consideration.

The flux values obtained in the presence of these amines are higher than those for not only K_2CO_3, but also for the corresponding amine solutions. In the case of the addition of DEA, a simple calculation could well predict the absorption rates, whereas the enhancement in the presence of MEA is more remarkable than the calculated value.

When taking the high stability of the MEA-carbamate into consideration, it is important to convert the carbamate to its free form. This is to be sure that the addition of amines promotes the CO_2 absorption rate in the carbonate solution; however, it is not clear whether the shuttle mechanism does take part in the reaction. If the residence time of the liquid in the contacting device is insufficient to hydrolyze the carbamate, then only Reaction(3.10) can contribute to the enhancement of the absorption rate.

Further examination was made of CO_2 absorption in $2M$ K_2CO_3 solution containing amine carbamate, prepared by bubbling pure CO_2 through aqueous solution of MEA and AMP. **Figures 3.11a** and **b** show the effects of the addition of the MEA- and AMP-carbamates on the CO_2 absorption, respectively, at two levels of the carbamation ratio*(C/A)*, defined as the molar ratio of carbamate to the total amine. For both amines of MEA and AMP, the presence of the carbamates causes a lowering of the absorption rate with an increase in the carbamation ratio. If the shuttle effect contributed to the present absorption system, the enhancement of the absorption rate should also be observed in the presence of the carbamate, since there is no significant difference in the salting-out effect on CO_2 solubilities in the amine and its carbamate solutions. From the above discussion, we can conclude that the residence time in the liquid is not long enough to diffuse the carbamate or its free amine through the liquid boundary film, owing to the small value of the liquid-phase mass-transfer coefficient in the laminar flow.

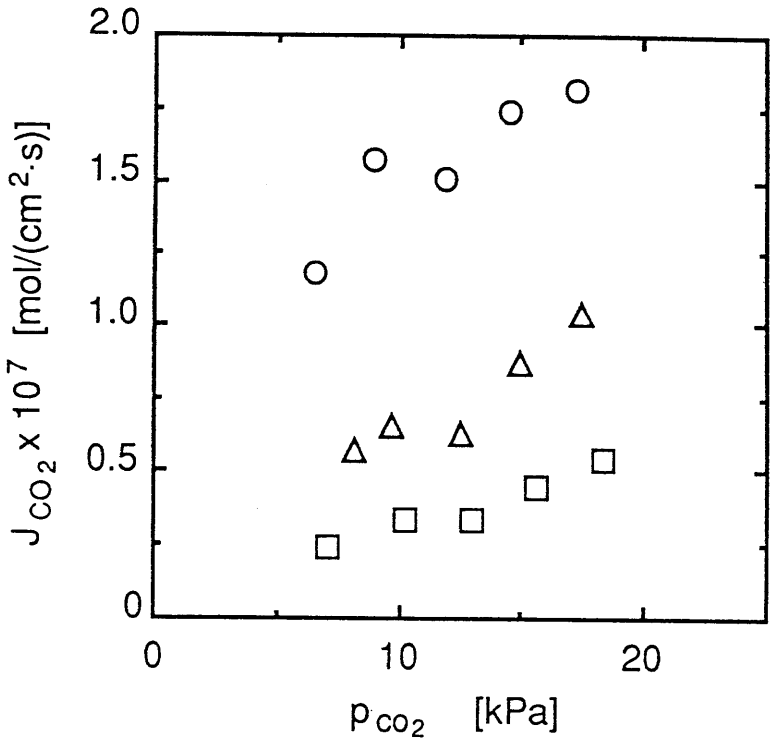

Fig.3.11a Effect of MEA carbamate addition to potassium carbonate solution on CO_2 fluxes. u_G: 10cm/s, u_L: 1.1cm/s, temp.: 293K, module: A. Molar ratio of carbamate to total amine; ○: null, △: 0.47, □: 0.65.

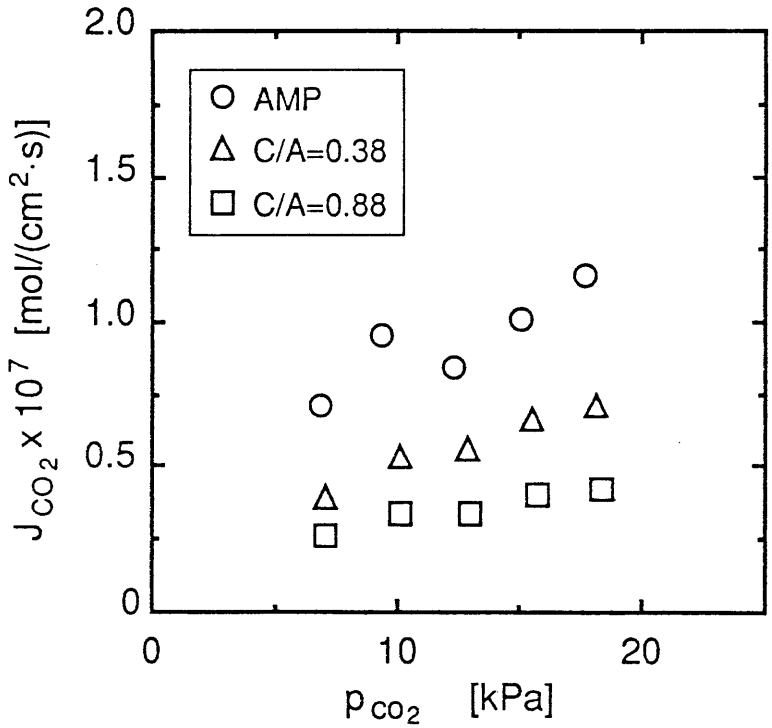

Fig.3.11b Effect of AMP carbamate addition to potassium carbonate solution on CO_2 fluxes. u_G: 10cm/s, u_L: 1.1cm/s, temp.: 293K, module: A.

3.2.6 Simultaneous membrane absorption of SO_2 and CO_2 using Na_2SO_3 solution

To examine the applicability of the present membrane absorber for flue gas desulfurization, the simultaneous membrane absorption of SO_2 and CO_2 from gaseous feed into aqueous Na_2SO_3 stream was conducted. In this system, the following reactions in the liquid film are considered to be significant.

$$SO_2 + SO_3^{2-} + H_2O \rightleftarrows 2HSO_3^- \quad (3.12)$$

$$CO_2 + SO_3^{2-} + H_2O \rightleftarrows HSO_3^- + HCO_3^- \quad (3.13)$$

$$SO_2 + HCO_3^- \rightleftarrows HSO_3^- + CO_2 \quad (3.14)$$

The values of the equilibrium constants K_1, K_2 and K_3 for Reactions(14), (15) and (16) are 2.76×10^5, 7.12 and 3.08×10^4, respectively[6] at infinite dilution at 298K. Reaction(3.12) proceeds much faster than the others: the value of k_r has five order of magnitude in $m^3/(mol \cdot s)$, being widely different from that for Reaction(3.13) (2.39×10^{-2} $m^3/(mol \cdot s)$)[6]. In the simultaneous membrane absorption of SO_2 and CO_2, the SO_2 dissolved in the liquid reacts instantaneously with a sulfite ion, and is depleted in the liquid boundary film, provided $C_B > C_{A2}$; a reaction plane is then formed.

Figure 3.12 shows the plots of the absorption rates of SO_2 and CO_2 against fluid velocity, u_L. The CO_2 flux decreases considerably with decreasing u_L, whereas the SO_2 flux is hardly influenced by u_L as long as sulfite ion in the liquid boundary film is not depleted. Thus, for flue gases containing a much lower SO_2 than CO_2 partial pressure, we can expect that the selective removal of SO_2 with respect to CO_2 is attained in the present membrane absorption under condition that the liquid flow rate is low, in other words the sulfite concentration near the gas-liquid interface is low.

Figure 3.13 shows the effect of the partial pressure of SO_2 on both the SO_2 and CO_2 fluxes for the simultaneous membrane absorption in 0.1*M* Na_2SO_3 at u_L of 1.2cm/s. The solid lines represent the calculated values from a theoretical equation based on a model with one reaction plane within the boundary film. In the calculation, we assumed that the dissolved SO_2 reacts instantaneously with SO_3^{2-} but CO_2 diffuses through the boundary film without reaction. Thus, the contribution of Reactions(3.13) and (3.14) are in the bulk, where the concentration of

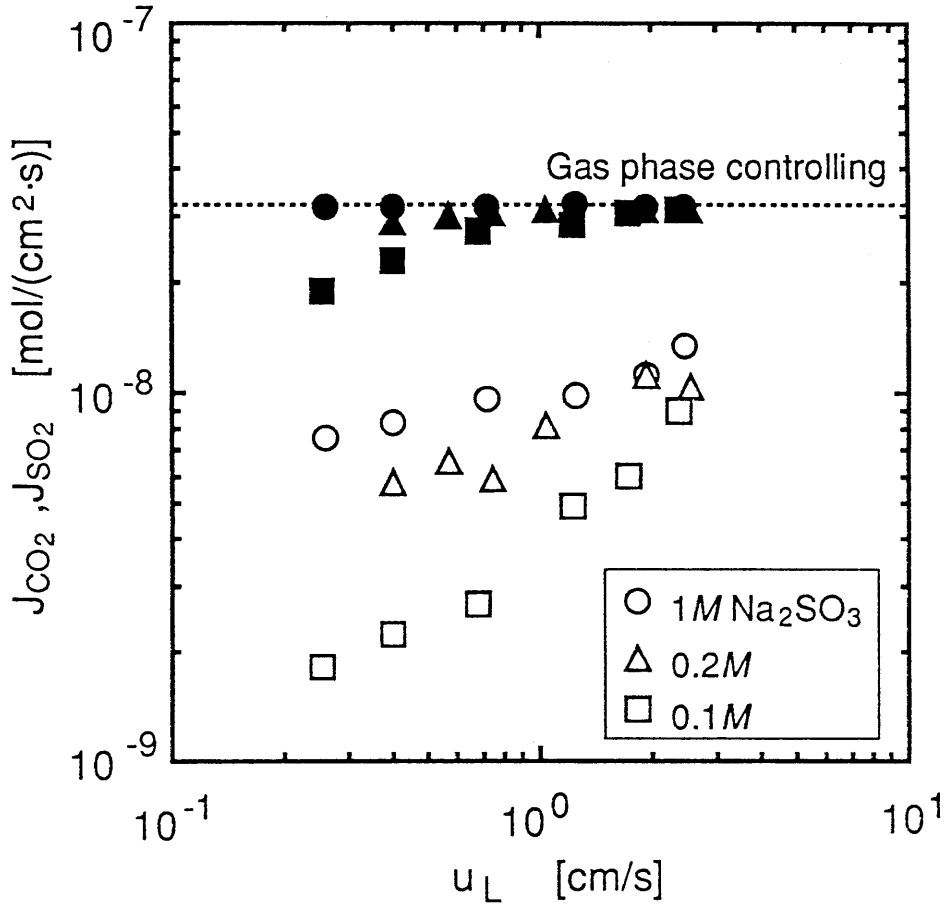

Fig.3.12 Dependence of CO_2 and SO_2 fluxes on liquid flow rate for simultaneous membrane absorption in aqueous Na_2SO_3 solutions. Feed gas: 9% CO_2, 0.5% SO_2, 90.5% N_2. Open key: CO_2, closed key: SO_2. u_G: 11.5cm/s, temp.: 298K, module: A.

sulfite ion was evaluated in succession through the module, because a remarkable concentration fall was observed in the effluent liquid. The enhancement factor for the SO_2 absorption was obtained from the following equation.

$$\beta = 1 + rq \tag{3.15}$$

where r is the diffusivity ratio D_B/D_A, being equal to 0.56 in the present situation and $q=C_B/C_{A2}$. The concentration of CO_2 in the liquid bulk was evaluated from the equilibrium constants K_1, K_2 and K_3. In each segment of the module, the local values of the CO_2 and SO_2 fluxes were calculated by an iterative method, and then the averaged fluxes over module were obtained by integrating local values from the inlet to outlet of the module. As can be seen in Fig.3.13, the absorption behavior of the two gases can also be reasonably interpreted by the model. This indicates that the absorption of CO_2 is suppressed in the presence of SO_2.

Here we define the selectivity of the SO_2 absorption to CO_2 as

$$\sigma_{SO_2/CO_2} = [J_{SO_2}/p_{SO_2}] / [J_{CO_2}/p_{CO_2}] \tag{3.16}$$

In **Fig.3.14** the σ values are plotted against the SO_2 partial pressure at p_{CO_2} of 5, 10, 15 and 20kPa, together with the calculated line from the model described above. The SO_2 selectivity varied with p_{SO_2} unusually, depending on p_{CO_2}. Such complicated behavior may be attributed to the presence of the membrane between the gas and liquid phases as well as the reaction kinetics of each gas in the liquid. Qualitatively, the σ behavior with the SO_2 partial pressure can be explained as follows. If there was no membrane between the gas and liquid phases and the gas-phase diffusional resistance was of no significance, then the σ value should increase with a decrease in p_{SO_2} because of the increase in the enhancement factor. At lower p_{SO_2}, however, the absorption of SO_2 is in the gas phase (including membrane phase) diffusion controlling; also the rate of Reaction(3.13) is very slow. On the other hand, as p_{SO_2} increases, the enhancement factor decreases; this leads to lowering of the σ value.

Apparently there are considerable deviations in the experimental points from each theoretical line; however, such deviation is responsible for the experimental errors in measuring the concentration of CO_2, that is in the absorption rate as shown in Fig.3.13. For example, if the error in each gas composition is within 10% for p_{SO_2}=300Pa and p_{CO_2}=20kPa, then the σ-value would vary in the range from 245 to 368.

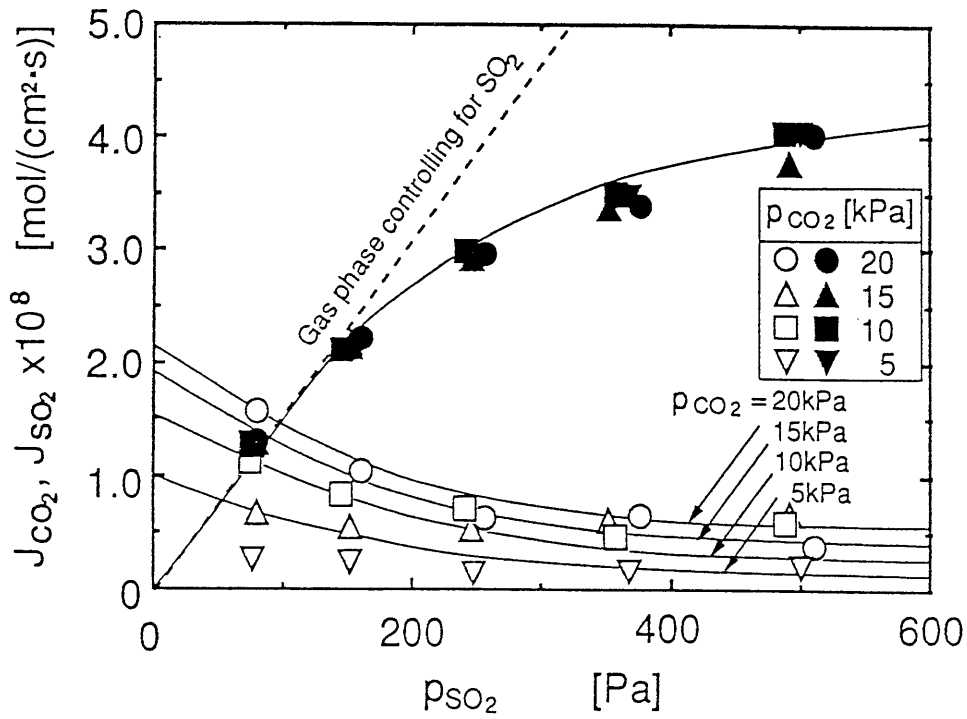

Fig.3.13 Effect of partial pressure of SO_2 on SO_2 and CO_2 fluxes in 0.1*M* Na_2SO_3 aqueous solution. Open and closed keys denote CO_2 and SO_2, respectively. Solid and dashed lines represent calculated values. u_G: 11cm/s, u_L: 1.2cm/s, temp.: 293K, module: A.

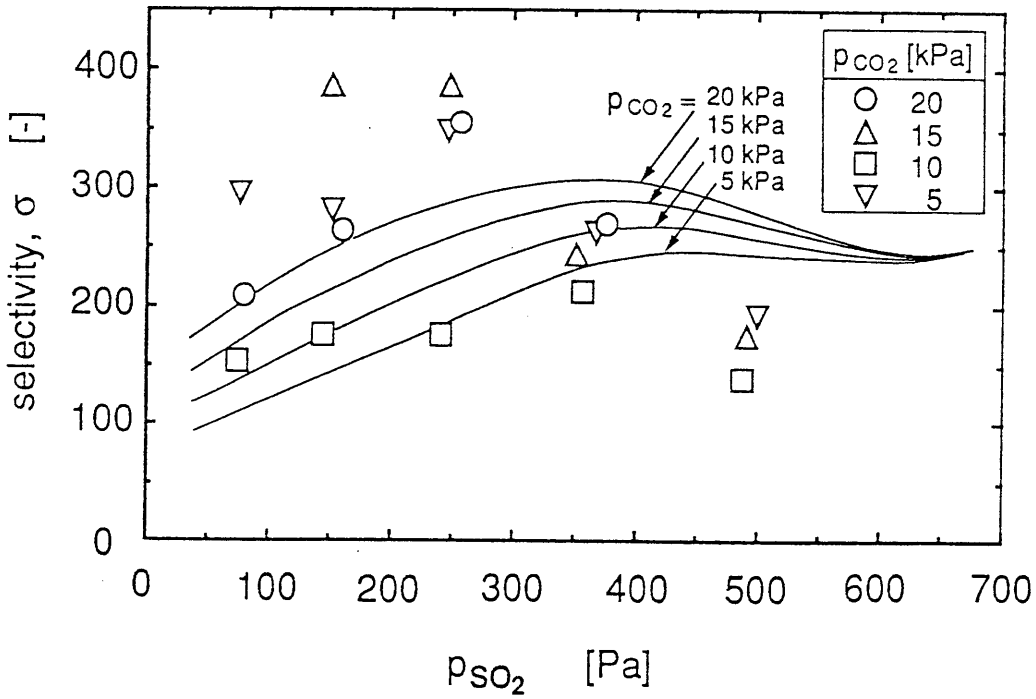

Fig.3.14 Effect of partial pressure of SO_2 and CO_2 on the selectivity of SO_2 in the simultaneous absorption in 0.1*M* Na_2SO_3 aqueous solution. Solid lines represent calculated values. u_G: 11cm/s, u_L: 1.2cm/s, temp.: 293K, module: A.

Consequently, the SO_2 selectivity goes through a maximum with increasing p_{SO_2} as shown in Fig.3.14. It is to be noted that a further increase in p_{SO_2} brings about the increase in σ from the contribution of Reaction(3.14), which increases free CO_2 concentration in the liquid film as well as the enhancement factor for SO_2.

CONCLUSIONS

Membrane absorption of CO_2 and/or SO_2 was examined using a hydrophobic microporous HF membrane module, with a view to developing an energy-saving process for acid gas removal from flue gases. The following results were obtained:

1) An empirical equation for the gas-phase mass-transfer coefficients on the shell side was derived in terms of the dimensionless parameters of *Sh*, *Re* and *Sc*, included geometrical factors of the HFs and the shell tube.

2) The rate of membrane absorption of CO_2 in aqueous solutions of alkalis and alkanolamines can be successfully described by a classical mass-transfer model incorporating gas diffusion through the pores subsequent to gas absorption accompanied by a chemical reaction.

3) For the simultaneous membrane absorption of SO_2 and CO_2 in Na_2SO_3 solution, a high selectivity of SO_2 to CO_2 was attained by selecting appropriate operating conditions, namely a low liquid flow rate and low solute concentration.

NOMENCLATURE

A_{av}	membrane area based on logarithmic mean diameter of HF	[cm^2]
A_i	membrane area based on inner diameter of HF	[cm^2]
A_o	membrane area based on outer diameter of HF	[cm^2]
C	concentration	[mol/cm^3]
d_e	hydraulic diameter	[cm]
d_i	inner diameter of HF	[cm]
d_o	outer diameter of HF	[cm]
d_s	inner diameter of the shell tube	[cm]

D	diffusivity	[cm^2/s]
H	Henry's constant	[$Pa \cdot cm^3/mol$]
J	membrane absorption flux	[$mol/(cm^2 \cdot s)$]
k_C	mass-transfer coefficient	[cm/s]
k_G	mass-transfer coefficient in the gas phase	[$mol/(cm^2 \cdot s \cdot Pa)$]
k_L	mass-transfer coefficient in the liquid phase	[cm/s]
k_M	mass-transfer coefficient in the membrane phase	[$mol/(cm^2 \cdot s \cdot Pa)$]
K_G	overall mass-transfer coefficient	[$mol/(cm^2 \cdot s \cdot Pa)$]
L	module length	[cm]
n	number of HF	[-]
p	partial pressure	[Pa]
p^*	equilibrium partial pressure	[Pa]
R	gas constant	[$cm^3 \cdot Pa/(K \cdot mol)$]
Re	Reynolds number, $d_e u_G/\nu$ *or* $d_i u_L/\nu$	
Sc	Schmidt number, ν/D	
Sh	Sherwood number, $k_C d_e/D$	
T	temperature	[K]
u	fluid velocity	[cm/s]
Subscripts		
G	gas	
L	liquid	
1	outer surface of HF	
2	gas-liquid interface	
Greeks		
β	enhancement factor	[-]
δ	membrane thickness	[cm]
ε	porosity	[-]
ϕ	packing fraction	[-]
ν	kinematic viscosity	[cm^2/s]

REFERENCES

1) Qi, Zhang and Cussler, E. L.: *J. Memb. Sci.* 23, 321 (1985).
2) Nii, S., Takeuchi, H. and Takahashi, K.: *J. Chem. Eng. Japan.* , 25, No.1, 67 (1992).
3) Leveque, M.A.: *Ann. Mines Rec. Mem. L'Explotas. Mines.* , 13, 210 (1928).
4) Yang, M. C and Cussler, E. L.: *AIChE J.* , 32, 1910 (1986).
5) Takeuchi, H., Takahashi, K. and Nakano, M.: *Ind. Eng. Chem Res..* 29, 1471 (1990).
6) Prasad, R. and Sirkar, K. K.: *AIChE J.* , 34, 177 (1988).
7) van Krevelen, D.W. and Hoftyzer, P.J.: *Rec. Trav. Chim.* , 67, 563 (1948).
8) Kohl, A. L. and Riesenfeld, F.C.: *"Gas Purification 4th ed. "* Houston TX: Gulf Publishing Co., pp. 29-109 (1985).
9) Astarita, G., Savage, D.W. and Bisio, A.: *"Gas Treating with Chemical Solvents. "* New York, John Wiley & Sons Inc., pp. 201-228 (1983).
10) Blauwhoff, P.M.M., Versteeg, G.F. and Van Swaaij, W.P.M.: *Chem. Eng. Sci.* 39, No.2, 207 (1984).
11) Danckwerts, P.V. and Sharma, M.M.: *The Chemical Engineer,* October, CE244-CE280 (1966).
12) Savage, D.W. *"Recent Developments in Separation Science Vol. 7."* Boca Raton, Florida: CRC Press, pp. 73-102 (1982).
13) Wilke, C.R. and Chang, P.: *AIChEJ.*, 1, 264 (1955).
14) Dankwerts, P.V.: *Chem. Eng. Sci.* , 34, 443 (1979).
15) Caplow, M.: *J. Am. Chem. Soc.* , 90, 6975-6803 (1968).
16) Hikita, H. and Konishi, Y.: *Chem. Eng. J.* , 27, 167 (1983).

Chapter 4.

PERVAPORATION WITH SWEEPING GAS IN POLYMERIC HOLLOW FIBER MEMBRANE MODULE - SEPARATION OF ALCOHOLS FROM AQUEOUS SOLUTION*

INTRODUCTION

Pervaporation processes have been an area of deserving special attention for the separation of organic liquid and water from a liquid mixture, because of the advantages of higher separation factor, lower operating cost and scalability in use. It is successfully applied to dehydrating aqueous alcohol solutions of relatively low water content near their azeotrope. This application has been commercially developed with the capacities ranging from 2,000 to 150,000 liter per day[3].

In alcohol fermentation process, pervaporation is rather favorable for continuous alcohol recovery from fermentation broth. This method is useful for enhancing the productivity from a reduction of product inhibition, and lowering the separation costs[2]. For this application, there have been numerous efforts for the development of alcohol selective membranes using silicone-based polymers such as polydimethylsiloxane (PDMS)[1] and polytrimethylsilylpropyne (PTMSP)[4]. In general, these materials are rubbery in nature; thus, previous studies are mainly made on a flat-sheet membrane with supporting solid matrix.

In conventional pervaporation, partial pressure difference of permeant between both sides of the membrane is provided by reducing the total pressure on the downstream side, a driving force for permeation through the membrane being then established. Thus the system needs a vacuuming system and solid matrix supporting membrane as well. Alternatively, permeant partial pressure on the permeate side can be reduced by sweeping the vapor with inert gas stream. This method can realize a pervaporation operation in simple manner without vacuuming system, in which a rubbery hollow fiber(HF) membrane module is applied. HF

---

* This article was presented at The 3rd Korea -Japan Symp. on Sep. Tech., Seoul, pp. 451-455 (1993).

modules have advantages of providing a large surface area per unit volume and of operability at low fluid velocity. Thus, such a gas sweeping pervaporation mode has the possibility of large scale separation processes. This view will be demonstrated in the present paper with the object of confirming its applicability to the separation of alcohols from aqueous solution using PDMS-HF membrane module.

4.1 THEORETICAL BASIS FOR EXPERIMENTAL MEASUREMENTS

In pervaporation using HF module, liquid and sweeping gas flow on the shell and lumen side, respectively. Assuming that a permeant diffusing through the membrane vaporizes on the permeate side of the module, one can express the permeant flux at a steady state on the basis of the solution-diffusion model as

$$J = k_M(\bar{C}_1 - \bar{C}_2) = k_G(p_2 - p_0) \quad (4.1)$$

where $\bar{C}$ is the alcohol concentration in the membrane phase, given as $\bar{C}=mC$; the subscript *1* denotes the liquid-membrane interface, *2* the gas-membrane interface, and *0* the bulk of gas phase. The partial pressure on the permeate side of the module, p_2 , can be evaluated from the vapor-liquid equilibrium(VLE) assuming the liquid concentration in equilibrium with $\bar{C}_2$. When the VLE of dilute alcohol solution is expressed as $p=HC$, the following equation is obtained.

$$J = (k_M m_2/H_2)(m_1 H_2 C_1/m_2 - p_2) = k_G(p_2 - p_0) = K(p_1^* - p_0) \quad (4.2)$$

where the overall mass-transfer coefficient, K, based on the gas phase and the hypothetical pressure of alcohol in the aqueous feed, p^*, are given as

$$1/K = H_2/(m_2 k_M) + 1/k_G \quad (4.3)$$

$$p_1^* = m_1 H_2 C_1/m_2 \quad (4.4)$$

The membrane transfer coefficient, k_M, is defined as $k_M = D_M/\delta$, where the alcohol diffusivity in membrane phase, D_M, can be determined as will be mentioned later. The gas film mass-transfer coefficient, k_G, for laminar flow inside a solid tube can be evaluated from the Leveque solution[5].

Since there is no available data for the VLE at a reduced pressure, partial pressure of alcohol on the permeate side was evaluated in terms of the activity coefficient from the Wilson equation with the saturated vapor pressure from the Antoine equation.

4.2 EXPERIMENTAL

Two PDMS membranes of flat-sheet and HF used in this study were supplied by Nagayanagi Ind. Co. Ltd.(Japan). The flat-sheet membranes were of 90 and 500μm in thickness; the thicker membrane was used only for diffusion cell experiment. The HF was of 0.31cm in outside diameter and 0.28cm in inside diameter. Two membrane modules consisting of different number of HFs were used in pervaporation experiments and the specifications are given in **Table 4.1**: Module A was for the operation at high gas velocity, Module B being for low gas velocity.

Schematic diagram of the experimental apparatus is shown in **Fig.4.1**. Sweeping gas(pure N_2) was introduced on the lumen side of HF at the top of the module, and an aqueous solution of ethanol or isopropanol as the feed was supplied on the shell side at the bottom of the module. After having reached a steady state, the permeant vapor in the effluent gaseous stream was collected in a cold trap submerged in liquid nitrogen at a time interval. The permeation rate of alcohols across the membrane was determined from the measurements of amount of the permeate and of the composition by Karl Fischer titration.

Solubility of alcohols in the membrane was determined by an immersion method at 303K, whereby the concentration change in the solution was obtained from the refractive index in a flow injection mode. Diffusivity of alcohols in the membrane was determined by a diaphragm cell method using flat-sheet membranes of different thickness.

4.3 RESULTS AND DISCUSSION

4.3.1 Membrane properties

Figure 4.2 shows the concentrations of ethanol and isopropanol in the membrane phase in equilibrium with the respective liquid phases, indicating that isopropanol is as soluble as ethanol to the PDMS membrane by a factor of 2. The distribution ratio of the alcohols, m, was defined as the tangent$(\bar{C}/C)$ at an arbitrary liquid concentration. The effect of permeant concentration on the alcohol diffusivity through the membrane at 304K is shown in **Fig.4.3**. This plot gives the concentration dependency of membrane-transfer coefficient.

For the pervaporation in the gas sweeping mode, typical results are shown in **Fig.4.4** as a plot of the composition of the permeate against that of the aqueous feed, which gives an extent of alcohol separation. The

Table 4.1 Specification of membrane module.

Module	Number of HF [-]	HF length [cm]	Shell tube I.D. [cm]	Memb. Area [cm^2]
A	1	33.6	0.9	32.7
B	5	31.5	1.7	153.4

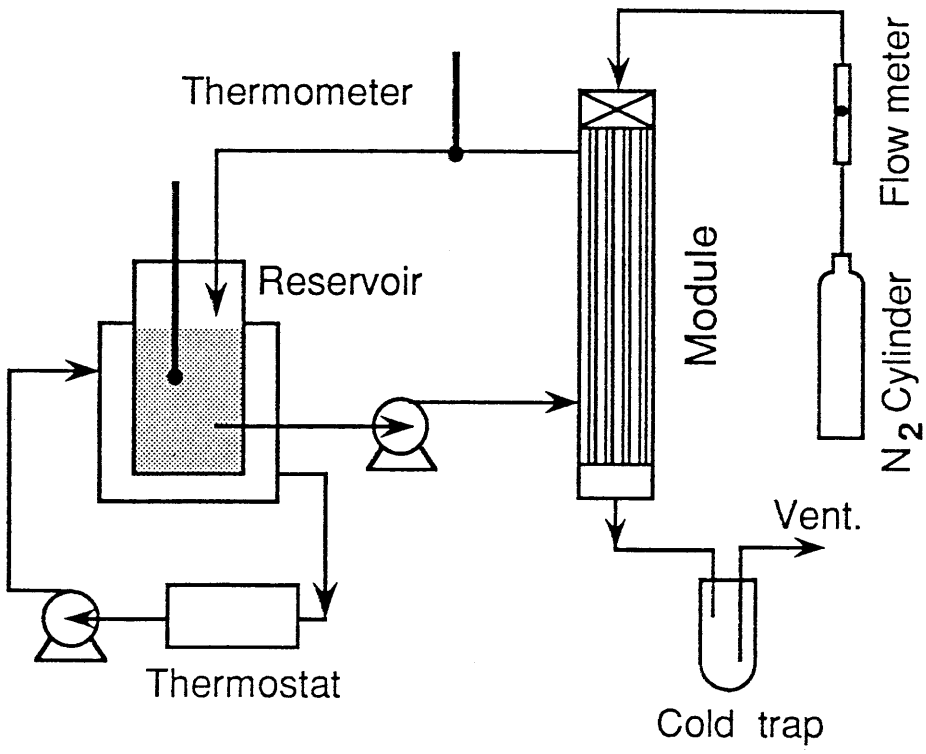

Fig.4.1 Schematic diagram of experimental apparatus.

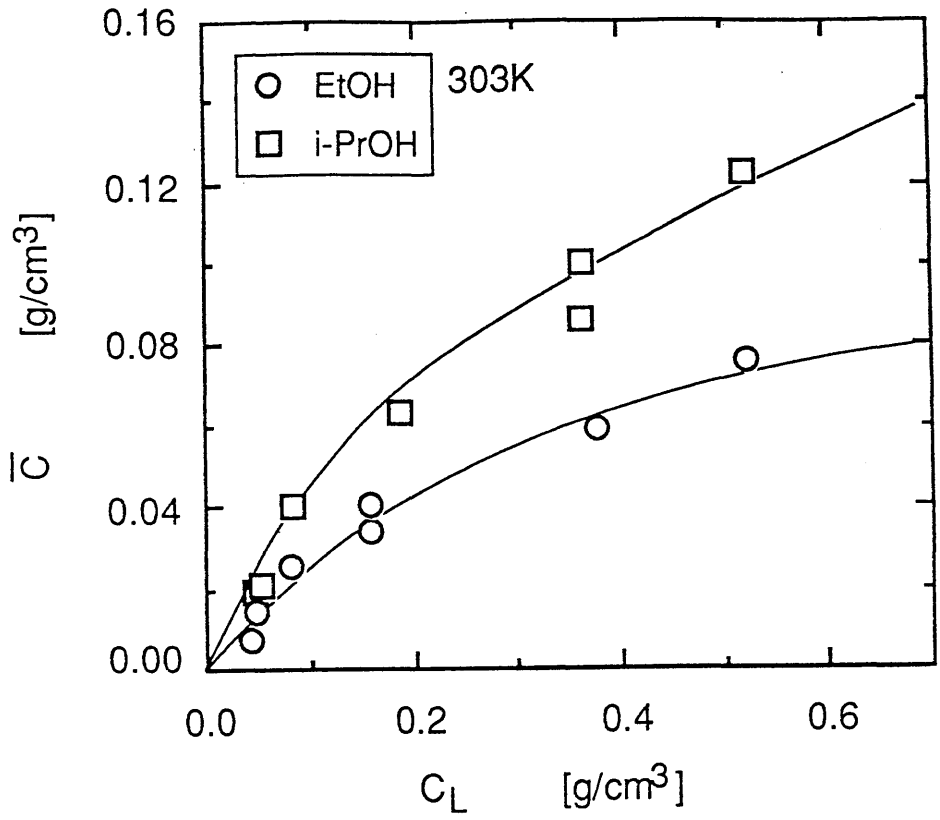

Fig.4.2 Solubilities of ethanol and isopropanol in PDMS membrane.

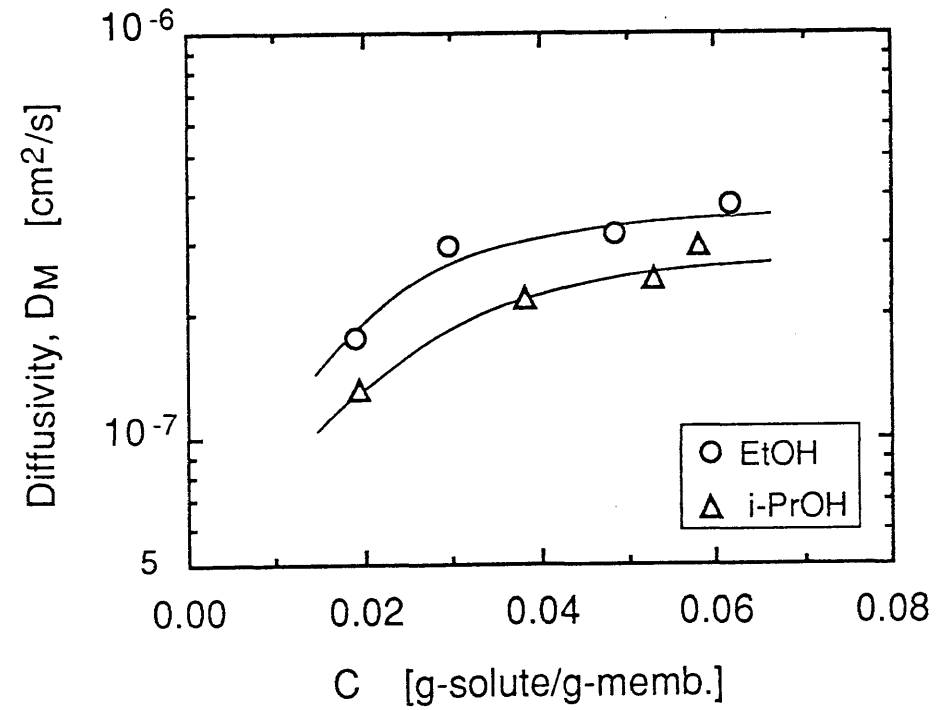

Fig.4.3 Plot of D_m vs. C for ethanol and isopropanol in PDMS membrane at 304K.

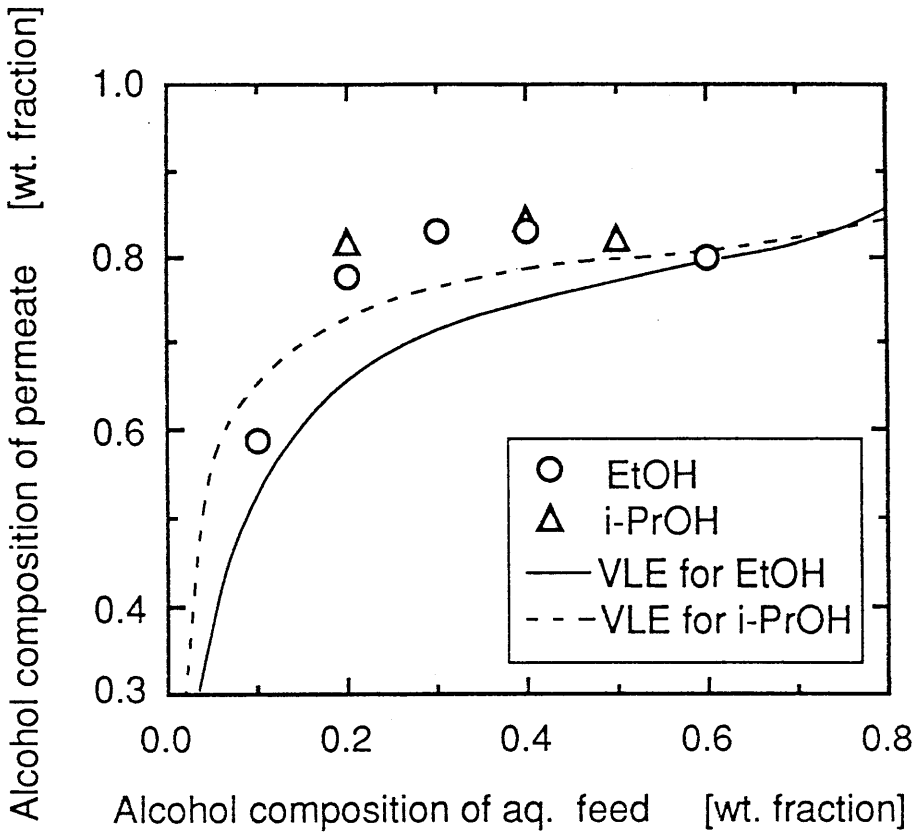

Fig.4.4 Plot of permeate composition vs. feed composition for pervaporation of aqueous solution of ethanol and isopropanol.

solid and dashed lines represent the VLE for the binary systems of ethanol/water and isopropanol/water, respectively. For the feed concentration below 60wt%, it is found that the permeate compositions are higher than the VLE compositions; the present membrane is preferential to ethanol and isopropanol. Thus, the further pervaporation experiments were carried out for the aqueous feed up to 60wt% alcohol.

4.3.2 Effect of gas flow rate on flux

The effect of gas flow rate on the ethanol and isopropanol fluxes is shown in **Figs.4.5a** and **4.5b**, respectively, as a plot of J vs.u_G for various alcohol concentrations, wherein the solid lines represent the calculated values. The calculation was made as follows. The module was supposed to divided into ten parts, within the each part, the value of alcohol flux was assumed. Then the value of $\overline{C}_2$. was obtained from Eq. (4.1) using the k_M value. From the plot of $\overline{C}$ vs. C_L, (Fig.4.2), C_2 was derived. While, the amount of alcohol permeated in the part of the module was calculated from the assumed flux, then the value of p_0 was obtained. The calculated flux was given from Eq.(4.1) using the k_G value. The calculated and observed fluxes were compared and the flux was reassumed. The calculation was repeated until the difference of the both fluxes were within allowable error. The calculated flux in Fig.4.5 were the averaged flux over module. **Figure 4.6** represents a plot of typical calculation result of the local values of the ethanol flux against the partial pressure through the module. In the plot, a remarkable decrease in the local alcohol flux is observed with an increase of x/L, the distance in the direction of the sweeping gas flow from the top of the module. Thus, the flux value shown in Fig.4.5 is an average flux over module, obtained by integrating the local values from the inlet to outlet of the module.

In Figs.4.5a and 4.5b the observed flux values are in a reasonable agreement with those from the model prediction. The permeation of alcohols is controlled by the diffusion through the membrane at higher gas velocity; it was found that the ratio of gas-film resistance to the total resistance is within 0.3%(e.g. $1/k_G=6.5\times10^4$, $1/K=2.1\times10^6$ at $u_G=108cm/s$ for 60wt% ethanol.) At lower gas velocity, however, the alcohol fluxes decrease remarkably with increasing the concentration of alcohol in the

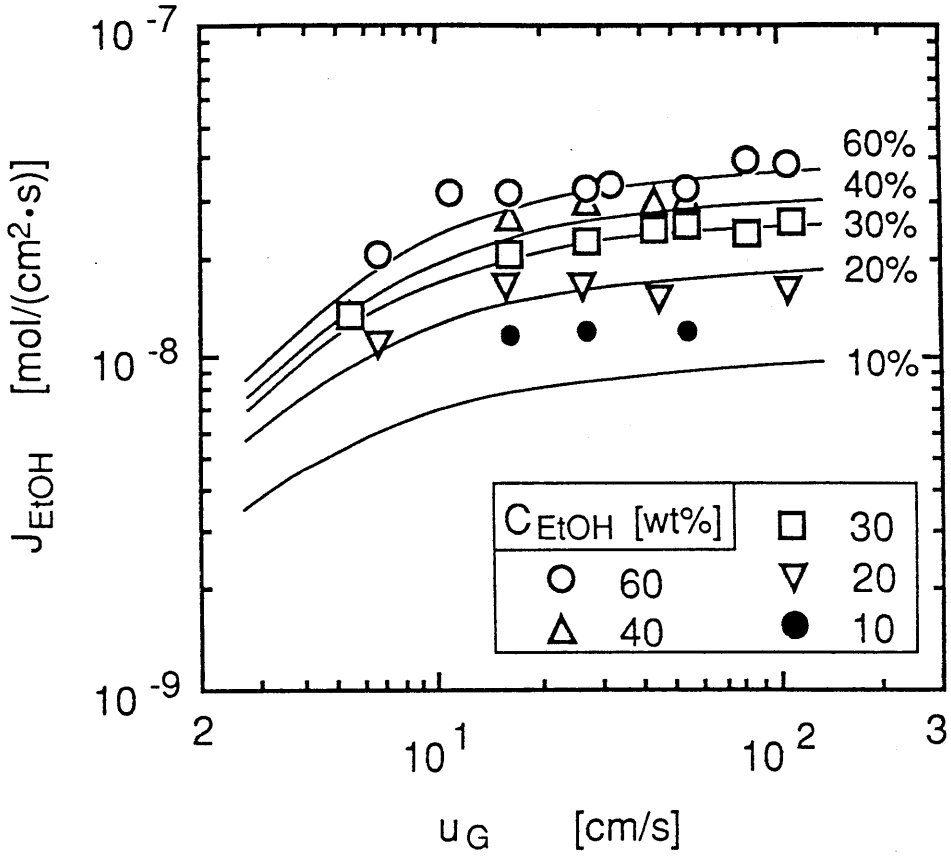

Fig.4.5a Effects of ethanol concentration and gas velocity on ethanol flux. Solid line represent the calculated value.

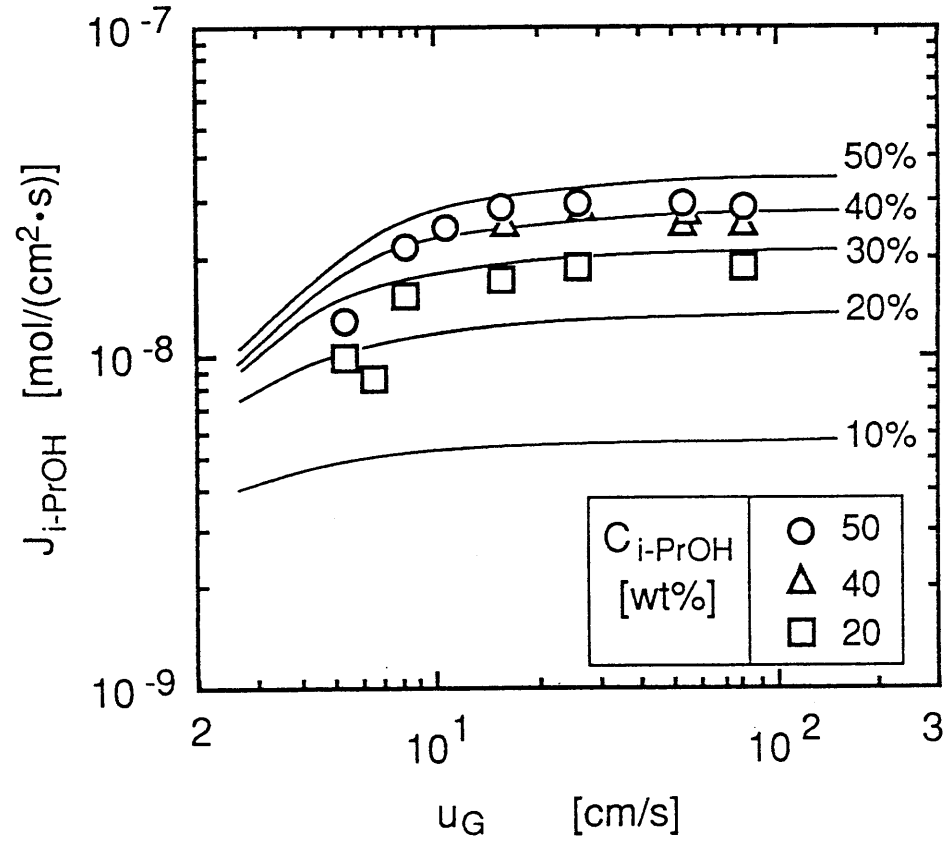

Fig.4.5b Effects of isopropanol concentration and gas velocity on isopropanol flux. Solid line represent the calculated value.

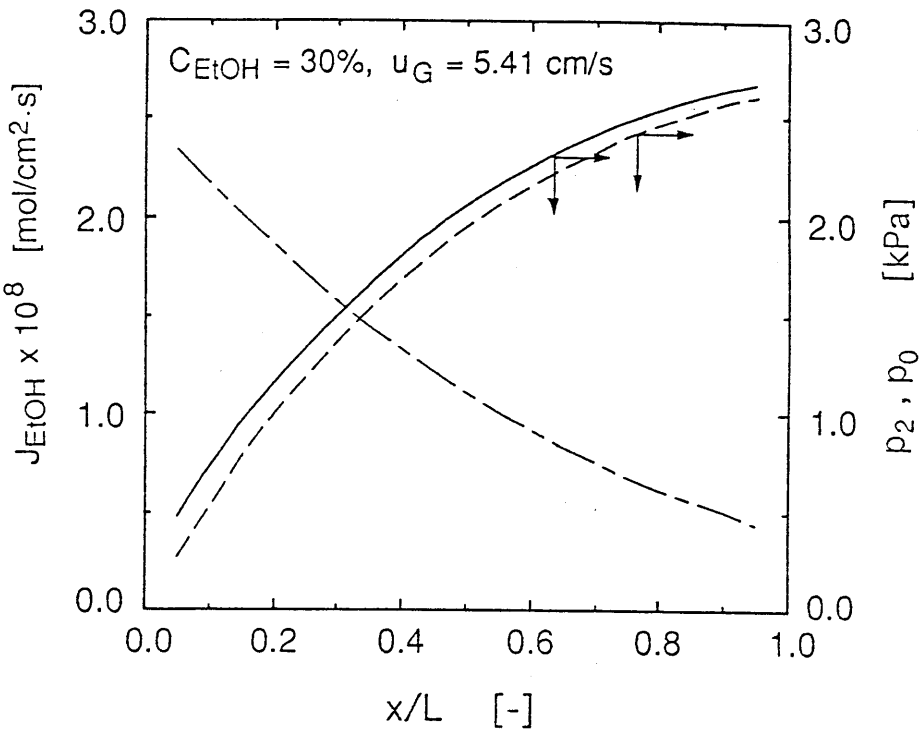

Fig.4.6 Variation of both local values of ethanol flux and partial pressure of ethanol through module. Solid, dashed and dash-dotted lines represent p_2, p_0 and J_{EtOH}, respectively.

feed. This can be attributed to the condensation of the water vapor permeated in the effluent gas.

Figure 4.7a and **b** show the effect of gas flow rate on the water flux, J_W, during the pervaporation from aqueous ethanol and isopropanol solution, respectively. The figures implys that the J_W values show the similar dependence of the gas flow rate for the aqueous feeds with the different alcohol concentrations. This result suggests that the water permeation occurred independent of the alcohol permeation. The reason for the dependence was not clear. Although the calculation of J_W was made on the basis of the permeation model presented in the section 4.1, the values were not in accordance with the observed values. The model gave much higher values than observed values and the calculated values were varied with the alcohol concentration in feed solutions.

4.3.3 Effect of gas flow rate on alcohol separation factor

Alcohol separataion factor is here defined by

$$\alpha = (X_{AR}/X_{WR})/(X_{AF}/X_{WF}) \tag{4.5}$$

where suffix F denotes the feed side, R the recovery side, A the alcohol and W the water. **Figures 4.8a and 4.8b** show the effect of gas flow rate on the separation factor of alcohols to water during the pervaporation. The alcohol selectivity increases with decrease in the gas flow rate as well as in the alcohol concentration in the feed solution. This was caused from the increase in the partial pressure of the alcohol at the gas-membrane interface, p_2.

4.3.4 Effect of downstream pressure on alcohol flux in vacuuming PV

Further examination was made on the applicability of the present model to conventional pervaporation operation in downstream vacuum mode. The effect of permeate side pressure on the ethanol flux through a PDMS flat membrane is shown in **Fig.4.9** with the calculated lines. The membane used here was the SRX membrane which was prepared by casting a silicone dispersed solution manufactured by Toray Dow Corning Silicone Co. Ltd. The model could predict well the experimental data obtained at the pressures ranged from 0.013 to 2.7kPa. This indicates that the performance of the pervaporation process can be evaluated from the only flux datum observed at a given downstream pressure.

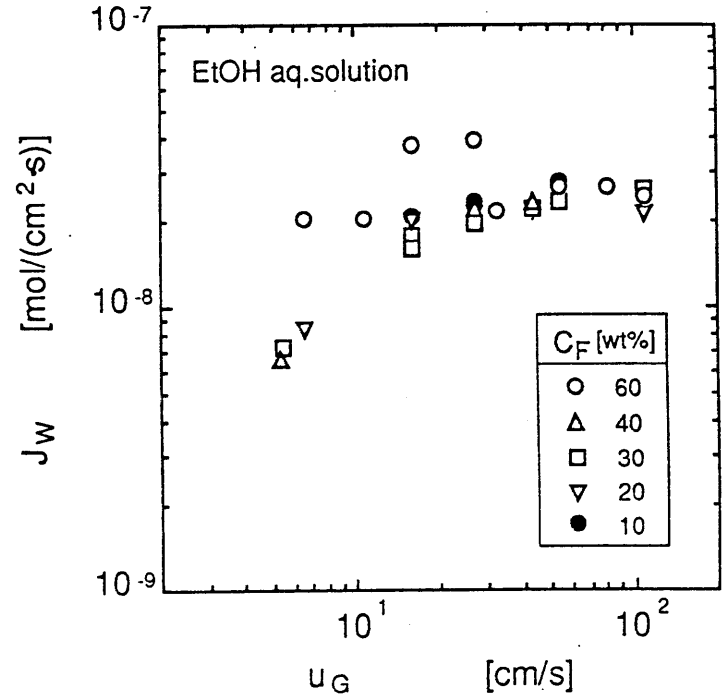

Fig.4.7a Effect of gas velocity on water flux during pervaporation of ethanol from aqueous solutions.

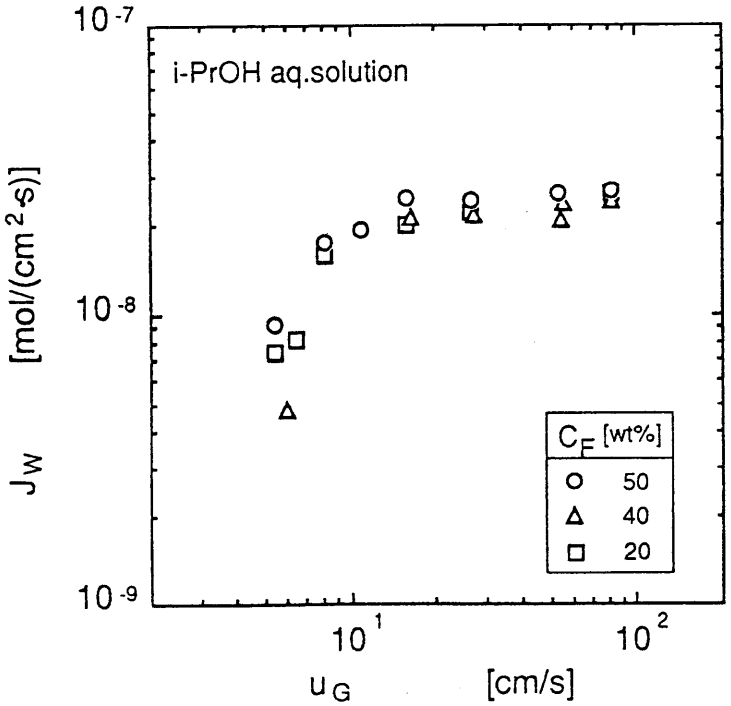

Fig.4.7b Effect of gas velocity on water flux during pervaporation of isopropanol from aqueous solutions.

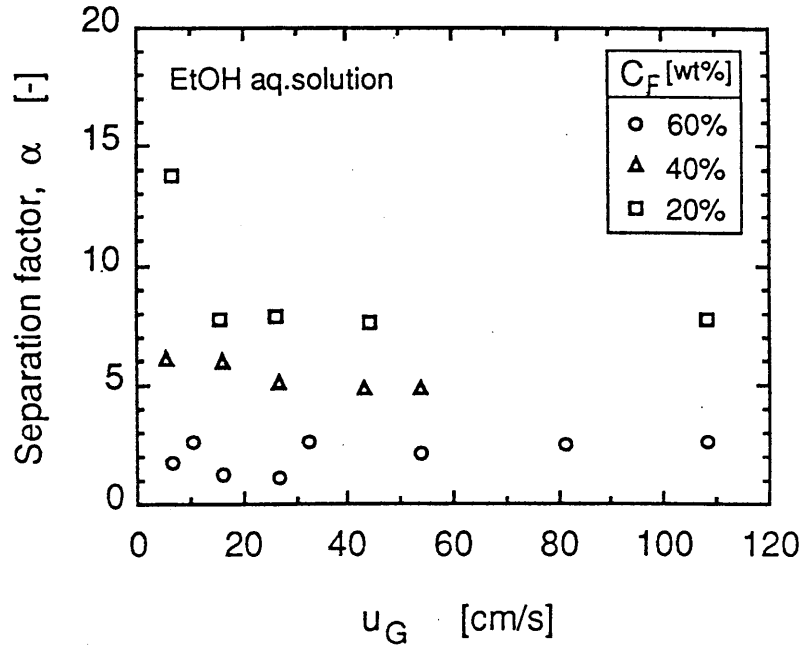

Fig.4.8a Effect of gas velocity on ethanol separation factor to water.

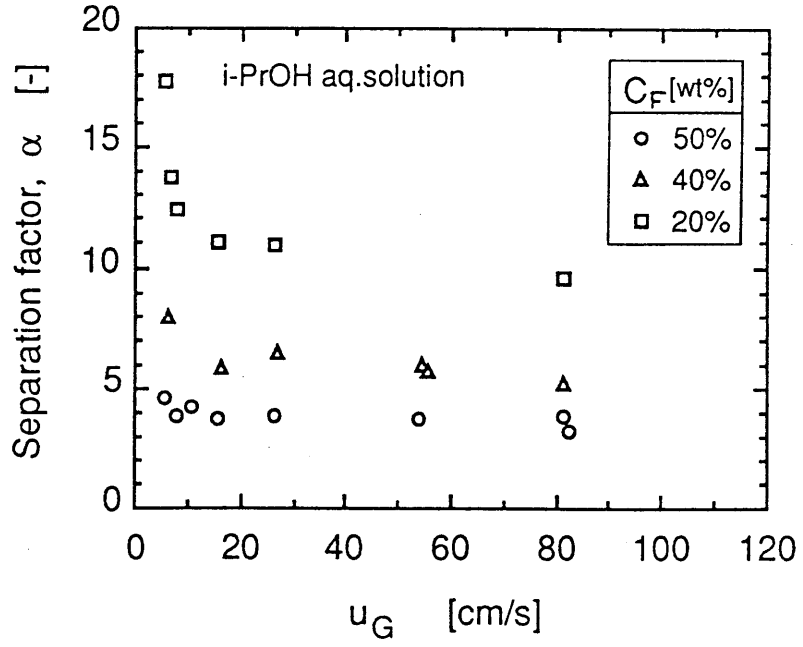

Fig.4.8b Effect of gas velocity on isopropanol separation factor to water.

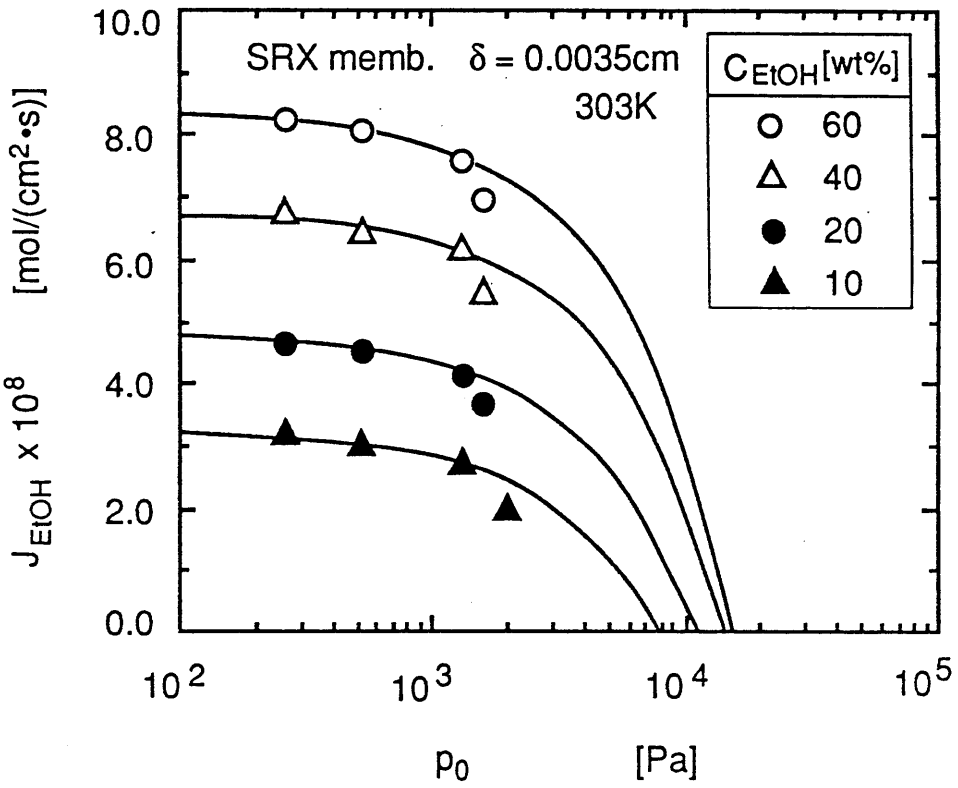

Fig.4.9 Effect of downstream pressure on ethanol flux for conventional pervaporation, where aqueous feed side was under ambient pressure.

CONCLUSIONS

A unique operation of pervaporation, in which the permeant vapor is swept by an inert gas flowing on the permeate side, was examined experimentally and theoretically on the permeation of ethanol and isopropanol and the separation from each aqueous solution using a PDMS-HF membrane module. It was illustrated that the permeation rate of alcohol through the membrane can be successfully expressed by a solution-diffusion-evaporation model. This operation mode could also be applied for the conventional pervaporation under vacuum on the downstream side. Separation factors of alcohols to water in the present mode decreased with increasing gas velocity, and the permeation flux was controlled by the diffusion in the membrane .

NOMENCLATURE

$\bar{C}$	concentration in the membrane phase	[mol/cm^3]
D_M	solute diffusivity in the membrane phase	[cm^2/s]
H	constant for the relation between alcohol vapor and concentration	[Pa•cm^3/mol]
J	flux of the permeate through membrane	[mol/(cm^2•s)]
k_M	mass-transfer coefficient in the membrane phase	[cm/s]
k_G	mass-transfer coefficient in the gas phase	[mol/(cm^3•s•Pa)]
K	overall mass-transfer coefficient	[mol/(cm^3•s•Pa)]
L	module length	[cm]
m	distribution ratio of alcohol	[-]
p	partial pressure	[Pa]
p^e	equilibrium partial pressure	[Pa]
p^*	hypothetical partial pressure defined by Eq.(4.4)	[Pa]
S	separation factor defined by Eq.(4.6)	[-]
u_G	gas velocity per cross sectional area of HF	[cm/s]
X	mole fraction	[-]
x	distance from the top of the module	[cm]
α	separation factor defined by Eq.(4.5)	[-]
δ	membrane thickness	[cm]

Subscripts

0 bulk of gas-phase
1 liquid-membrane interface
2 gas-membrane interface
A alcohol
F feed side
R recovery side
W water

REFERENCES

1) Feng, X. and Huang, R.Y.M.: *J. Memb. Sci.*, 74 171 (1992).
2) Hickey, P.J. and Slater, C.S.: Separation and Purification Methods, 19, 93 (1990).
3) Huang, R.Y.M.: *"Pervaporation membrane separation processes"*, Elsevier, Amsterdam, (1991).
4) Ishihara, K., Nagase, Y. and Matsui, K.: Makromol. Rapid Commun., 7, 43(1986).
5) Leveque, M.A.: *Rec. Mem. L'Explotas. Mines*, 13 201 (1928).

Chapter 5.

BULK LIQUID MEMBRANE WITH POROUS PARTITION MEMBRANE

INTRODUCTION

Supported liquid membranes(SLMs) have been studied extensively for the application of gas separation, concentration of metal ion from an aqueous solution and separation of organic acid from fermentation products[3]. SLM has advantages of a small amount of membrane solution with carrier, simple preparation and operation, and without containing surfactant which is used for an emulsion type liquid membrane having problems of a loss of membrane solution as fine droplets, contamination of products with the surfactant, etc. However, there are some problems associated with the use of the SLM: the loss of membrane solution from the supporting porous membrane by evaporation or dissolution of membrane solution into the feed and recovery solutions, which leads to the breakdown of the liquid membrane and the accumulation of substances which interfere with mass transfer across the liquid membrane. For overcoming these problems, studies have been made on continuous regeneration and prolongation of the lifetime of the SLMs[1,2,4,7]. Takahashi and Takeuchi[4] used a flat-sheet SLM in horizontal configuration, wherein a small amount of membrane solution was forced to flow with the recovery solution to stabilize the SLM. Fujinawa and Hozawa[1] used a vertical laminated film module with a reservoir of the membrane solution at the top of the module, where one end of the film was soaked into the reservoir. Nakano et al.[2] used a vertical hollow fiber SLM module wherein the membrane solution was supplied by buoyant force to the pore-continua within supporting solids. These studies aimed at refilling the pore of the solid with the membrane solution by supplying it continuously.

In the present study, we proposed a novel operation mode of a liquid membrane as shown in **Fig.5.1**, i.e. a large amount of membrane solution is forced to flow on the feed and recovery sides, wherein both aqueous phases are partitioned by a hydrophobic porous membrane and

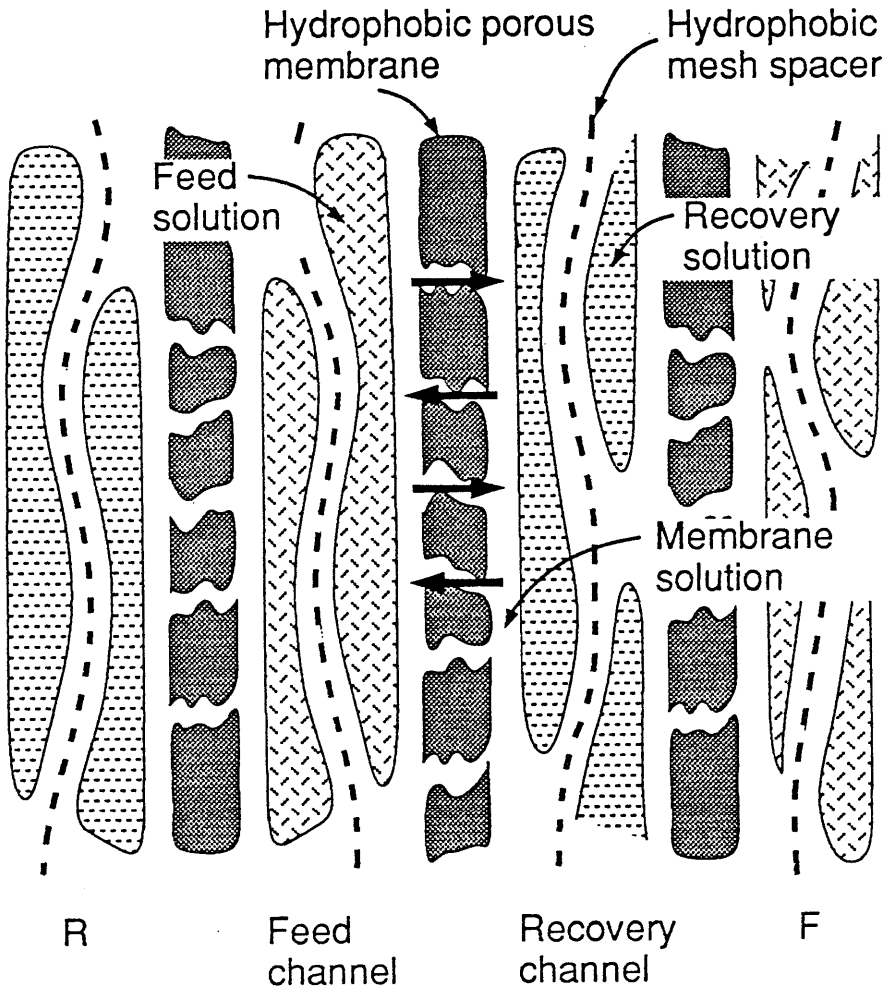

Fig.5.1 Conceptual figure of bulk liquid membrane operation.

the membrane solution can move freely through the pore of membrane. The solute dissolves into the membrane solution, then it is transferred across the porous membrane with the bulk motion of the membrane solution, i.e. the organic phase acts as a bulk liquid membrane. The movement of membrane solution across the membrane can enhance the mass-transfer rate, which enables a rapid separation of the solute.

In the operation, a large interfacial area between aqueous and organic phases can be realized by decreasing the channel depth and inserting a hydrophobic mesh spacer. Although relatively large amount of membrane solution is needed for the operation in comparison with the SLM, this method might be effective to concentrate and separate unstable substances just as antibiotics from dilute solution rapidly.

This view will be demonstrated by the comparison of the fractions of solute removal from feed solution between the bulk liquid membrane operation(BLM) and the SLM operation. In addition, mass-transfer coefficients for aqueous and organic phases and the porous membrane were measured at various aqueous and organic flow velocities.

5.1 EXPERIMENTAL

Hydrophobic porous membrane used in this study is Duragard 2500 of 25μm in thickness, 0.45 porosity, and 0.4x0.04μm pore size, which is made of polypropylene. On both sides of the membrane, flow channels of rectangular cross section(1x10mm) are set on PTFE sheets of 1mm thickness. A mesh having hydrophobic surface is inserted within the flow channel. Experimental setup for the BLM operation is schematically shown in **Fig.5.2a**. The membrane module shown in **Fig.5.2b** was installed vertically. In the figure of module A, broken line indicates the flow channel on the opposite side of the membrane, and hatched parts existence of flow channels on both sides of the membrane. Effective membrane length is 98cm.

Feed solution was an aqueous solution of I_2-KI, the membrane solution was n-heptane and the recovery solution was aqueous solution of $Na_2S_2O_3$. Iodine in the feed solution was extracted by the membrane solution, then was transferred from feed side to recovery side across the porous membrane and was stripped from the membrane solution by the recovery solution. The feed solution was mixed with the organic membrane solution just before the inlet of the module, then the two phase

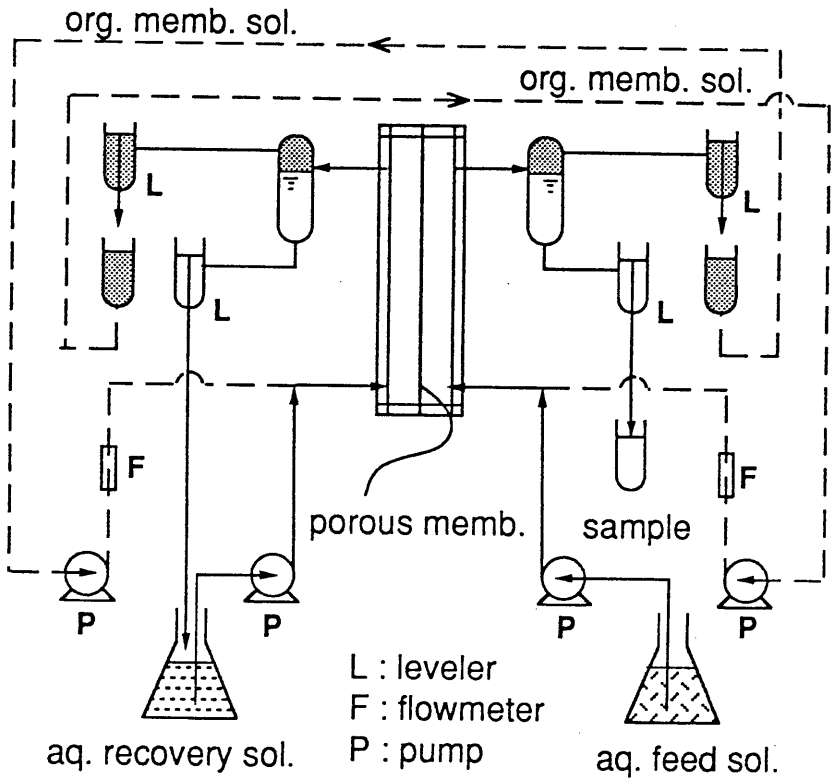

Fig.5.2a Schematic diagram of experimental apparatus.

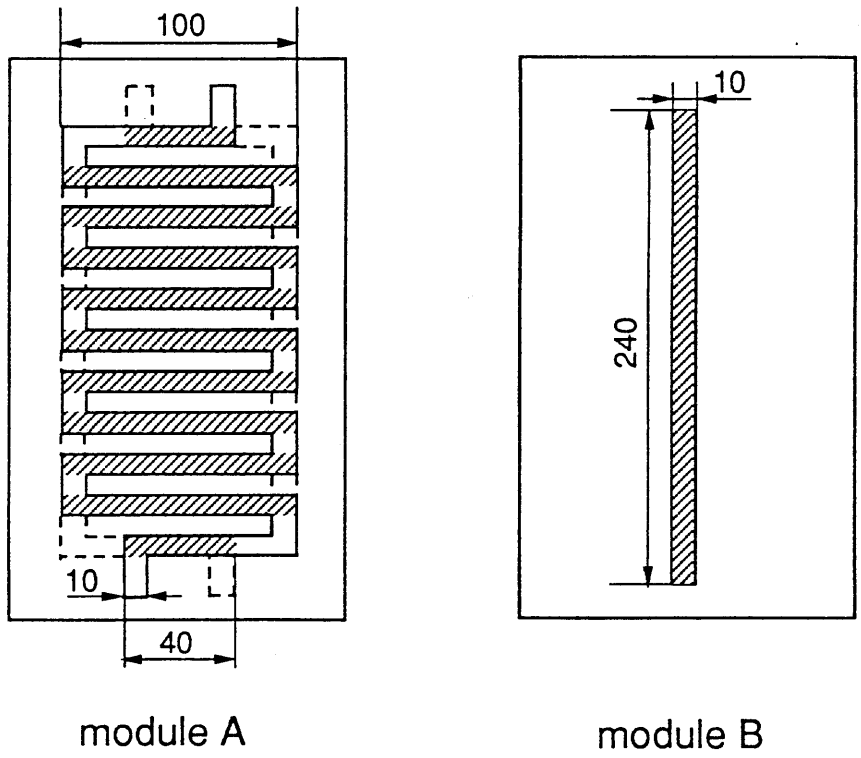

Fig.5.2b Details of flow channel of membrane modules. Hatched part refers to effective membrane area.

mixture was supplied to the feed side channel at the bottom of the module. Another two phase mixture of the recovery solution and the membrane solution was fed to the recovery side channel and flowed upward in parallel with the feed side flow. The two phase mixture leaving from each channel of the module was sent to a phase separator in which interface level was adjusted by two levelers for aqueous and organic phases. The membrane solution from the recovery side was pumped to the feed side and that from the feed side to the recovery side, i.e. the membrane solution was circulated between the channels on the feed and the recovery side. The recovery solution from the leveler was returned to the reservoir. The iodine concentrations in aqueous solution on the feed side were determined by the titration with aqueous solution of $Na_2S_2O_3$. Experiments without circulation of the membrane solution were also carried out, in which iodine free n-heptane was supplied to both channels and the iodine concentrations in the membrane solutions coming out from the module were measured by a spectrophotometer.

For the comparison between the BLM and the SLM, experiments without supply of membrane solution were carried out as an operation of the SLM. Flow rates of aqueous solutions and organic solutions at the outlet of channels were measured by taking the solution from the leveler with a measuring tube for a given time, and those of organic solutions at the inlet of channels with flow meters.

Mass-transfer characteristics were determined with module B (Fig.5.2b), which had a short flow path. In Module A, it is difficult to measure the mass-transfer coefficient because the organic phase at the outlet was almost in equilibrium with aqueous phase. Overall capacity coefficients based on the aqueous phase within the flow channel were obtained by the extraction of iodine from I_2-KI aqueous solution into n-heptane with a single flow mode. Distribution coefficients of iodine between the organic and aqueous phases were measured between the solutions of individual runs. Capacity coefficients for the organic phase were also measured from stripping experiments of iodine from n-heptane to $Na_2S_2O_3$ aqueous solution in a single flow mode. The iodine reacts with $Na_2S_2O_3$ at the interface, and there is no mass-transfer resistance in aqueous phase. For the measurement of mass-transfer coefficient in the organic phase across the porous membrane, two phase mixture of deionized water and iodine n-heptane solution was supplied to the feed-

side channel, and another two phase mixture of deionized water and iodine free n-heptane to the recovery-side channel. Concentrations in organic phases from both channels were measured as well as flow rates.

5.2 RESULTS AND DISCUSSION

5.2.1 Comparison between SLM and BLM

Figure 5.3 shows the iodine concentration ratios of outlet to inlet aqueous solution of feed-side channel for the BLM with and without the circulation of the membrane solution, and those for the SLM. The ratio increases with the increase in aqueous flow velocity, because the residence time decreases with U_{aqF}. The fraction of iodine removed from the feed solution in the BLM operation is much higher than that in the SLM. For U_{aqF}=0.005m/s, the BLM(with circulation) can achieve the outlet concentration as small as about 1/3 for the SLM in spite of small residence time of the BLM: under the same U_{aqF}, residence time of the BLM is smaller than that of the SLM, because the membrane solution is supplied with the feed solution in case of the BLM. In the present experiments, U_{orF}=U_{orR}=0.02m/s, the residence time of the BLM is about 1/5 of the SLM for U_{aqF}=0.005m/s. The BLM can realize a large recovery fraction with a small residence time. Flow velocities to get C_{aqFo}/C_{aqFi} = 0.4 are 0.02 and 0.005m/s for the BLM and the SLM, respectively, i.e., the throughput of the BLM is 4 times as large as that of the SLM for the same separation. Thus it is expected that highly efficient separation and concentration is achieved in this novel operation mode. For the experiments without circulation of membrane solution, iodine free heptane was supplied to both channels, then the values of C_{aqFo}/C_{aqFi} were smaller than those in the case of circulation of membrane solution as shown in Fig.5.3.

5.2.2 Mass-transfer characteristics

To analyze the separation process of the BLM, it is necessary to get the mass-transfer characteristics: mass-transfer coefficient between aqueous and organic phases in the flow channel and mass-transfer coefficient in organic phase across the porous membrane. For two phase flow in a single flow channel where iodine is extracted from aqueous phase into organic phase, a mass balance differential equation is expressed as

$$K_{aq}a\,(C_{aq} - C_{or}/m)\,dl = -\,U_{aq}\,dC_{aq} \qquad (5.1)$$

where $K_{aq}a$ is an overall capacity coefficient based on aqueous concentration, m an iodine distribution ratio between aqueous and organic phases and U_{aq} aqueous phase flow velocity. In the present study, the value of m was in the range from 6 to 8. The distribution ratio of iodine between n-heptane and I_2-KI aqueous solution and changes of distribution ratio with [KI] were given in the previous paper[5,6]. When iodine free n-heptane is supplied, iodine concentration in organic phase is given by

$$C_{or} = (C_{aqi} - C_{aq})\,U_{aq}/U_{or} \qquad (5.2)$$

By substituting Eq.(5.2) into Eq.(5.1), following equation is derived

$$K_{aq}a\,dl = -\frac{U_{aq}\,dC_{aq}}{(U_{or}m + U_{aq})\,C_{aq} - U_{aq}C_{aqi}} \qquad (5.3)$$

$K_{aq}a$ is obtained by integrating Eq.(5.3) from the inlet to outlet of the channel as follows.

$$K_{aq}a = \frac{U_{aq}U_{or}m}{L(U_{or}m + U_{aq})}\,ln\left(\frac{U_{or}mC_{aqi}}{(U_{or}m + U_{aq})C_{aqo} - U_{aq}C_{aqi}}\right) \qquad (5.4)$$

where C_{aqi} and C_{aqo} are iodine concentrations in aqueous phase at the inlet and the outlet of the channel, respectively. **Figure 5.4** shows effects of U_{or} and U_{aq} on overall capacity coefficient, $K_{aq}a$, which increases both with U_{or} and U_{aq}.

Capacity coefficients in organic phase, $k_{or}a$, were obtained with back-extraction from n-heptane solution of iodine to aqueous solution of $Na_2S_2O_3$. Since concentration of $Na_2S_2O_3$ in aqueous phase was high enough to reduce iodine even at the outlet of the module, the iodine concentration in aqueous phase(i.e., at the interface) is considered to be zero. The mass balance equation for the organic phase of differential length dl and unit width of the channel is written as

$$-\,U_{or}\,dC_{or} = k_{or}a\,C_{or}\,dl \qquad (5.5)$$

By integrating Eq.(5) from inlet to outlet of the channel, $k_{or}a$ is given by

$$k_{or}a = (U_{or}/L)\,ln\,(C_{ori}/C_{oro}) \qquad (5.6)$$

where C_{ori} and C_{oro} are the iodine concentrations in organic phase at the inlet and the outlet of the channel, respectively. The effects of U_{or} and U_{aq} on $k_{or}a$ are shown in **Fig.5.5**, and the following correlation was derived.

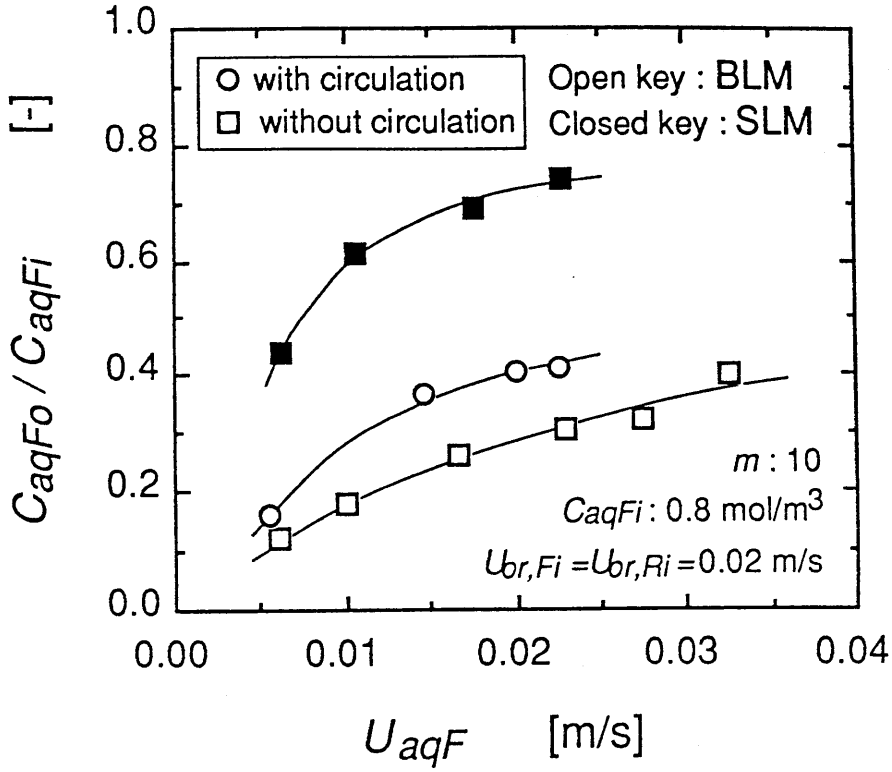

Fig.5.3 Comparison between concentration ratio of outlet to inlet solution in BLM and SLM operations.

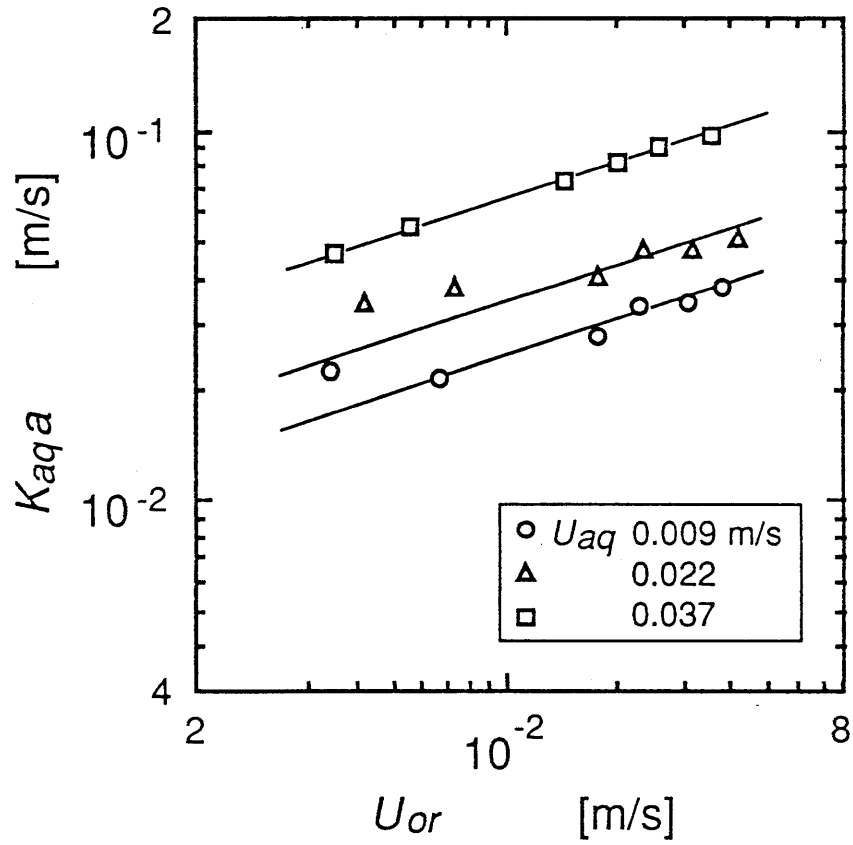

Fig.5.4 Effects of both U_{or} and U_{aq} on $K_{aq}a$.

$$k_{or}a = 5.2\ U_{aq}^{0.51}\ U_{or}^{0.45} \quad (5.7)$$

The dependency of $k_{or}a$ on Uaq was somewhat larger than that on U_{or}. This might come from the fact that organic phase flowed along the porous membrane and the mesh spacer in the channel because these materials were hydrophobic and the effect of organic phase motion on the mass-transfer resistances near the interface was smaller than that of aqueous phase motion.

For the conditions of experiments in Fig.5.4, $k_{or}a$ were calculated from Eq.(5.7), and capacity coefficients, $k_{aq}a$, in aqueous phase were determined with values of $K_{aq}a$ and $k_{or}a$ by use of the additive rule of mass-transfer resistances. Values of $k_{aq}a$ were also correlated with aqueous and organic phase flow velocities as

$$k_{aq}a = 2.6\ U_{aq}^{0.68}\ U_{or}^{0.33} \quad (5.8)$$

For the transfer of solute in the membrane solution across the porous membrane, there are two different modes: one is the diffusional transfer attributed by the concentration gradient, the other is a bulk transfer due to the motion of membrane solution through the pore of membrane. As the transfer coefficient implying the contribution of these transfers, we introduce a mass-transfer coefficient, k_B, for membrane solution across the porous membrane. On the assumption that amount of iodine dissolved in deionized water is negligible, mass balance for the differential section dl shown in **Fig.5.6** is given as

$$-h\ d(U_{orF}C_{orF})/dl = k_B\ (C_{orF} - C_{orR}) + v\ C_{orF} \quad (5.9)$$

where h is the depth of the channel and v the apparent velocity of membrane solution across the porous membrane. $k_B\ (C_{orF} - C_{orR})$ contains the bulk transfer expressed by $v_R\ (C_{orF} - C_{orR})$ as well as the diffusional transfer. Since dU_F is equal to $-v\ dl/h$, Eq.(5.9) is reduced to

$$-h\ U_{orF}\ dC_{orF}/dl = k_B\ (C_{orF} - C_{orR}) \quad (5.10)$$

By assuming that there is no accumulation in the porous membrane, following equations are given

$$C_{orR} = (U_{orFi}\ C_{orFi} - U_{orF}\ C_{orF})/U_{orR} \quad (5.11)$$

$$U_{orF} = U_{orFi} - v\ l/h \quad (5.12)$$

$$U_{orR} = U_{orRi} + v\ l/h \quad (5.13)$$

$$U_{orF} + U_{orR} = U_{orFi} + U_{orRi} \quad (5.14)$$

Eqs.(5.11) to (5.14) are substituted in Eq.(5.10), and rearranged as follows

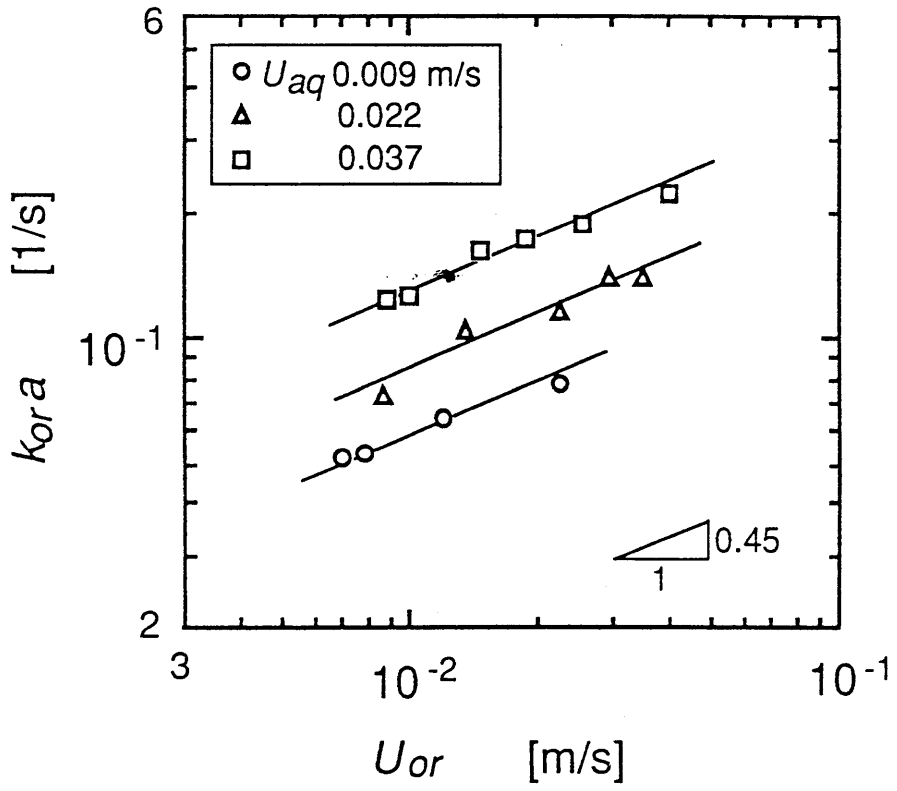

Fig.5.5 Effects of both U_{or} and U_{aq} on $k_{or}a$.

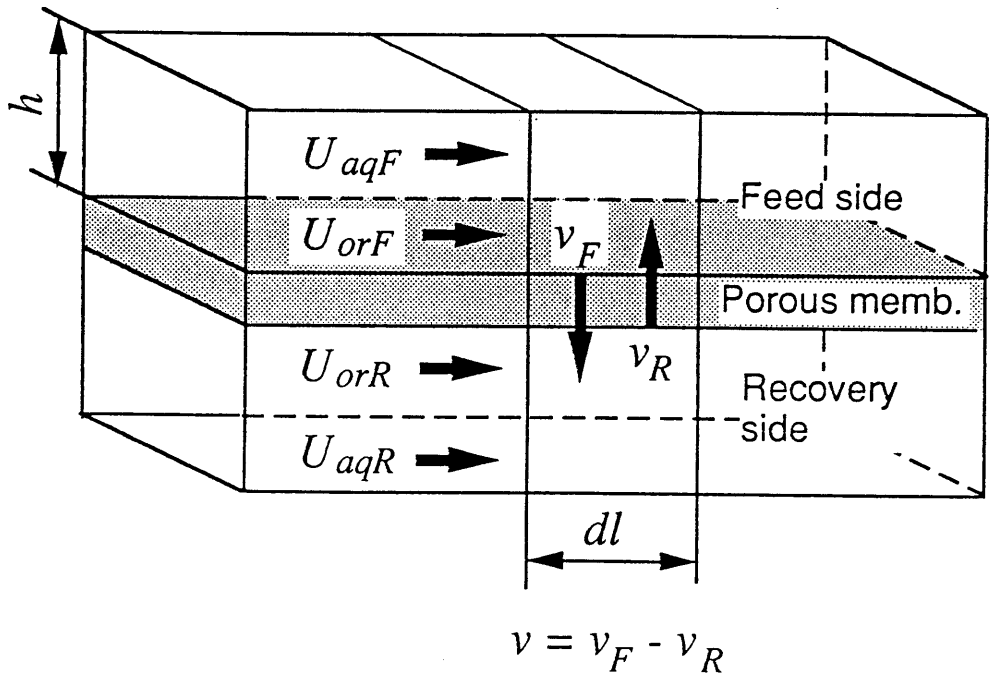

$$v = v_F - v_R$$

Fig.5.6 Mass balance in BLM membrane module.

$$k_B \left(\frac{dl}{U_{orFi} - vl/h} + \frac{dl}{U_{orRi} + vl/h} \right)$$

$$= - \frac{(U_{orFi} + U_{orRi})\, h\, dC_{orF}}{(U_{orFi} + U_{orRi})\, C_{orF} - U_{orFi}\, C_{orFi}} \qquad (5.15)$$

Eq.(5.15) is integrated between l=0 and l=L, and k_B is obtained as

$$k_B = v \frac{ln\left[U_{orRi}\, C_{orFi} / \{(U_{orFi} + U_{orRi})\, C_{orFo} - U_{orFi}\, C_{orFi}\}\right]}{ln\left\{U_{orRo}\, U_{orFi} / (U_{orFo}\, U_{orRi})\right\}} \qquad (5.16)$$

Figure 5.7 shows the effects of $\overline{U_{or}}$ and U_{aq} on k_B in the BLM operation. $\overline{U_{or}}$ is the average organic phase velocity on feed side and recovery side. In the experiments, aqueous phase velocities were equal on each side of the module. As can be seen in the figure, k_B does not depend on aqueous phase velocity but increases with 0.37power of average organic phase velocity, i.e., the motion of membrane solution across the porous membrane increases with $\overline{U_{or}}$. The obtained correlation is as follows;

$$k_B = 6.5\, \overline{U_{or}}^{0.37} \qquad (5.17)$$

Since the pore size and porosity of Duragard 2500 was relatively small, the values of k_B were not so high. It is expected that higher value of k_B can be achieved by use of the partition membrane of larger pore size and porosity.

5.2.3 Simulation of BLM

For simulating the solute concentration at the outlet of the module under various conditions, it is needed that a formulation of differential mass balance shown in Fig.5.6 is established. The feed, the membrane and the recovery solutions flow in parallel with concentration change in the flow direction. Membrane solution moves across the porous membrane from feed side to recovery side with velocity v_F and in opposite direction with v_R. A differential mass balance on the solute in feed solution is given by Eq.(5.1), and rearranged

$$dC_{aqF}/dl = - K_{aq}a\, (C_{aqF} - C_{orF}/m)/U_{aqF} \qquad (5.18)$$

in the recovery-side channel,

$$dC_{aqR}/dl = K_{aq}a\, (C_{orR}/m - C_{aqR})/U_{aqR} \qquad (5.18')$$

In the present case of iodine transfer with the recovery solution of $Na_2S_2O_3$, the iodine concentrations in the aqueous phase and at the

interface between aqueous and organic phases within the recovery channel were zero, and Eq.(5.18') was not used in the calculation.

For the organic phase in the feed-side channel

$$h\,U_{orF}\,dC_{orF} = K_{aq}a\,(C_{aqF} - C_{orF}/m)\,h\,dl - \{k_B\,(C_{orF} - C_{orR}) + v\,C_{orF}\}\,dl \quad (5.19)$$

$$dC_{orF}/dl = K_{aq}a\,(C_{aqF} - C_{orF}/m)/U_{orF} - \{k_B\,(C_{orF} - C_{orR}) + v\,C_{orF}\}/(h\,U_{orF}) \quad (5.20)$$

and in the recovery side-channel

$$h\,U_{orR}\,dC_{orR} = \{k_B\,(C_{orF} - C_{orR}) + v\,C_{orF}\}\,dl - K_{aq}a\,(C_{orR}/m - C_{aqR})\,h\,dl \quad (5.21)$$

$$dC_{orR}/dl = \{k_B\,(C_{orF} - C_{orR}) + v\,C_{orF}\}/h\,U_{orR} - K_{aq}a\,(C_{orR}/m - C_{aqR})/U_{orR} \quad (5.22)$$

In the present case, $-\,k_{or}a\,C_{orR}/U_{orR}$ is used instead of the last term in Eq.(5.22). The change of organic phase velocity in flow direction is written as

$$dU_{orF}/dl = -\,v/h \quad (5.23)$$

The concentrations of C_{aqF}, C_{aqR}, C_{orF} and C_{orR} are obtained by solving the set of differential equations (5.18), (5.18'), (5.20), (5.22) and (5.23) according to the Runge Kutta method.

Figure 5.8 shows the plot of outlet concentrations of aqueous and organic phases in the feed side and organic phase in the recovery side on the experimental conditions of without circulation of membrane solution. Solid lines represent the calculated values obtained from the set of equations by using mass-transfer coefficients estimated from Eqs.(5.7), (5.8) and (5.17). The deviation between the observed values and the solid lines might come from the different flow pattern of two phases in the module A and the module B shown in Fig.5.2b. Mass-transfer coefficients were determined with the module B of vertical flow channel, whereas the BLM operation was carried out with the module A of horizontal flow channel. Within horizontal flow channel, it was observed that organic phase tends to flow in upper part and aqueous phase flows in lower part of the channel. In vertical flow channel, the two phase flow was uniform. Thus there is a possibility of overestimate of capacity coefficients, $k_{or}a$ and $k_{aq}a$ for applying the BLM operation of horizontal flow channel.

To fit the calculated values to the observed values, the effects of capacity coefficients on the calculated concentrations at the outlet of the

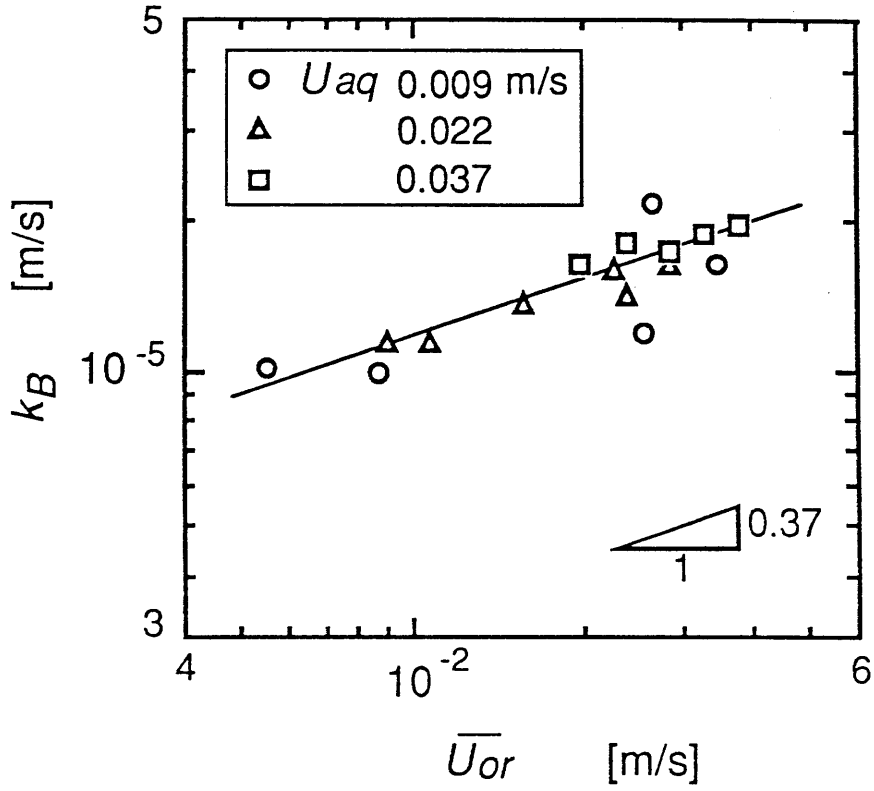

Fig.5.7 Effects of both $\overline{U_{or}}$ and U_{aq} on k_B.

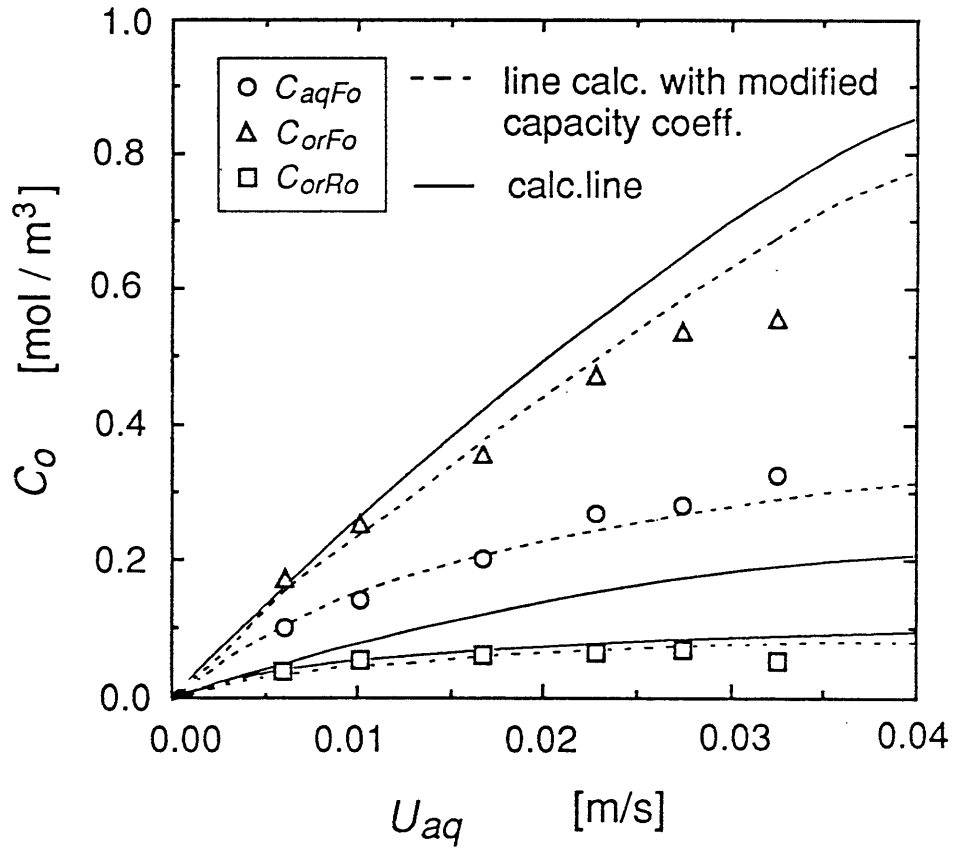

Fig.5.8 Comparison between calculated and observed values for concentrations at outlet of module.

module were examined. The decrease of $k_{or}a$ and $k_{aq}a$ led to the rise of C_{aqFo} and the fall of C_{orFo}. In the figure, dashed lines represent the calculated values obtained by reducing capacity coefficients $k_{or}a$ and $k_{aq}a$, i.e., 65% of the estimated values. The dashed lines are in a good agreement with the observed values. This suggests that the effective interfacial area in the horizontal flow might be about 65% of that in the vertical flow configuration. It was concluded that, the model presented in this study was applicable for predicting concentrations at the outlet of the module with a simple correction of capacity coefficients. For the observed results in Fig.8, the ratio of C_{orFo}/C_{aqFo}=1.7 which is much smaller than the equilibrium distribution ratio(in this experiments m = 10). This indicates that the mass transfer across the porous membrane acts effectively to reduce the concentration of C_{orF}.

CONCLUSIONS

Mass transfer characteristics in a novel operation mode of bulk liquid membrane with the porous partition membrane were studied systematically with the iodine transfer experiments. It was found that the BLM operation is effective for the rapid mass-transfer operation rather than the SLM operation. It was established that the basic equation including coefficient for bulk-transfer of membrane solution across the porous membrane; this coefficient was correlated with organic phase velocity. The model developed in the present study predicted well the concentrations of aqueous and organic phases in the feed-side and the recovery-side at the outlet of the module with a simple correction of capacity coefficients estimated from the correlations obtained for the different flow pattern of two phase flow.

NOMENCLATURE

a	specific interfacial area	[m^2/m^3]
C	concentration	[mol/m^3]
h	depth of a flow channel	[m]
k_{or}	mass-transfer coefficient in organic phase	[m/s]
k_B	mass-transfer coefficient for bulk transfer of the membrane liquid across porous membrane	[m/s]

K_{aq}	overall mass-transfer coefficient based on aqueous phase concentration	[m/s]
l	distance in flow direction	[m]
L	total flow length from inlet to outlet of the module	[m]
m	distribution ratio of iodine between organic and aqueous phases	[-]
$\overline{U_{or}}$	average velocity of organic phase in feed and recovery side	[m/s]
v	net velocity of membrane solution across the porous partition membrane	[m/s]
v_F	velocity of membrane solution from feed-side to recovery-side across porous membrane	[m/s]
v_R	velocity of membrane solution from recovery-side to feed-side across porous membrane	[m/s]

Subscripts

aq	aqueous phase
F	feed side
i	inlet
o	outlet
or	organic phase
R	recovery side

REFERENCES

1) Fujinawa, K. and Hozawa, M.: *Proceedings of the World Congress III of Chem. Eng.*, Vol. III, 8J-353, 342 (1986).
2) Nakano, M., Takahashi, K. and Takeuchi, H.: *J. Chem. Eng. Japan*, 20, 326 (1987).
3) Noble R.D., Way, J. D.: *"Liquid membranes theory and applications"*, ACS symposium series 347, Am. Chem. Soc, Washington, (1987).
4) Takahashi, K., and Takeuchi, H.: *J. Chem. Eng. Japan*, 18, 205 (1985).
5) Takahashi, K., Nakano, M. and Takeuchi, H.: *Kagaku Kogaku Ronbunshu*, 13, 256 (1987).
6) Takeuchi, H., Takahashi, K. and Nakano, M.: *Ind. Eng. Chem. Res.*, 29, 1471 (1990).
7) Tanigaki, M., Eguchi, W. and Mori, Y.: *Proceedings of the World Congress III of Chem. Eng.*, Vol. III, 8J-351, 334 (1986).

Chapter 6.

COUNTERION EFFECT ON THE EXTRACTION OF LITHIUM BY 18-CROWN-6*

INTRODUCTION

There has been much recent interest in macrocyclic polyether as complexing agents, because of the ability of these compounds to act as selective agents for metal extraction, to serve as phase-transfer catalysts, and to transport metal ions across hydrophobic membranes. Such neutral ionophores as crown ethers contain hard oxygen atoms as potential donors in their binding sites; interaction of cation with the oxygen atoms for ionophoric cavity is expected[6]. Thus, the selective extraction of metals by various synthetic cyclic polyethers have been extensively reported. These studies, however, have been focused mainly on the inclusion of cations within the ring cavity from aqueous media; little is known regarding the quantitative relation on the effect of counterions.
In the case of neutral ionophores, complexation occurs between the cation and the binding sites of the ionophore; thus, it is expected that the extraction and transport of the cation are affected by the solvation energy of the accompanying anion, i.e., the anion-solvent interaction. In the present communication, this view will be demonstrated on the extraction of Li^+ by 18-crown-6 as a typical neutral cyclic polyether. This system is characteristic of very low extractability; therefore, it is favorable to examination under conditions with little variation of the concentration of the free ligand during the extraction.

6.1 EXPERIMENTAL

Commercially available 18-crown-6, 1,4,7,10,13,16-hexaoxacyclo octadecane(Aldrich) was dissolved in chloroform and washed with a large amount of water. Aqueous solutions of lithium salts were prepared by dissolving LiI, $LiNO_3$, $LiClO_3$, LiCl and Li_2SO_4 of analytical grade with deionized water in the concentration range of 0.5~2mol/dm^3.

---

* This chapter is appeared in J. Chem. Eng. Japan, **25**, No. 2, 220-223(1992).

Equal volumes ($20cm^3$) of aqueous and organic phase were placed in a $50cm^3$ flat-bottomed flask and shaken for 30min using a shaker regulated at 298K. After reaching equilibrium, the liquid mixture was settled in a funnel at the same temperature as in the extraction. The organic phase separated from the aqueous phase was scrubbed with $20cm^3$ of deionized water for 30min, whereby all the salts were back-extracted three times. The Li^+ concentration was determined by atomic absorption spectroscopy, and then the equilibrium concentration in the organic phase was calculated from mass balance.

6.2 RESULTS AND DISCUSSION

6.2.1 Effect of crown concentration on distribution ratio of lithium ion

The distribution ratios of Li^+, $D(=[\overline{Li}]/[Li])$, for the extraction from aqueous solutions of LiCl and LiI are plotted in **Fig.6.1** against the crown concentration, $[\bar{L}]$, in the organic phase, where $[\overline{Li}]$ and [Li] are the equilibrium concentrations in the organic and the aqueous phase, respectively. The value of D is directly proportional to $[L]$. This concentration dependence can be explained from the mechanism of an ion-pairing extraction with crown ether as

$$Li^+ + L + X^- \overset{K_a}{\rightleftarrows} Li^+LX^- \overset{K_D}{\rightleftarrows} \overline{Li^+LX^-} \qquad (6.1)$$

where L is the ligand in the aqueous phase near the liquid-liquid interface and the overbar denotes the organic phase;

$K_a = [Li^+LX^-] / [Li^+][L][X^-]$ and

$K_D = [\overline{Li^+LX^-}] / [Li^+LX^-]$.

Equation (6.1) leads to the following relation between the distribution ratio and the counterion concentration:

$$D = [\overline{Li}] / [Li] = [\overline{Li^+LX^-}] / ([Li^+] + [Li^+LX^-])$$

$$= K_D \left(1 + \frac{1}{K_a[L][X^-]}\right)^{-1} \qquad (6.2)$$

$$\cong K_D K_a [\bar{L}][X^-] = K_{ex}[\bar{L}][X^-] \qquad (6.2')$$

provided that $K_a[L][X^-] \ll 1$.

In a previous study[10], Takahashi *et al.* found that the permeation flux of alkali metal ions across a dibenzo-18-crown-6 containing

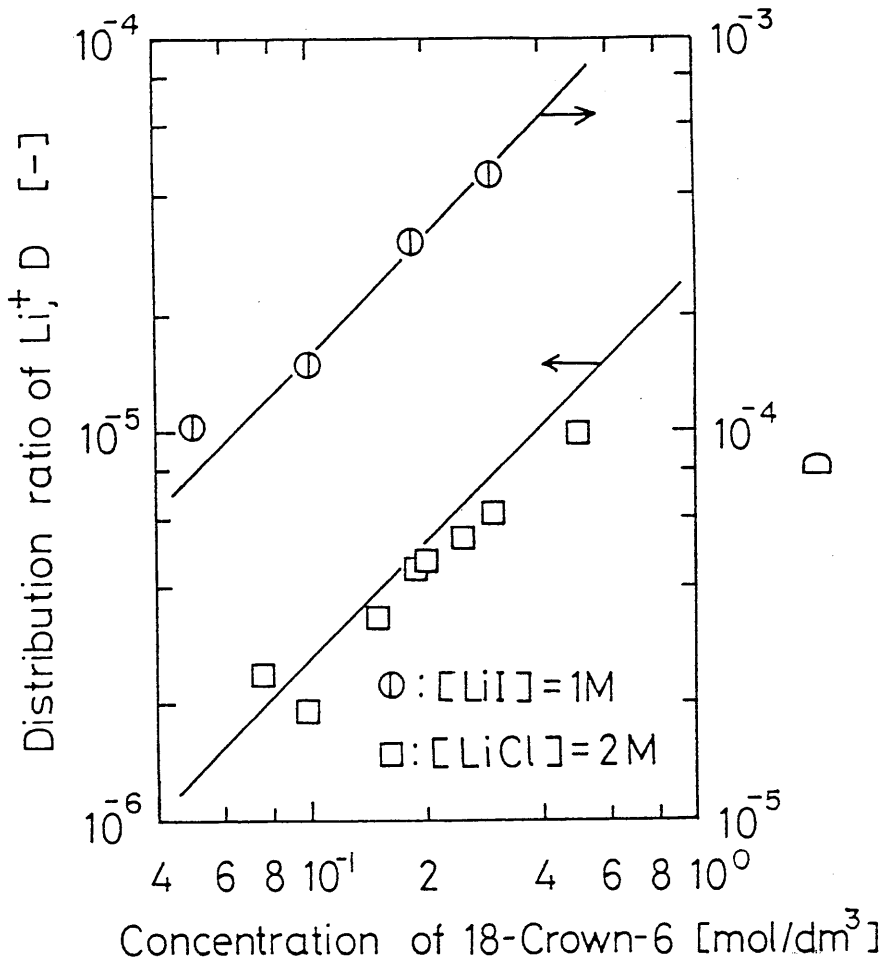

Fig.6.1 Effect of ligand concentration on the distribution ratio of Li^+. Solid lines represent the calculated values from Eqs.(6.2') and (6.4).

dichloroethane membrane is directly proportional to the concentration product of the cation and anion. In other words, the concentration of the complexes in the organic membrane is related to the product as the effective driving force through the membrane; their result can be explained well by Eq.(6.2).

6.2.2 Effect of counterion on distribution ratio of lithium ion

Figure 6.2 shows the results for various lithium salts as a log-log plot of D versus C_{salt}, indicating that the extractability of 18-crown-6 is in the order $I^- > NO_3^- > ClO_3^- > Cl^-$ and is almost nil for the sulfate, although the data are not given here. This sequence corresponds to the Hofmeister or lyotrophic series of anions[2].

The thermodynamic stability of a complex is, in general, inversely proportional to the solvation of the ligand and of ion or complex. Therefore, complex formation will be weaker in solvents where the acceptor is strongly solvated. Li^+ forms stable complexes with water molecules, in which the cation is coordinated by four water molecules[6]; also, counterions are strongly solvated in water.

Here we attempted to introduce the Jones-Dole parameter[3], B, to quantify the effect of the anion on Li^+ extraction. The dependence of fluidity of electrolyte solution on the concentration[1] is given by

$$\phi / \phi_0 = 1 + A\sqrt{C} + BC \qquad (6.3)$$

The coefficients A and B depend on the solute species. A $\sqrt{C}$ is the contribution of the interionic electrostatic interaction. The linear term, BC, arises from ion-solvent interaction. The constant B is highly specific and is an additive property of the separate ions. Generally, $|A| < |B|$, so that the relative magnitude of the terms in Eq.(6.3) depends on the concentration. Values of B for various ions are available elsewhere[7,8,9], and the approximate value can also be evaluated from Eq.(6.3) with its viscosity data. According to Podolsky[7], the parameter B is proportional to the perturbation of the activation energy accompanying transformation of a lattice particle from a water to anion.

Figure 6.3 shows a semilogarithmic plot of D versus B-coefficient of the anions, together with literature values of K_{ex} for the halides extraction by benzo-15-crown-5[4]. The relationship between $\ln D$ or $\ln K_{ex}$ and B-coefficient is approximately linear, and the equation of the

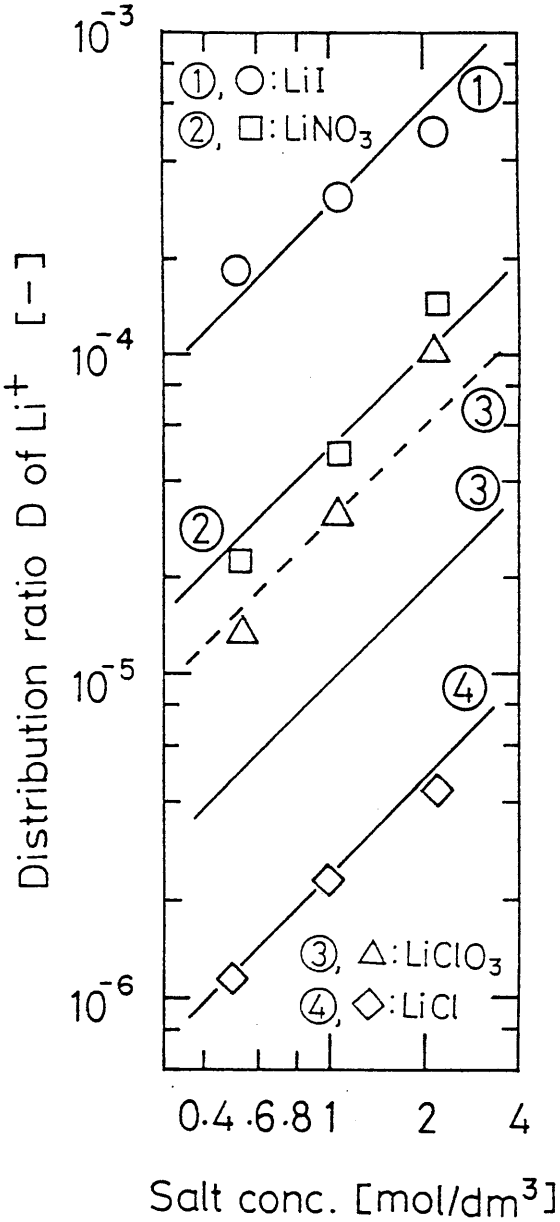

Fig.6.2 Effect of the anionic species on the distribution ratio of Li^+ for $[\bar{L}]=0.186M$. Solid lines represent the calculated values for Li-salts from Eqs.(6.2') and (6.4).

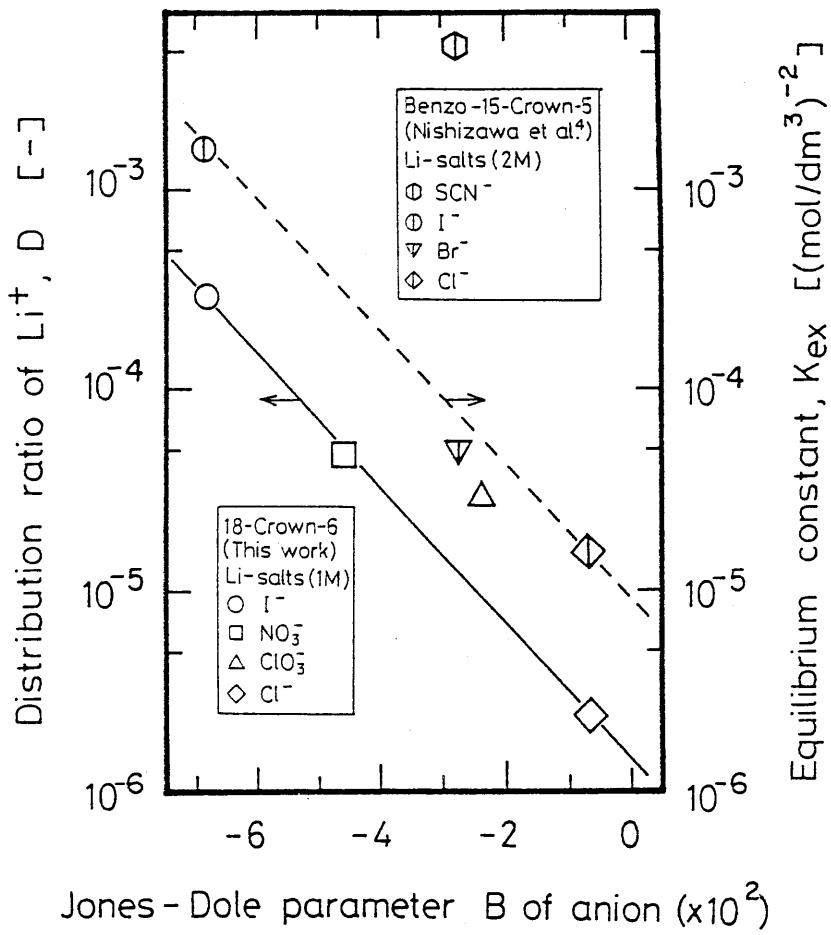

Fig.6.3 Correlation of distribution ratios of Li^+ with the Jones-Dole parameter, *B*.

best straight line(solid line) can be obtained for the 18-crown-6 system on the basis of Eq.(6.2').

$$K_{ex} = 7.58\text{x}10^{-6} \exp(-78.05B) \qquad (6.4)$$

In Figs.6.1 and 6.2, the solid lines represent the calculated values from Eqs.(6.2') and (6.4); the data points fall very close to the respective lines except for $LiClO_3$. The dashed line for $LiClO_3$ in Fig.6.2 illustrates the calculated value with a B-value, -0.038. In addition, for LiSCN in literature data[4] there is a large deviation from the dashed line in Fig.6.3. This may be attributed for the suspicious value of B. Taking the Hofmeister series of anion into account, one has an expectation of allowing numerically greater B value for SCN^-. To ascertain the effect of the concentration of anion on the distribution ratio of Li^+, further experiment was conducted with the mixed-salts solution of $LiNO_3$ and $NaNO_3$. The results are shown in **Fig.6.4**. The value of D increases with increasing nitrate concentration at the constant $[Li^+]$; the anion-concentration dependence of D has the same tendency as in the single-salt system, as can expect from Eq.(6.2').

In conclusion, the merit of introduction of the Jones-Dole parameter is that it can satisfactorily explain known facts or past findings on the effect of counterion on metal extraction by cyclic polyethers.

NOMENCLATURE

A	constant	$[(dm^3/mol)^{1/2}]$
B	constant	$[dm^3/mol]$
C	concentration in aqueous phase.	$[mol/dm^3]$
D	distribution ratio of lithium	[-]
K_a	equilibrium constant	$[(mol/dm^3)^{-2}]$
K_D	distribution coefficient of complex	[-]
K_{ex}	extraction constant	$[(mol/dm^3)^{-2}]$
L	neutral ligand (crown ether)	[-]
X	anionic species	[-]
ϕ	fluidity (= reciprocal of viscosity)	$[(Pa\ s)^{-1}]$
[ ]	concentration	$[mol/dm^3]$

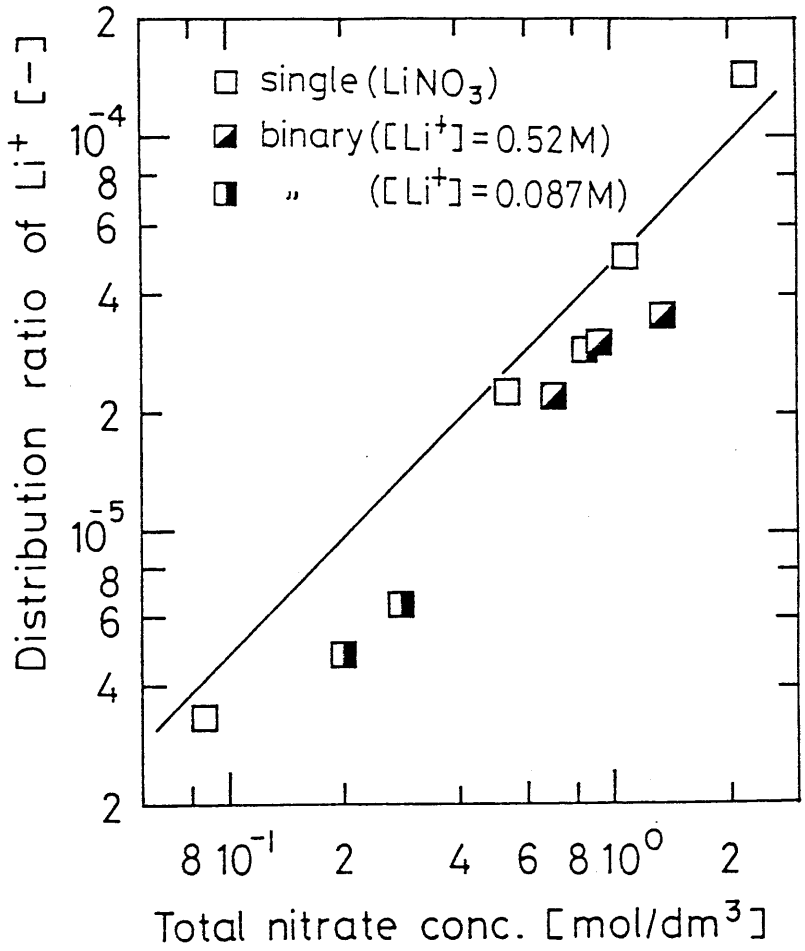

Fig.6.4 Effect of the anion concentration on the distribution ratio of Li^+ for both single and binary systems ($LiNO_3$ and $NaNO_3$). Solid line represents the calculated value for $[\overline{L}]$=0.186*M*.

REFERENCES

1) Bingham, E. C.: *J. Phys. Chem.*, 45, 885 (1941).
2) Christensen, J. J., Lamb, J. D. and Izatt, R.M.: *J. Am. Chem. Soc.* 100, 3219 (1978).
3) Jones, G. and Dole, M.: *J. Am. Chem. Soc.* 51, 2950 (1929).
4) Nishizawa, K., Ishino, S. and Watanabe, H.: *J. Nucl. Sci. Technol.*, 21, 694 (1984).
5) Nishizawa, K. and Takano, T.: *Sep. Sci. & Technol.* 23, 333 (1988).
6) Olsher, U., Izatt, R. M. Bradshaw, J. S. and Dalley, K.: *Chem. Rev.* 91, 137 (1991).
7) Podolsky, R. J.: *J. Am. Chem. Soc.* 80, 4442 (1958).
8) Ratcliff, G. A. and Holdcroft, J. G.: *Trans. Inst. Chem. Engrs.* 41, 315 (1963).
9) Robinson, R. A. and Stokes, R. H.: *"Electrolyte Solutions"*, p516, Butterworths Sci. Pub., London, (1959).
10) Takahashi, M., Imanaka, M. and Takeuchi, H.: *Kagaku Kogaku Ronbunshu*, 7, 494, (1981).

Chapter 7.

MAXIMUM THROUGHPUT IN MULTISTAGE MIXER-SETTLER EXTRACTION COLUMN*

INTRODUCTION

In multistage countercurrent extraction column, it is desirable to achieve a high mass-transfer rate and an operability in wide flow rate range of each phase. With the strong agitation, the dispersed droplets are split into fine droplets which realize a large interfacial area. As the drop size decreases with agitation rate, however, the coalescence of dispersed phase becomes difficult and the dispersed drop tends to flow with the continuous phase. These negative effects lowers the throughput. Therefore, there have been attempts for overcoming of these drawbacks.

Scheibel[4] sets the packed bed between the mixing part alternatively for promoting the coalescence of the droplets. For the same purpose, Steiner[5] used a three dimensional lattice made of PTFE. Bails-Stitt[1] realized a high extraction efficiency under a vigorous agitation by applying the electrostatic field for the coalescence of aqueous dispersed phase. Gaubinger *et al.*[2] used a concentric cones for dividing the flow channels of two phases and achieved a stable operation.

The holdup and drop size distribution were measured in the single stage mixer-settler apparatus with divided flow channels for both phases suggested by Takahashi and Takeuchi. From the measurement of pressure distribution in the stage, it was suggested that a lifter-turbine impeller realizes a stable operation with strong agitation and rapid coalescence of dispersed droplet. In the present study, the effect of agitation rate on the maximum throughput was examined with the Mixer-Settler column consisting of three stages. The effect of setting a coalescer between the mixer and the settler is also investigated. In addition, the pressure differences were measured between stages and between the mixer and the settler in the next stage.

---

* This chapter is appeared in Kagaku Kogaku Ronbunshu, **19**, No. 3, 440-445(1993).

7.1 EXPERIMENTAL

Schematic diagram of experimental apparatus is shown in **Fig.7.1**. The MS column consists of three stages. A stage is divided into two parts, the upper one is settler and the lower one is mixer. On the bottom of the column, a non-woven fabric was mounted for coalescing small droplets of dispersed phase. As a dispersed phase, n-heptane was fed at the bottom of the column, then flows to the mixer in the bottom stage through the riser tube. After passing through the column, the phase is returned to the reservoir via a leveler. As a continuous phase, deionized water was supplied at the mixer in the top stage through the downspout. After settling on the top stage, the water flows down to the mixer on the middle stage. The water comes out from the bottom of the column and returned to the reservoir.

The flow rate of dispersed phase is considered to be controlled by the pressure difference between the upper and lower ends of the riser tube. Pressure differences between the settlers and between the mixer and the settler in the next stage were measured with manometer from the experiments of supplying only continuous phase. The pressure tap was set at the both settlers and at a beneath of the impeller, where the end of a tap tube is open for upper direction.

Details of MS column is shown in **Fig.7.2(a)** and **(b)**. The column is made of acrylic resin, whose inside diameter is of 60mm. There are three stages within the column, each stage is separated with the PTFE plate of 3mm in thickness into two parts as mentioned above. The total height of one stage is of 90mm: the settler of 40mm in height and mixer of 50mm in height. These parts are partitioned with the doughnut-shaped PTFE plate of 3mm in thickness and the open space of the plate has the diameter of 30mm. As an impeller, a six-blade lifter turbine of 30mm in diameter is used. On the partitioning plate, various coalescers are set. The properties of these coalescers are shown in **Table 1**, wherein the table, "Mesh" is a glass fiber mesh coated with PTFE. "Lattice" is a three dimensional lattice which is assembled with mesh. "Foam" is a urethane foam of three-dimensional network structure.

The maximum throughput was measured under conditions of the constant flow rate of dispersed phase and the agitation rate. With increasing the continuous phase flow rate, the phase begins to accumulate at the upper part of the settler as shown in Fig.7.2(b). The maximum

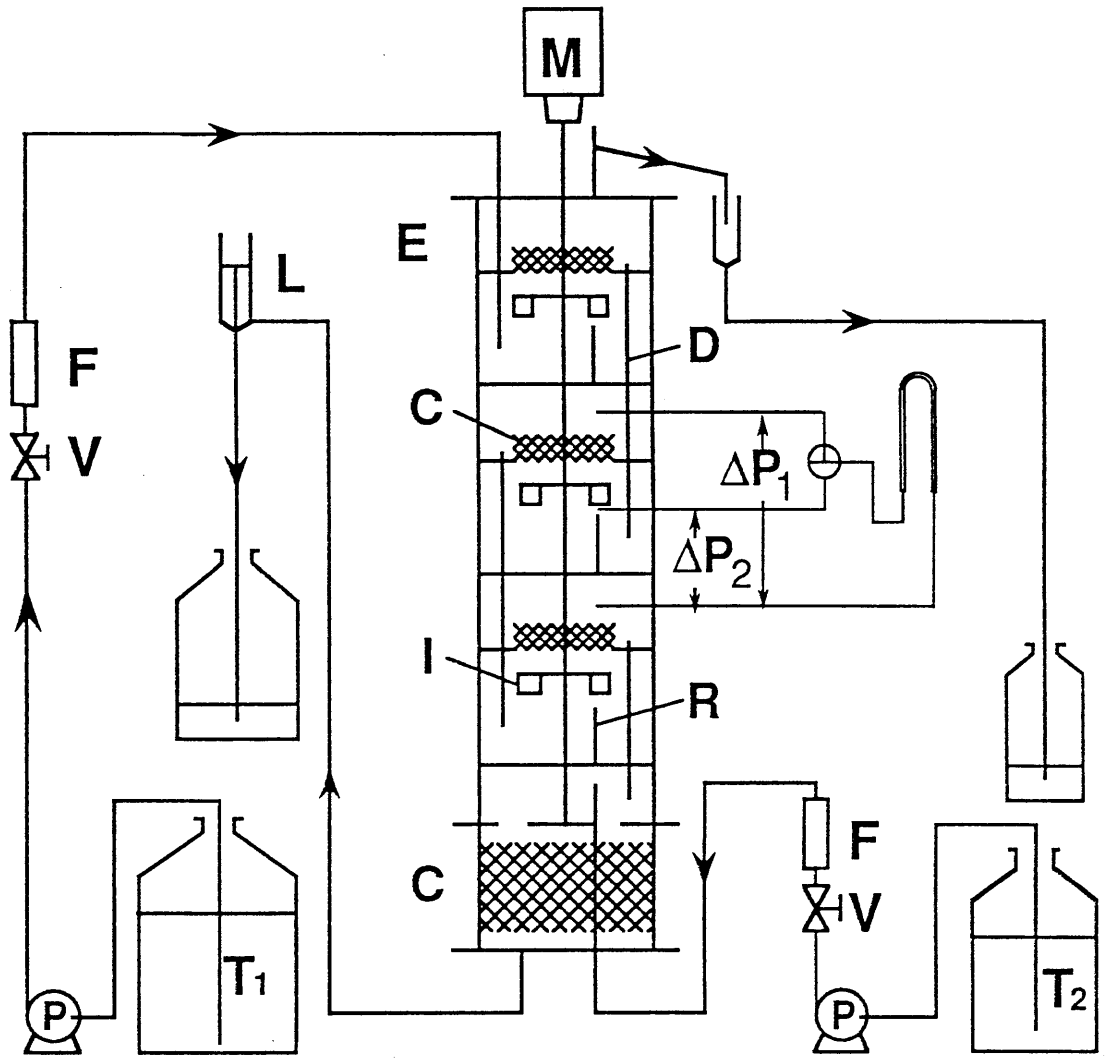

E: extraction column
C: drop coalescer
T_1 : tank for aqueous phase
T_2 : tank for organic phase
I: 6-blade lifter-turbine
D: down spout for aqueous phase
R: riser for organic phase
L: level er
F: flow meter
P: pump
V: valve

Fig.7.1 Schematic diagram of experimental apparatus.

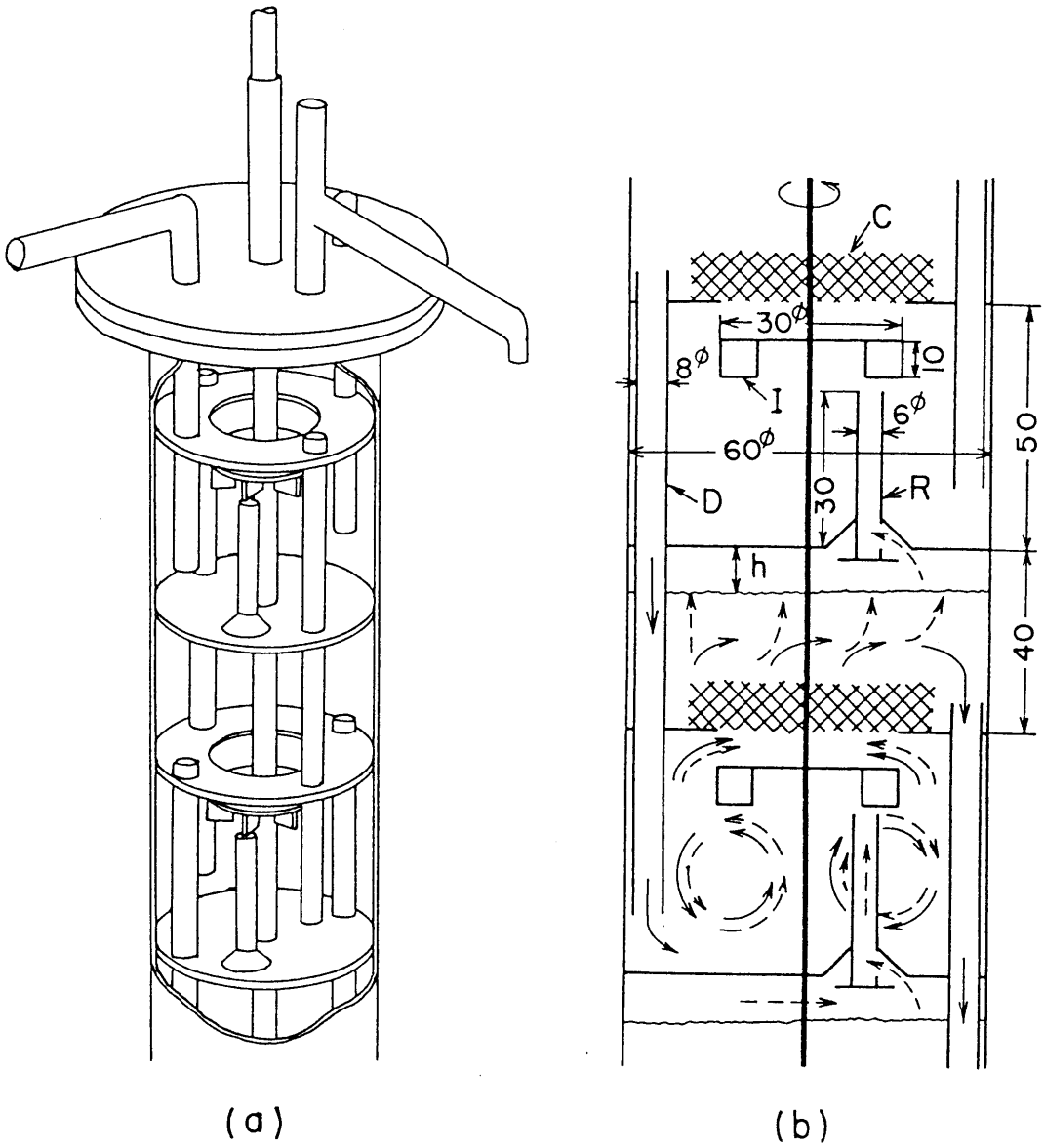

Fig.7.2 Mixer-settler extraction column. I: 6-blade lifter turbine, D: downspout for aqueous phase, R: riser for organic phase, C:drop coalescer.

Table 7.1 Poresize and thickness of coalescers.

Coalescer	d_p [mm]	t [mm]	
Mesh	1.7x2.0	0.8	Spun glass coated with PTFE
Lattice	2.0x2.0	10	Made of mesh
Foam	4.5	10	Urethane
Foam	1.8	10	Urethane
Foam	1.2	10	Urethane
Foam	0.9	10	Urethane

throughput, U_{WF}, was determined as the flow rate when the height of the accumulated dispersed phase, h, exceeds 20mm.

In MIXCO column, the maximum throughput was also measured. The operation was performed with the same shell tube as the MS column. The column is partitioned in five stages with four doughnut shaped PTFE plate of the open space of 31mm in diameter, the top and the bottom stage are used for the phase separation. At each center of three stages, a six-flat blade turbine of 30mm in diameter are mounted.

7.2 RESULTS AND DISCUSSION

7.2.1 Maximum flow rate

In MIXCO column, the increase in U_W is a cause for the carry-over of small droplets of dispersed phase accompanied with the downward flow of continuous phase. The dispersed phase coalesced and accumulate at the top of the settler, then moves upward to next stage. When U_W is further increased, the bottom stage becomes to be filled with the dispersed phase. At this flow rate, we define the maximum flow rate, U_{WF}, in MIXCO column. **Fig.7.3** shows a plot of maximum flow rate, U_{WF}, versus the flow rate of dispersed phase, U_O. U_{WF} decreased rapidly with the increase in U_O. Solid lines represent the upper limits of the flow rate for two phases in the stable countercurrent operation. In the region of upper right of the line, the column could not be operate stable. U_{WF} was significantly affected with agitation rate. With increasing mixing strength, the droplets are splitted into smaller ones and these flowed down with the continuous phase. This leads to the significant fall of U_{WF}.

On the other hand, within the one stage of MS column, the behavior of the dispersion in the mixer and coalescence in the settler is shown in the photograph of Fig.7.4. **Figure 7.4(a)** shows the condition without coalescer, where many small droplets are observed and the phase separation cannot occur in the settler. With mounting the lattice coalescer, the coalescence of the droplets is much improved as shown in **Fig.7.4(b)**, wherein the small droplets was not observed in the settler, and the interface between organic and aqueous phases was shown clearly.

Figure 7.5 shows the plot of the height of dispersed phase accumulated in the settler, h, against U_W. In the region of low U_W, the dispersed phase does not accumulate, but once starts to accumulate, the

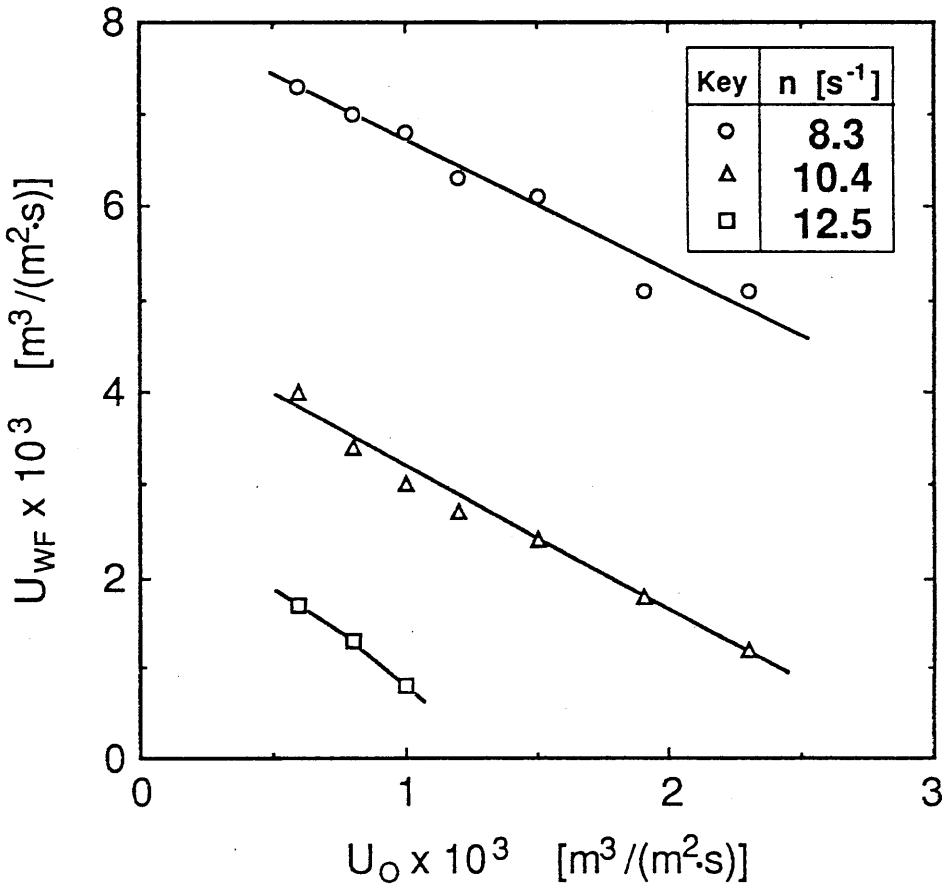

Fig.7.3 Maximum throughput for MIXCO column.

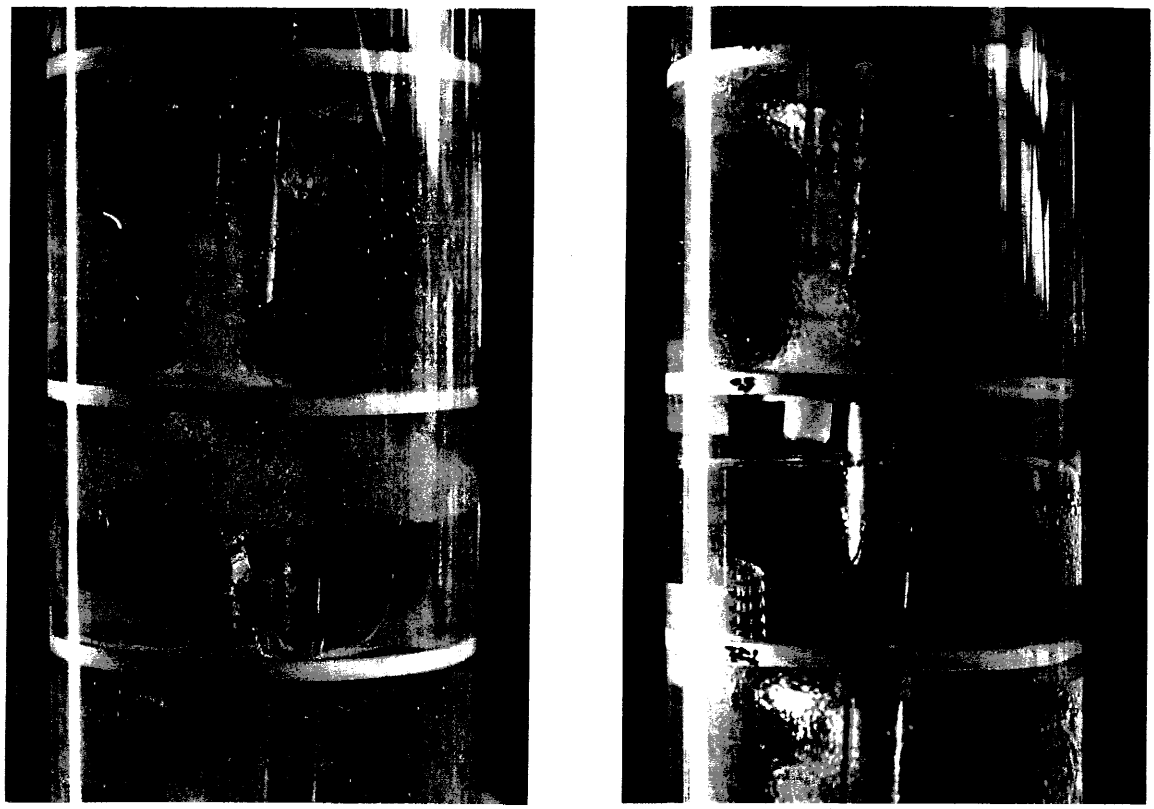

(a) (b)

Fig.7.4 Photograph of mixer-settler column, (a) without coalescer, (b) with lattice coalescer.

height of dispersed phase steeply increases with U_W. From the plot, the maximum throughput was determined as the U_W where the value of h reaches 20mm. In MS column, the maximum throughput increases with the agitation rate; such a favorable behavior have not been ever observed in other type of extraction column. **Figure 7.6** shows the dependence of the U_{WF} on U_O with the effect of mounting a coalescer. In low U_O without coalescer, the U_{WF}s are larger than these for with coalescer, then significantly decrease with U_O. This might be caused by the increase of flow resistance and the pressure drop. The carry-over of dispersed phase droplets with the continuous phase makes increase in the apparent viscosity of the two phase flow. Furthermore the attachment of the dispersed phase droplet on the wall of a downspout increases the flow resistance. These negative effect on the throughput was enhanced with the agitation rate. On the other hand, the U_{WF} with coalescer at low U_O is lower than those values without coalescer because of the pressure drop caused by the coalescer. However, the decrease in U_{WF} was not so significant and the U_{WF} was kept higher in wide U_O range as observed in the case without coalescer. This suggests that an effective coalescence of the droplets makes the operation in MS column stable. Whether coalescer was mounted or not, the value of U_{WF} increased with the agitation rate in the MS column contrary to the MIXCO column, where the throughput decrease with the agitation rate. The reason for this excellent performance is considered to be from the suction force derived from the lifter-turbine blade. **Figure 7.7** shows the effect of agitation rate on the total throughput to compare between MIXCO column and MS column. The observed behavior in MIXCO column was a common characteristics among conventional countercurrent extraction columns. In MS column with lifter-turbine impeller, however, the high agitation rate realizes both large interfacial area and high throughput. This provides the great advantage for the continuous countercurrent operation.

The effect of various coalescer on the maximum throughput is shown in **Fig.7.8**. Although the mesh coalescer is the thinnest among the three, the U_{WF} is lower than the U_{WF} for lattice of the same material. The difference might be due to the structure of the mesh. On the mesh coalescer which is mounted horizontally, the dispersed phase easily coalesced and made the mesh clog. This might be led to the increase of pressure drop between the mixer and the settler. On the lattice coalescer,

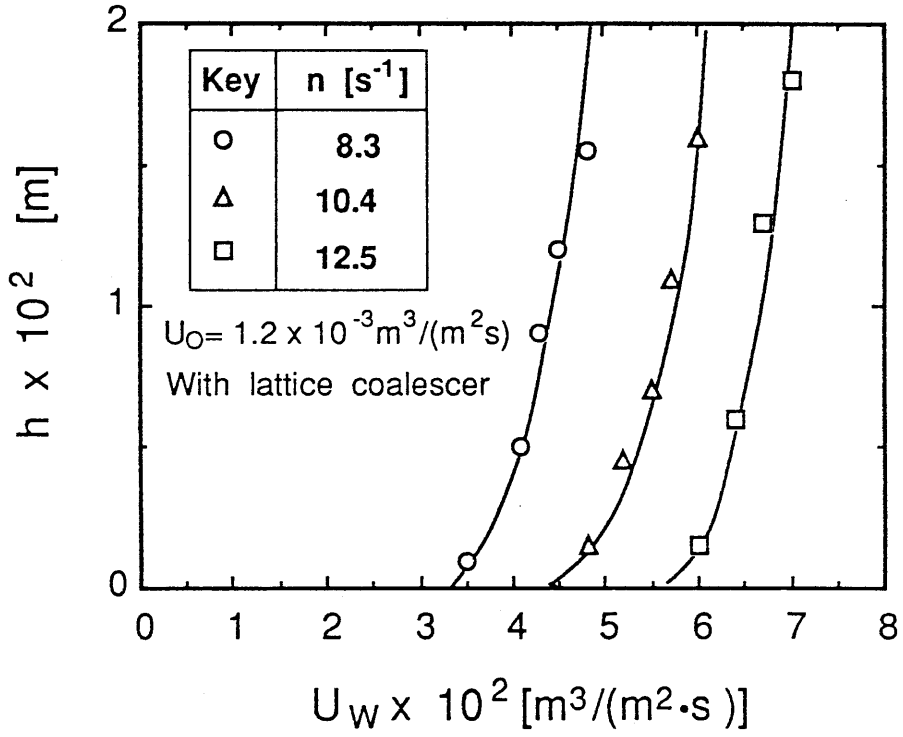

Fig.7.5 Thickness of dispersed phase accumulated in settler of mixer-settler column.

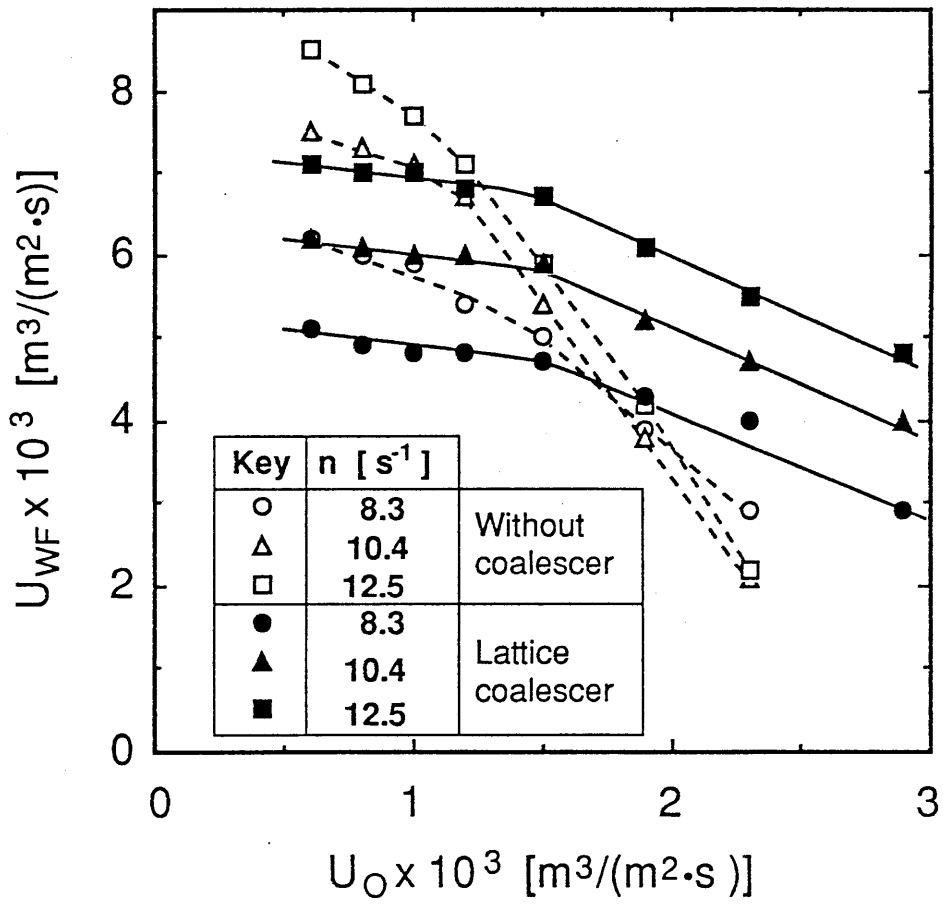

Fig.7.6 Maximum throughput for mixer-settler column.

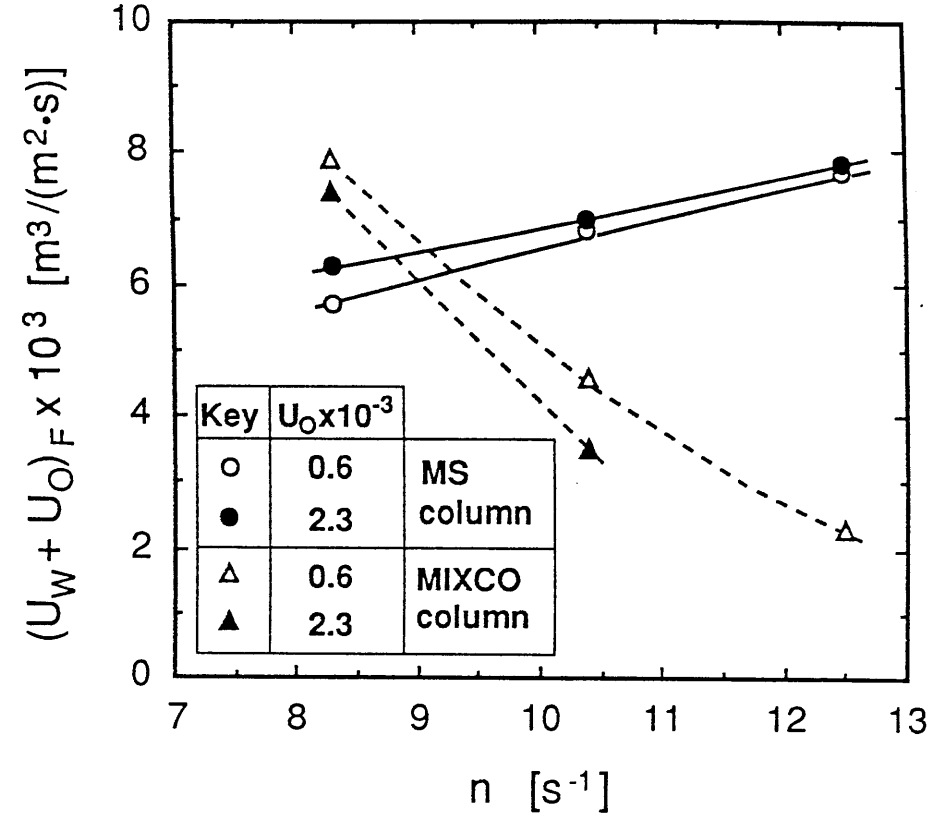

Fig.7.7 Effect of agiatation rate on total throughput.

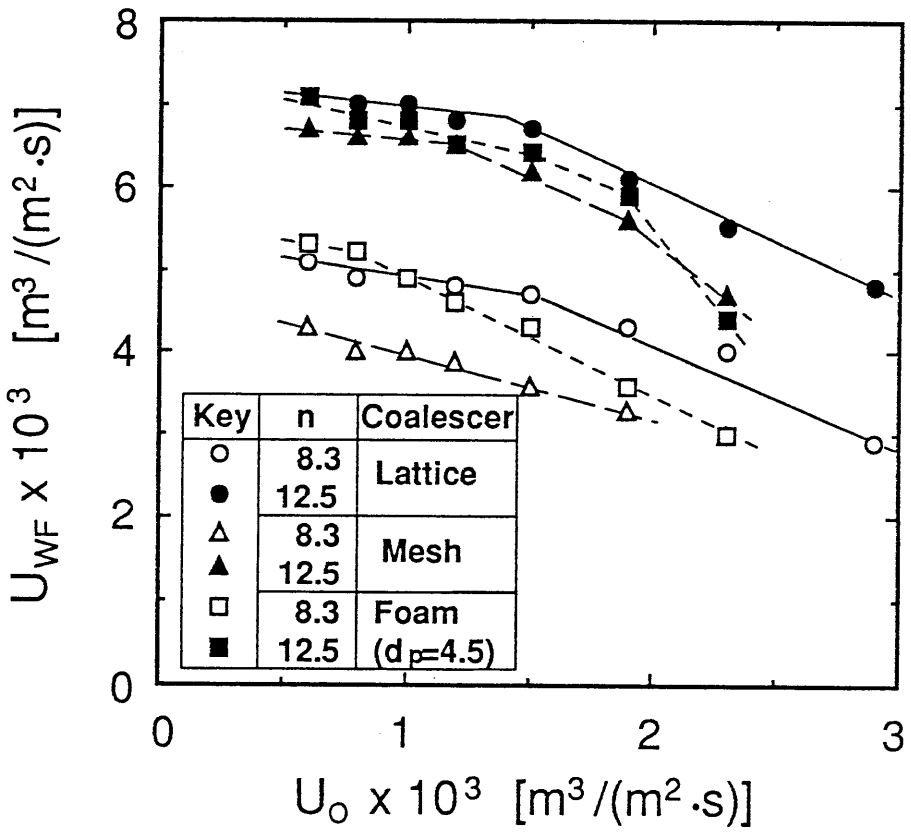

Fig.7.8 Maximum throughput for various coalescer.

the dispersed phase attached on the fiber moves easily along the fiber and drained away. Thus even for the relatively large drops at low agitation rate, effective coalescence was achieved without increasing the pressure drop. When urethane foam is used as a coalescer, the U_{WF} decreases significantly with U_O, and lots of uncoalesced small droplets were observed. **Figure 7.9** shows the effect of pore size of the urethane foam on the U_{WF}. The U_{WF} decreased with the decrease in the pore diameter, i.e., the increase in pressure drop. For the coalescer of d_p less than 1.2mm, small droplet of dispersed phase was well trapped and it was not observed that the droplets passed through the coalescer.

7.2.2 Pressure drop

In MS column without coalescer, both the pressure differences between the settlers, ΔP_1, and between the mixer and the settler, ΔP_2 are plotted against U_W^2 in **Fig.7.10**. When there was no agitation, ΔP_1 was equal to ΔP_2 and ΔP increased in proportio to U_W^2. Under conditions of supplying only continuous phase and closing the end of the riser tube, ΔP_2 was expressed as the pressure difference of ΔP_1 plus the pressure difference between the mixer and the settler. The results of $\Delta P_1 = \Delta P_2$ suggested that the dominant pressure drop is between the both ends of downspout. Since the rotation of lifter-turbine yields a suction force, the pressure drop ΔP_1 decreases with the agitation rate. In addition, ΔP_2 decreases remarkably with the agitation rate and at last the value became negative, i.e., the pressure in the settler of lower stage became higher than that in the mixer of upper stage. This pressure difference made the flow of dispersed phase upward, therefore, the total throughput increased with U_O in MS column as shown in Fig.7.7. As the driving force to flow the dispersed phase upward, the buoyant force should also be taken into consideration. The buoyant force arose from the dispersed phase accumulated in the riser and the settler. It was expressed in the form $g\,\Delta\rho(h_R + h)$, where $\Delta\rho$ is the density difference between phases(in these experiments, 315 kg/m^3) and h_R the length of a riser(in there experiments, 0.033m). If the accumulation height in settler is 2cm, the buoyant forced becomes to 164Pa. As increase in the flow rate of continuous phase, the total driving force $\Delta\rho(h_R + h) - \Delta P_2$ becomes zero and the dispersed phase does not flow. So it was considered that the throughput reaches a maximum. From the plot of Fig.10, the value of

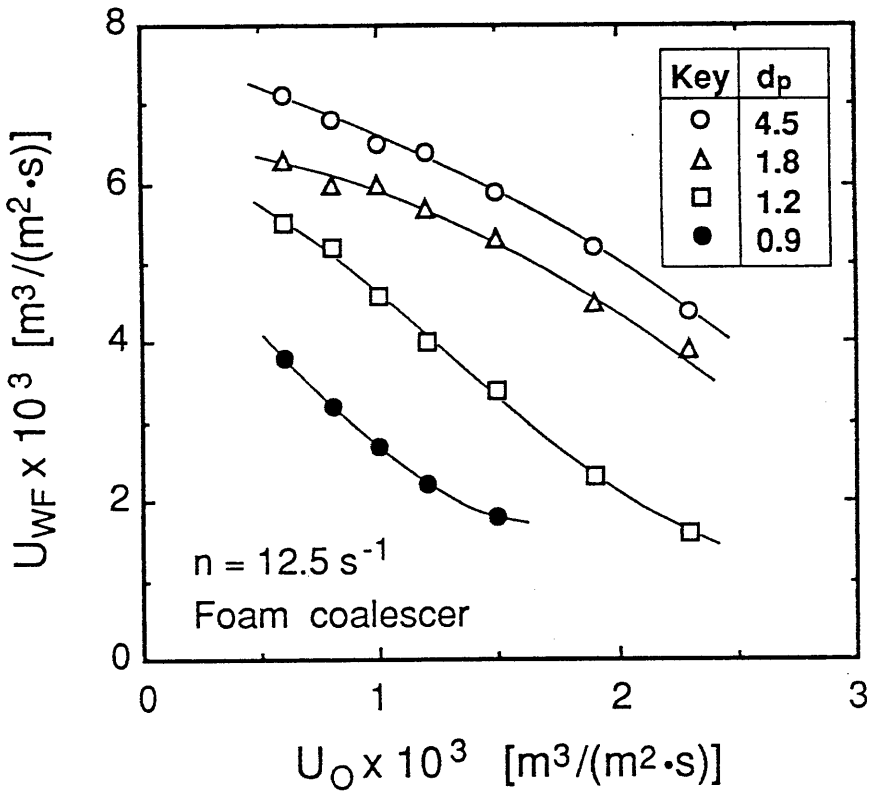

Fig.7.9 Effect of poresize of foam coalescer on throughput.

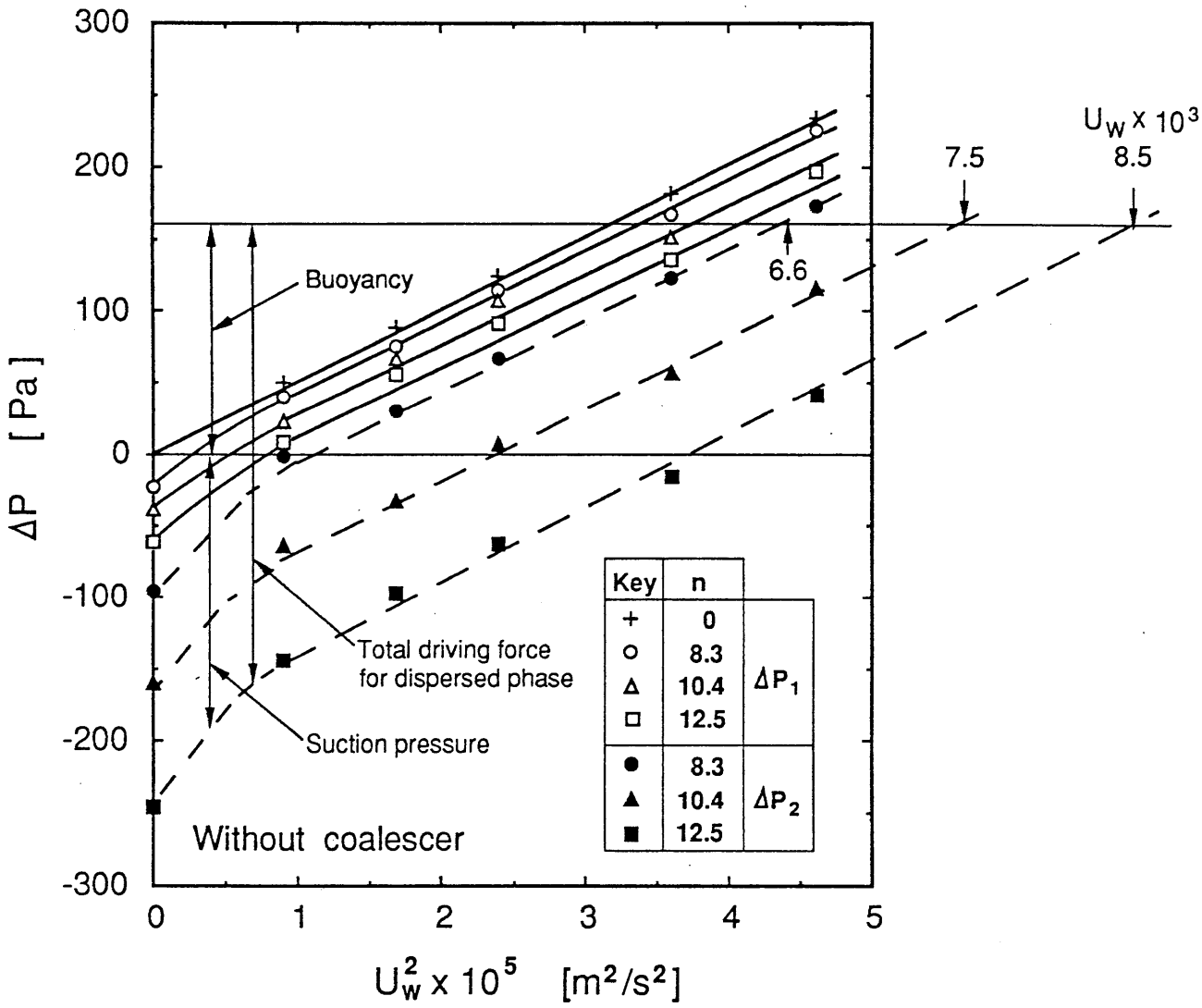

Fig.7.10 Pressure drop of single stage and pressure difference between ends of riser.

U_W at ΔP_2 is equal to 164Pa $U_W = (4.4 \times 10^{-5})^{0.5} = 6.6 \times 10^{-3}$ $m^3/(m^2 \cdot s)$ for $n = 8.3 s^{-1}$. For $n = 10.4$ and $12.5 s^{-1}$, U_W values are obtained from the interpolation of the curves. These values are 7.5×10^{-3} and $8.5 \times 10^{-3} m^3/(m^2 \cdot s)$, respectively. On the other hand, the observed values of U_{WF} without coalescer at $U_O = 0.6 \times 10^{-3} m^3/(m^2 \cdot s)$ are 6.2×10^{-3}, 7.5×10^{-3} and $8.5 \times 10^{-3} m^3/(m^2 \cdot s)$ at $n = 8.3$, 10.4 and $12.5 s^{-1}$, respectively. These values are in good agreement with the values predicted from the relation of $\Delta \rho (h_R + h) - \Delta P_2 = 0$.

Figure 7.11 shows the effect of hole size of coalescer on ΔP_1 and ΔP_2. For the coalescer of 4.5mm in hole diameter, ΔP_1 is about as high as the value without coalescer for $n = 0$. When the hole diameter is small and there is no agitation, the pressure drop increases and the value of ΔP_1 becomes larger than that without coalescer. The increase in ΔP_2 is more significant than that in ΔP_1 because the pressure drops of two coalescers were included in ΔP_2. Even if there was agitation, the pressure drop arose from the coalescer gave the same effect on the ΔP_2. For these coalescers, the values of U_{WF} were estimated from the interpolation of the curve of ΔP_2 versus U_O and the buoyant force as mentioned before. The values of U_{WF} for the foam coalescer of the largest hole and of the smallest hole were 8.5×10^{-3} $m^3/(m^2 \cdot s)$ and $7.2 \times 10^{-3} m^3/(m^2 \cdot s)$, respectively. In Fig.9, the observed U_{WF} values at $U_O = 0.6 \times 10^{-3}$ $m^3/(m^2 \cdot s)$ for each coalescer was 7.1×10^{-3} and $3.8 \times 10^{-3} m^3/(m^2 \cdot s)$, respectively. These observed values were lower than the estimated values, even if the observed values were extrapolated to $U_O = 0$. This might be the effect of the increase of pressure drop due to the attachment of the dispersed phase on a coalescer. Thus when the dispersed phase was supplied, the value of ΔP_2 in Fig.7.9 might be lower than those in Fig.7.11. With the lattice coalescer, the pressure drop of the lattice itself was as low as the urethane foam of larger hole. As observed in Fig.7.6, the flow of dispersed phase lowered the U_{WF} at low U_O ,owing to the decrease in pressure drop. Furthermore, the decrease of U_{WF} with the lattice coalescer is less significant than that for the foam coalescer. This is because the excellent performance of coalescence of the dispersed droplet with the lattice coalescer. The dispersed phase attached on the lattice flows along the fiber and moves upward rapidly, thus the pressure drop was not affected significantly by the increase in U_O. The lattice coalescer has the surface of PTFE which is highly resistant to the various

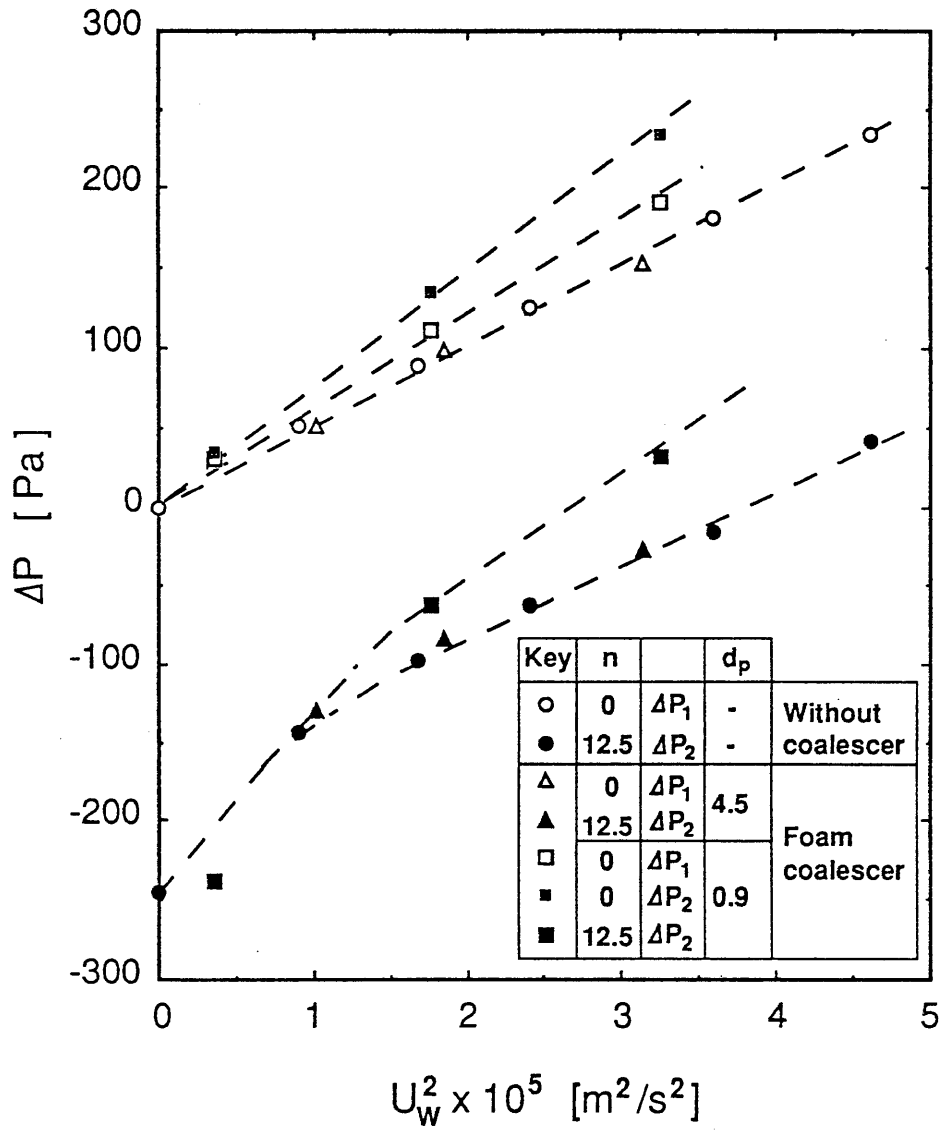

Fig.7.11 Effect of coalescer on pressure difference.

organic solvents, strong acids and bases. For the extraction, this is also an advantage of a lattice coalescer.

CONCLUSIONS

In a multistage mixer-settler extraction column, the fine droplets of the dispersed phase is desirable for enhancing the mass transfer. Generally the strong agitation for making a fine droplets leads to the decrease in the throughput and unstable countercurrent operation. In the present study, we proposed a Mixer Settler column using lifter-turbine impeller. It was observed that the maximum throughput increase with an agitation rate. This excellent performance was achieved by the suction force at the beneath of lifter-turbine impeller. This effect was clarified by measuring the pressure differences between the settlers and between the mixer and the next settler. Furthermore, the insertion of hydrophobic matrix between between the mixer and settler coalescer enhanced the coalescence of dispersed phase droplets between the mixer and the settler, and the coalescer makes the countercurrent operation stable under wide flow conditions. Especially, in high flow rate of dispersed phase, the maximum flow rate was greatly improved by the coalescer. A lattice of a mesh sheet coated with PTFE gave a superior performance as a coalescer.

NOMENCLATURE

d_p	pore size of coalescer	[m]
g	gravitational acceleration	[m^2/s]
h	height of dispersed phase accumulated in settler	[m]
h_R	height of riser for organic phase	[m]
n	agitation rate	[s^{-1}]
ΔP_1	pressure drop of one stage	[Pa]
ΔP_2	pressure difference between outlet and inlet of organic phase riser	[Pa]
U	flow rate per unit cross sectional area of column	[$m^3/(m^2 \cdot s)$]
$\Delta\rho$	density difference between aqueous and organic phases	[kg/m^3]

Subscript

F flooding

O organic phase

W aqueous phase

REFERENCES

1) Bailes, P. J. and Stitt, E. H.: *Chem. Eng. Res. Des.*, 65, 514 (1987).
2) Gaubinger, W., Husung, G. and Marr, R.: *Ger. Chem., Eng.*, 6, 74 (1983).
3) Kirou, V. J. and Tavlarides, L. L.: *AIChE J.*, 34, 283 (1988).
4) Scheibel, E. G.: *Chem. Eng. Progr.*, 44, 681 (1948).
5) Steiner, L., E. von Fisher and Hartland, S.: *AIChE Symp. Ser.*, 80, No.238, 130 (1984).
6) Takahashi, K. and Takeuchi, H.: *J. Chem. Eng. Japan,* 23, 12 (1990).
7) Takahashi, K. and Takeuchi, H.: *"Solvent Extraction 1990"* Elsevier, p.1357-1362 (1992).

Chapter 8.

STAGE EFFICIENCY OF MIXER-SETTLER EXTRACTION COLUMN*

INTRODUCTION

Multistage countercurrent extraction is useful for the separation of liquid mixtures, and an extraction column of high performance which achieves large throughput and a high stage efficiency is desirable. Mechanical agitation can promote stage efficiency due to the large interfacial area with small dispersed drops. As the drop size decreases with agitation speed, however, the relative velocity between the dispersed drops and the continuous phase decreases, which makes the throughput small[5]. Moreover, axial mixing, which lowers the stage efficiency, becomes significant at high agitation speed. To increase the relative velocity between phases, it is desirable that the small drops be coalesced in the section between stages. Scheibel[6] set up the mixing part and the packing part alternately to promote drop coalescence in the packing part. For the same purpose, Steiner *et al.*[7] used a three-dimensional lattice as a partition of the mixing stages. In the case of aqueous dispersion, Bails-Stitt[1] used an electrostatic coalescence to obtain stable operation under a vigorous agitation. The division of flow channels into a dispersed phase channel and a continuous phase channel is also useful to obtain large throughput as an effective utilization of buoyancy.

Gaubinger *et al.*[2] achieved a large throughput and small axial mixing by dividing the flow channels with concentric cones. The section in which the drops are coalesced is a sort of settling part, and act as a suppresser of axial mixing. Horvath-Hartland[4] realized a high stage efficiency with a mixer-settler extraction column in which the interstage mixing was extremely small, but the throughput of the column was also small.

In the previous chapter, it was discussed about the maximum

---

* This chapter is **appeared** in J. Chem. Eng. Japan, **26**, No. 6, 715-719(1993).

throughput of the MS column, i.e., the maximum throughput was measured for a mixer-settler column(MS column), which had a drop coalescer between each mixer and settler, divided flow channels and a lifter-turbine impeller in the mixer. It was indicated that the drop coalescer was useful for the stable operation, especially at a large flow rate of dispersed phase, and that a large throughput was realized by the suction pressure induced with the lifter-turbine impeller as well as by the devision of flow channels. In the present study, the stage efficiency of the MS column is measured with iodine extraction from the aqueous phase into n-heptane, and the effects of the agitation speed, the flow ratio of the dispersed phase to the continuous phase and the distribution ratio of iodine between phases on the stage efficiency or the height of a transfer unit is studied.

8.1 EXPERIMENTAL

An experimental flow sheet with a MS column is shown in **Fig.8.1**. Details of the column were given in the previous paper[9]. The extraction column consists of three stages and a bottom-drop coalescer of nonwoven material and the inside diameter of the column is 60mm. Each stage is partitioned into an upper settler of 40mm in height and a lower mixer of 50mm in height. A 6-blade lifter-turbine of 30mm in diameter is used for agitation in the mixer and a three-dimensional lattice-drop coalescer is set on the stator ring of 30mm in opening diameter between the mixer and the settler. The lattice coalescer, which is made of glass fiber mesh coated with PTFE, is 10mm in height and 2.5x2.3mm rectangular pitch.

An aqueous solution(continuous phase) fed to the mixer of the top stage rises through the coalescer into the settler with the dispersed phase, goes down through two downspouts located at opposite sides of the column into the lower-stage mixer after settling into two phases and finally be led to the leveler from the bottom of the column. An organic solution(dispersed phase) fed at the bottom of the column rises from the mixer into the settler with the continuous phase, from the settler into the upper-stage mixer through a riser and overflows from the top of the column. The downspout is a glass tube of 5.5mm inside diamter and the riser is a PTFE tube of 4mm in inside diameter. The continuous phase and the dispersed phase flow countercurrently as a whole.

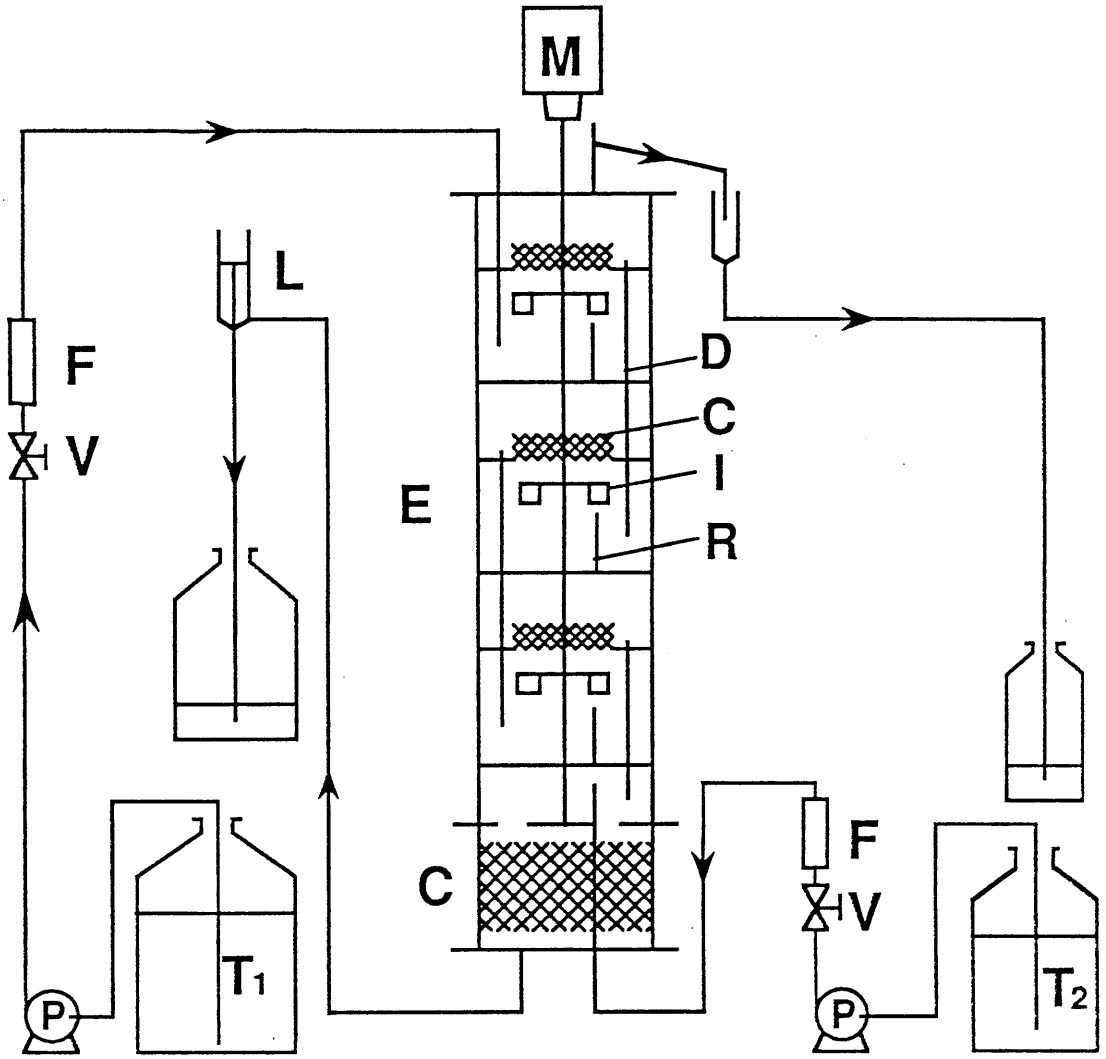

E: extraction column
C: drop coalescer
T_1 : tank for aqueous phase
T_2 : tank for organic phase
I: 6-blade lifter-turbine
D: down spout for aqueous phase
R: riser for organic phase
L: level er
F: flow meter
P: pump
V: valve

Fig.8.1 Schematic diagram of experimental apparatus.

Stage efficiencies were measured with the experiments of iodine extraction from an aqueous solution of I_2-KI into the dispersed phase of n-heptane. After the column was filled with the aqueous solution, iodine-free n-heptane was fed and the outlet aqueous solution and the outlet organic solution were taken at intervals of 5minutes. The iodine concentration of these samples were measured by a spectrophotometer. Steady state was achieved after flowing the solutions of over three times the column volume when the flow ratio of aqueous phase to organic phase was 4. Since the distribution ratio of iodine for the present system varies with concentration of iodic ion in the aqueous solution[8], aqueous solutions of various KI concentration were used in the experiment to change the distribution ratio. The distribution ratio for each experimental run was determined by measuring the iodine concentrations of the dispersed and the continuous phases after equilibrating two phases.

Stage efficiencies were measured with a MIXCO column for the comparison with the MS column. The same column shell as with the MS column was used, and the column was divided into five stages of 60mm in height by stator rings of 31mm in opening diameter. The top and the bottom stages were used as settlers, and a 6-blade turbine impeller of 30mm in diameter was set at the center of each stage for three stages. The time to reach steady state was about twice of that for the MS column.

8.2 RESULTS AND DISCUSSION

8.2.1 Stage efficiency

Liquid-liquid equilibrium for the extraction of iodine from aqueous phase into heptane is given by

$$y = m\,x \tag{8.1}$$

where y and x are the iodine concentrations in heptane and aqueous phase, respectively, and m distribution ratio of iodine which is expressed by $m = 36.6/(1 + 748[I^-])$[8], where $[I^-]$ is iodic ion concentration in $kmol/m^3$. Since mutual solubilities between n-heptane and water are very small, the operating line for the multistage countercurrent extraction is expressed by

$$y_n - y_{in} = (R/E)(x_{n+1} - x_{out}) \tag{8.2}$$

where R is the raffinate phase flow rate, E the extract phase flow rate, y_{in} the iodine concentration in organic phase fed to the bottom of the column, and x_{out} the iodine concentration in aqueous phase from the

bottom of the column. Stage number is counted from the top of the column. The stage efficiency E_{Oy} based on the concentration of organic phase is defined as follows.

$$E_{Oy} = (y_n - y_{n-1}) / (y_n^* - y_{n-1}) \quad (8.3)$$

where y_n^* ($=mx_n$) is the organic phase concentration in equilibrium with the aqueous phase of n-th stage. Under the assumption that stage efficiency does not vary with the stage number, the following relation is derived for N-stage column from Eqs.(8.1) to (8.3) as shown in **Appendix**.

$$E_{Oy}(mx_{out} - y_{in})(1 + r_y + r_y^2 + \cdots + r_y^{N-1}) - (y_{out} - y_{in}) = 0$$

where

$$r_y = E_{Oy}\{m/(R/E) - 1\} + 1 \quad (8.5)$$

The flow ratio is given by $R/E = (y_{out} - y_{in})/(x_{in} - x_{out})$. By using the measured values of x_{in}, x_{out}, y_{in}, y_{out} and m, E_{Oy} can be determined from Eq.(8.4).

Stage efficiencies E_{Oy} of the MS column and the MIXCO column are shown in **Fig.8.2** against the agitation speed n for the distribution ratio m = 6.0 and flow ratio R/E =4. E_{Oy} of MS column increased monotonously with increase in n and a high stage efficiency could be obtained with strong agitaion under the present experimental conditions. E_{Oy} of the MIXCO column stopped increasing at large values of n, and the values were smaller than those of the MS column in spite of the fact that the holdup of dispersed phase(i.e., the interfacial area) of the MIXCO column was larger than those of MS column. The stage efficiency of the MIXCO column might be affected by the axial mixing between stages. Since the axial mixing increased with agitaion speed, the difference in E_{Oy} between the two columns became large with n. The MS column may be a high-performance extraction column, which can achieve a high stage efficiency as well as a high throughput and stable operation at vigorous agitation. However, if the agitation speed continues to increase, a large part of dispersed drops will pass through the coalescer without coalescing and be accompanied by the continuous phase, and a decrease in stage efficiency follows. Though smaller drops can be coalesced with the coalescer of smaller mesh pitch, the pressure drop in the coalescer increases with the decrease in mesh pitch, which decreases the throughput[9].

The effect of throughput on the stage efficiency is given in **Fig.8.3** for a given R/E and m. U_O and U_W are superficial velocities of the dispersed and the continuous phases respectively, and $U_O + U_W = 1.33$m/s corresponds to $R + E = 3.75\text{x}10^{-6}\text{m}^3/\text{s}$ for the present column. E_{Oy} varied little with total throughput $U_O + U_W$. The holdup of dispersed phase increases with increase in U_O and decreases with increase in U_W, and the effect of U_O is larger than that of U_W[10], i.e., the holdup may increase by doubling $U_O + U_W$ at constant R/E. The residence time of dispersed phase decreases with increase in U_W, and the size of dispersed drop increases with decrease in residence time[11]. As effects of the flow rate on stage efficiency, the contribution of the holdup is positive and that of the residence time is negative, for the interfacial area is proportional to the holdup and inversely proportional to the the drop size. The former may be compensated by the latter in case of Fig.8.3.

On the other hand, E_{Oy} for a given m increased with the flow ratio R/E, and that for a given R/E decreased with the distribution ratio m as shown in **Figs.8.4** and **8.5**. These data are replotted against $m/(R/E)$ in **Fig.8.6**. Points for a given agitation speed are on one curve for both variations in R/E and n, i.e., the stage efficiency, depends on the ratio of the slopes between the operating line and the equilibrium line.

When the stage efficiency E_{Ox} defined by the following equation using the concentration of continuous phase, the dependency of the stage efficiency on m and R/E may be different from the above results.

$$E_{Ox} = (x_n - x_{n+1})/(x_n^* - x_{n+1}) \tag{8.6}$$

where $x_n^* = y_n/m$. In the same way as for E_{Oy}, the following equation can be derived.

$$(E_{Ox}r_x/m)(mx_{out} - y_{in})(1 + r_x + r_x^2 + \cdots + r_x^{N-1}) - (x_{in} - x_{out}) = 0 \tag{8.7}$$

where $r_x = 1/\{E_{Ox}(R/E)/m + 1 - E_{Ox}\}$. In Fig.8.5, E_{Ox} for the same data used to calculate E_{Oy} are also plotted against m. E_{Ox} increased with the increase in m in contrast with the change of E_{Oy}. The value of E_{Ox} was larger than E_{Oy} for $m > R/E$ and the reverse was also true. The change of E_{Ox} was large for $m < R/E$, while that of E_{Oy} was large for $m > R/E$.

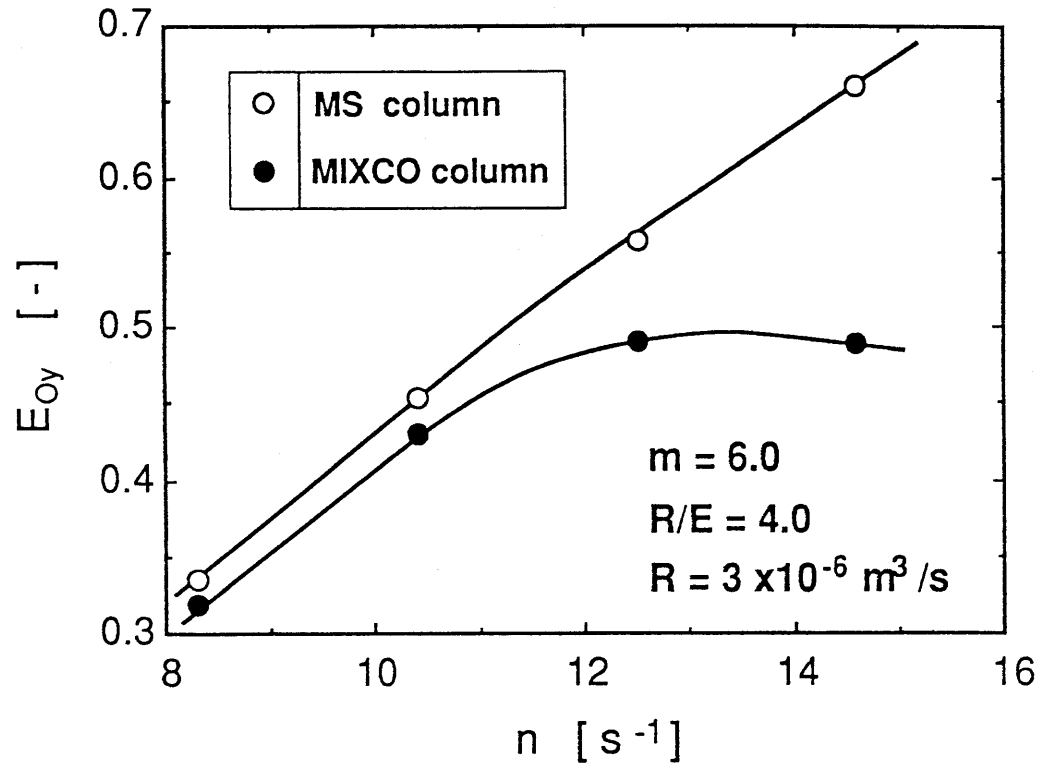

Fig.8.2 Comparison of E_{Oy} between MS column and MIXCO column.

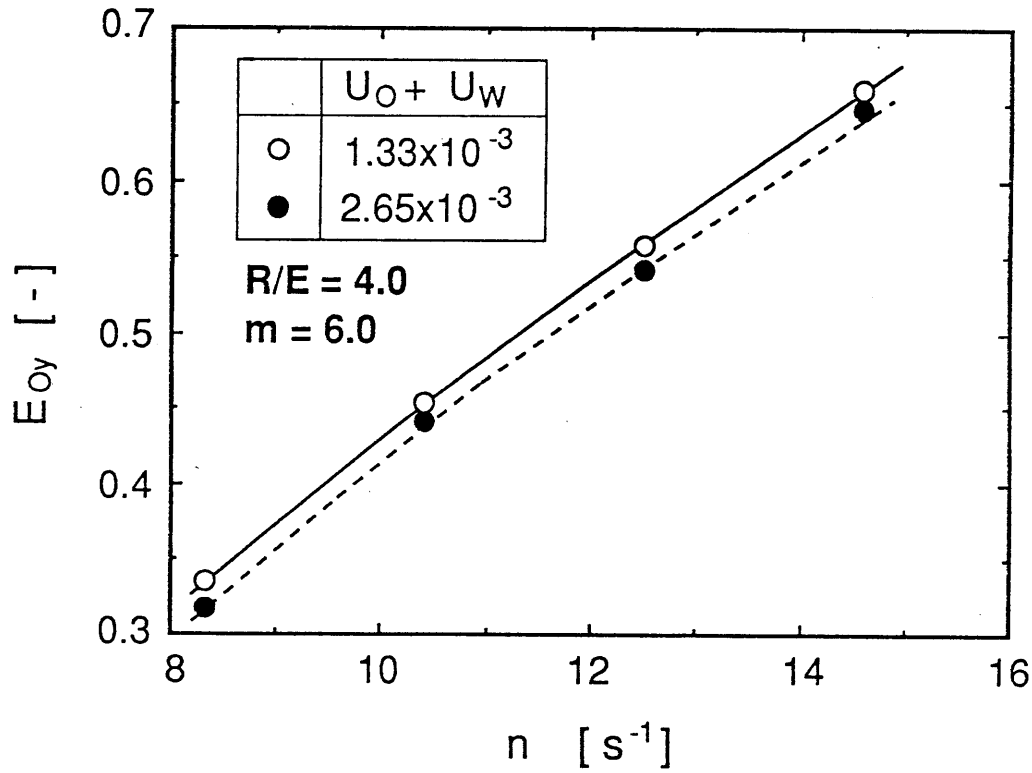

Fig.8.3 Effect of throughput on stage efficiency.

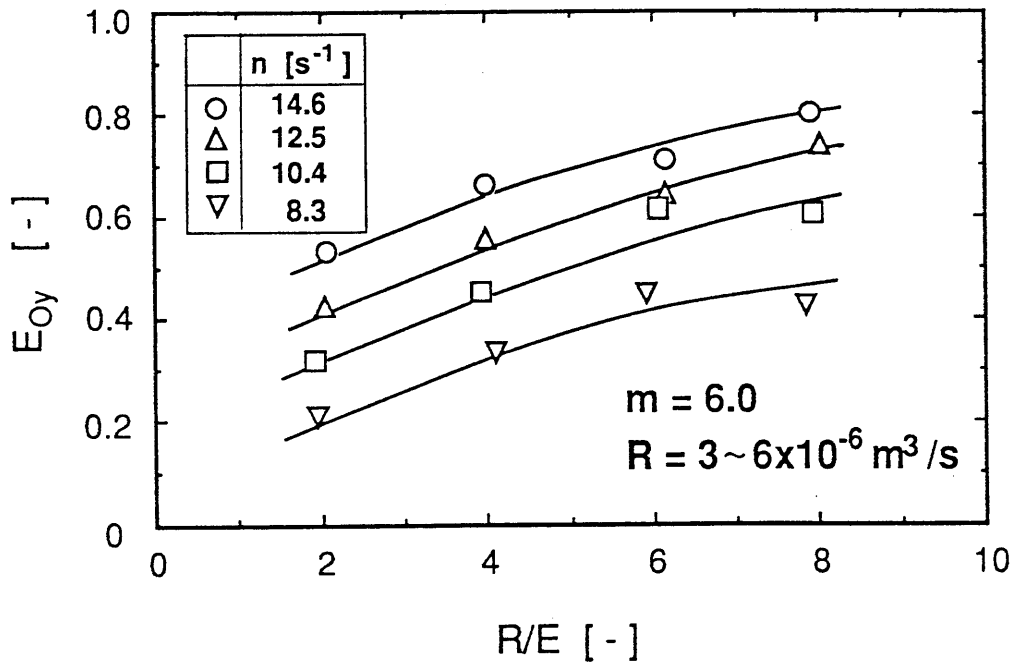

Fig.8.4 Effect of flow ratio on stage efficiency.

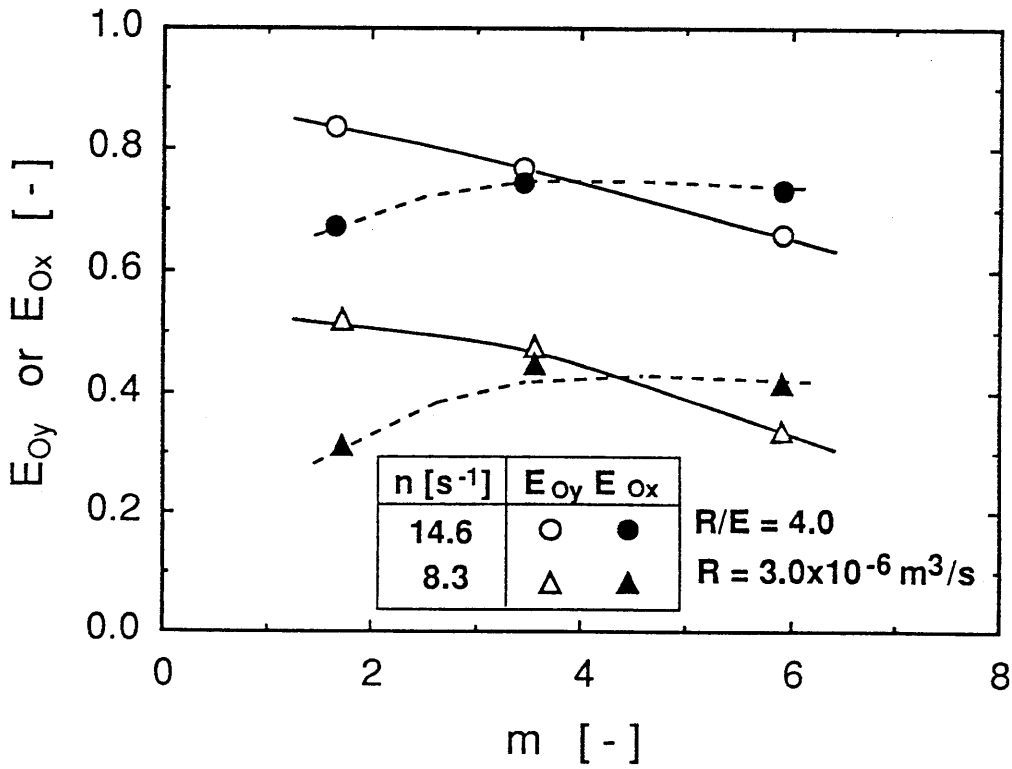

Fig.8.5 Effect of distribution ratio on stage efficiency.

8.2.2 Height of a transfer unit

Relation between the overall transfer unit N_{Oy} and E_{Oy} is given as follows in the same way as for the relation between the overall transfer unit and the point efficiency of the distillation column[3].

$$N_{Oy} = -ln\ (1 - E_{Oy}) \tag{8.8}$$

With E_{Oy} shown in Figs.8.4 and 8.5, N_{Oy} values were calculated by Eq.(8.8), and the values were converted to the overall height of a transfer unit by the relation of $H_{Oy} = Z/N_{Oy}$, where Z was the height of one stage (9cm in the present column). H_{Oy} is plotted against $m/(R/E)$ in **Fig.8.7.** Points for a given agitation speed are on a straight line. Bailes-Stitt[1] devised an extraction column which could be operated at vigorous agitation by use of electrostatic coalescence, and gave the height of a transfer unit of 13.4cm at agitation speed of $23s^{-1}$. The values of H_{Oy} of the MS column in Fig.7 were in the range of 4.5~12cm at agitation speed of $14.6s^{-1}$. This indicates that the MS column is excellent in the mass transfer characteristics as well as stable in operation.

The relation among the overall H_{Oy}, H_y of the dispersed phase and H_x of the continuous phase is expressed as follows.

$$H_{Oy} = H_y + \{m/(R/E)\}\ H_x \tag{8.9}$$

Under an assumption that the straight lines in Fig.8.7 correspond to Eq.(8.9), H_x can be determined from the slope of the line and H_y from the value on the ordinate. These values are plotted against the agitation speed in **Fig.8.8**, and correlated for the range of n = 8.3~$14.6s^{-1}$ as follows.

$$H_y = 0.76n^{-1.16} \tag{8.10}$$

Both H_y and H_x decreased with the agitaion speed, for the specific interfacial area increased due to the increase in dipersed-phase holdup and the decrease in drop diameter with n. The mass transfer coefficient of continuous phase might vary widely with n in comparison with dispersed phase, because the dependency of H_x on n was larger than that of H_y. Stage efficiencies E_{Oy} calculated by using Eq.(8.10) with the experimental conditions n, m and R/E are compared with the experimental values in **Fig.8.9**, and the average deviation was 4.3 %.

CONCLUSIONS

The stage efficiency of the mixer-settler extraction column increased monotonously with increase in agitation speed. Since stable operation was

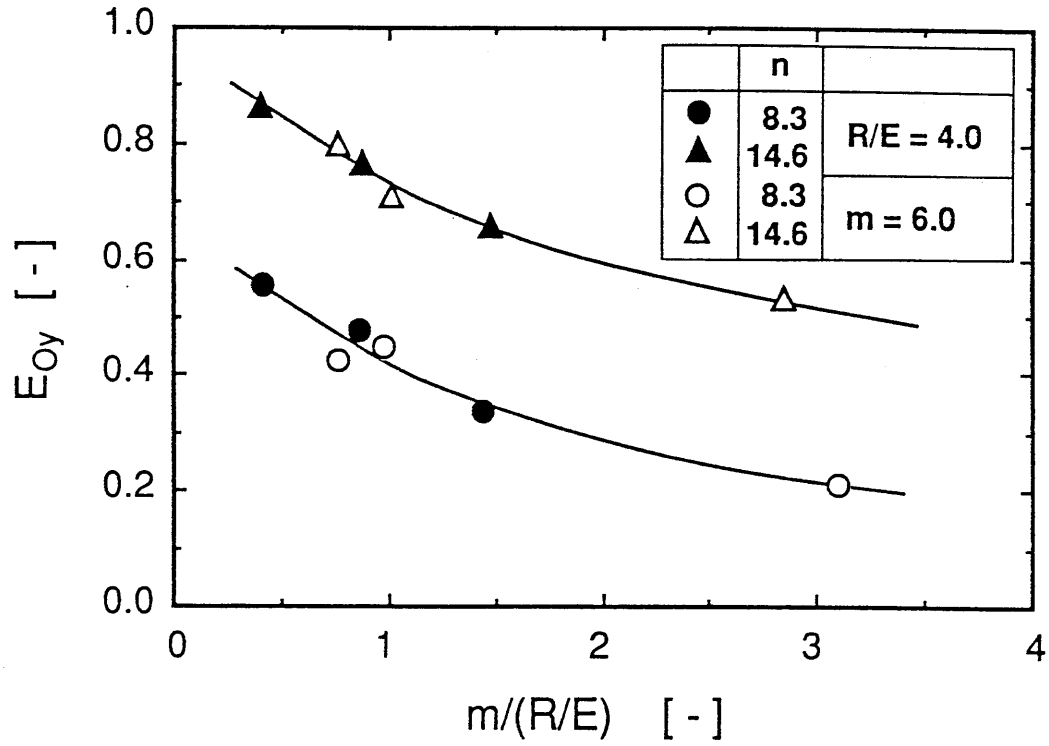

Fig.8.6 Effects of distribution ratio and flow ratio on stage efficiency.

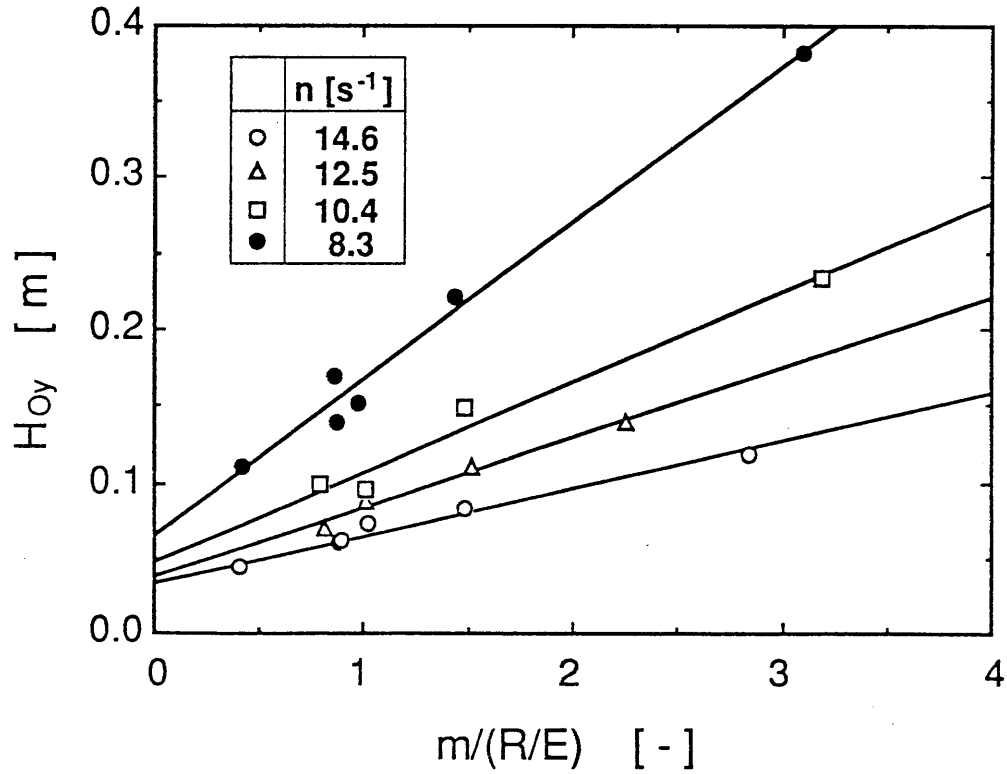

Fig.8.7 Height of a transfer unit against *m/(R/E)*.

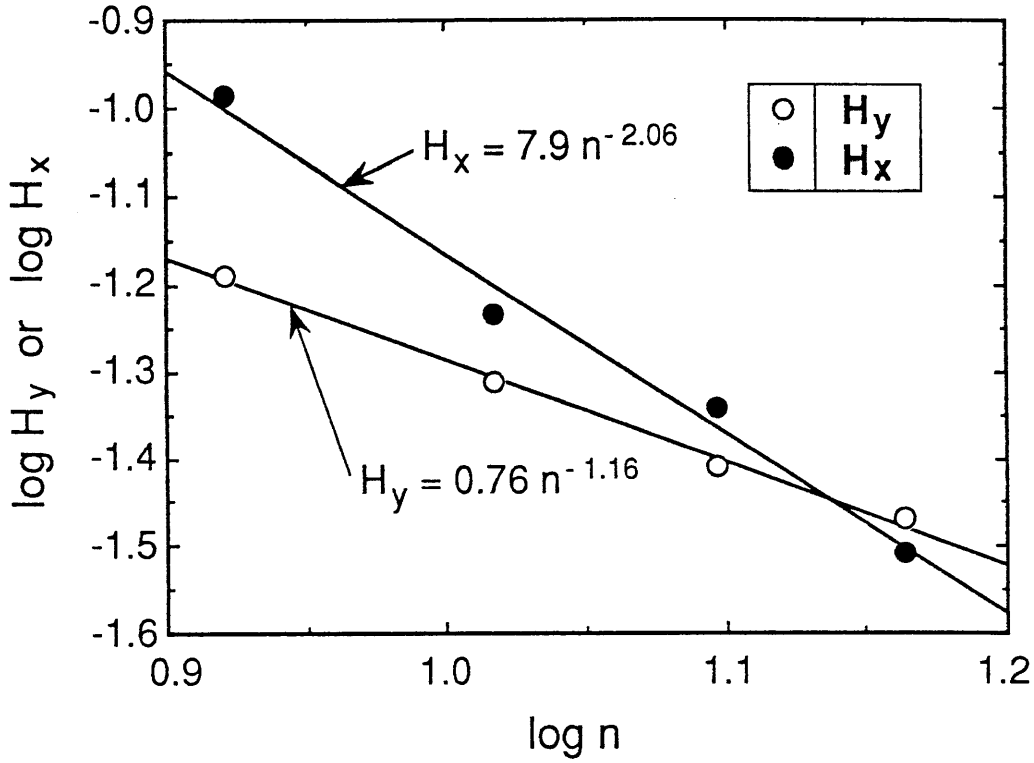

Fig.8.8 Correlation of height of a transfer unit against agitation speed

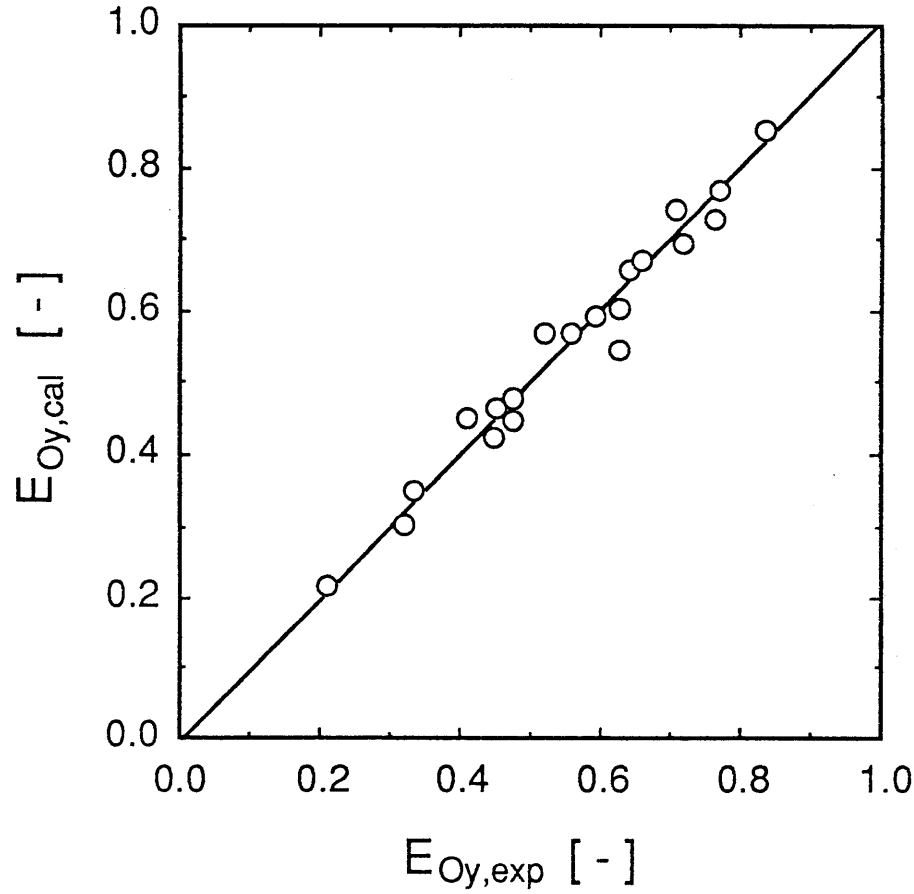

Fig.8.9 Comparison of calculated stage efficiencies with experimental ones.

possible at a high agitation speed with this extraction column, both a large stage efficiency and a large throughput, which is desiable for the countercurrent extraction column, could be achieved. The effect of flow ratio R/E and the distribution ratio m on the stage efficiency E_{Oy} were put together as the effect of $m/(R/E)$, i.e., E_{Oy} decreased with the ratio of the equilibrium line slope to the operating line one. The stage efficiencies EOy were converted to the overall height of a transfer unit H_{Oy}. The values of H_{Oy} at high agitation speed indicated that the mixer-settler extraction column had excellent mass transfer characteristics. H_{Oy} for each agitation speed was correlated with $m/(R/E)$ by a straight line, and H_x of the continuous phase and H_y of the dispersed phase were determined from the slope of the line and the value on the ordinate, respectively. These heights of a transfer unit of the two phases were correlated with the agitation speed, and the stage efficiency calculated with these correlation reproduced the experimental value with the average error of 4.3%.

APPENDIX

Determination of stage efficiency

In the present case, the equilibrium line and the operating line are given by Eqs.(8.1) and (8.2) in the chapter, which are straight lines on the x-y diagram as shown in **Fig.8.A.1**. Under the assumption that the stage efficiencies for every stage are given by a same value, points (x_{out}, y_1), (x_2, y_2), • • •, (x_n, y_n), • •, (x_N, y_{out}), which represent the concentrations of the dispersed and the continuous phases leaving the stage, are on a straight line as shown by $y = ax + b$ in Fig.8.A.1, and the following relation can be obtained.

$$y_n - y_{n-1} = (R/E)(x_{n+1} - x_n) \qquad (8.A.1)$$

$$y_{n-1} - y_n = a\,(x_{n+1} - x_n) \qquad (8.A.2)$$

From these equations,

$$y_{n+1} - y_n = r_y(y_n - y_{n-1}) \qquad (8.A.3)$$

where $r_y = a / (R/E)$. The series $\{y_n - y_{n-1}\}$ is a geometric progression, and the summation of the series is

$$\mathrm{SUM}\{y_n - y_{n-1}\} = y_{out} - y_{in}$$

$$(y_1 - y_{in})(1 + r_y + r_y^2 + \cdots + r_y^{N-1}) \qquad (8.A.4)$$

From the definition of stage efficiency,

$$E_{Oy} = \frac{(ax_n + b) - \{(R/E)(x_n - x_{out}) + y_{in}\}}{mx_n - \{(R/E)(x_n - x_{out}) + y_{in}\}} \qquad (8.A.5)$$

This equation is rearranged as follows.

$$\{a - mE_{Oy} - (1 - E_{Oy})(R/E)\}x_n + b - (1 - E_{Oy})\{y_{in} - (R/E)\,x_{out}\} = 0 \qquad (8.A.6)$$

To satisfy Eq.(8.A.6) for any value of x_n,

$$a = E_{Oy} + (1 - E_{Oy})(R/E) \qquad (8.A.7)$$

$$b = (1 - E_{Oy})\{y_{in} - (R/E)x_{out}\} \qquad (8.A.8)$$

And the following equations are derived.

$$r_y = a / (R/E) = E_{Oy}\{m / (R/E) - 1\} + 1 \qquad (8.A.9)$$

$$y_1 - y_{in} = E_{Oy}(y_1^* - y_{in}) = E_{Oy}(mx_{out} - y_{in}) \qquad (8.A.10)$$

By substituting Eq.(8.A.10) to Eq.(8.A.4),

$$E_{Oy}(mx_{out} - y_{in})(1 + r_y + r_y^2 + \cdots r_y^{N-1}) - (y_{out} - y_{in}) = 0 \qquad (8.A.11)$$

Eqs.(8.A.11) and (8.A.9) are Eqs.(8.4) and (8.5) in the text, respectively.

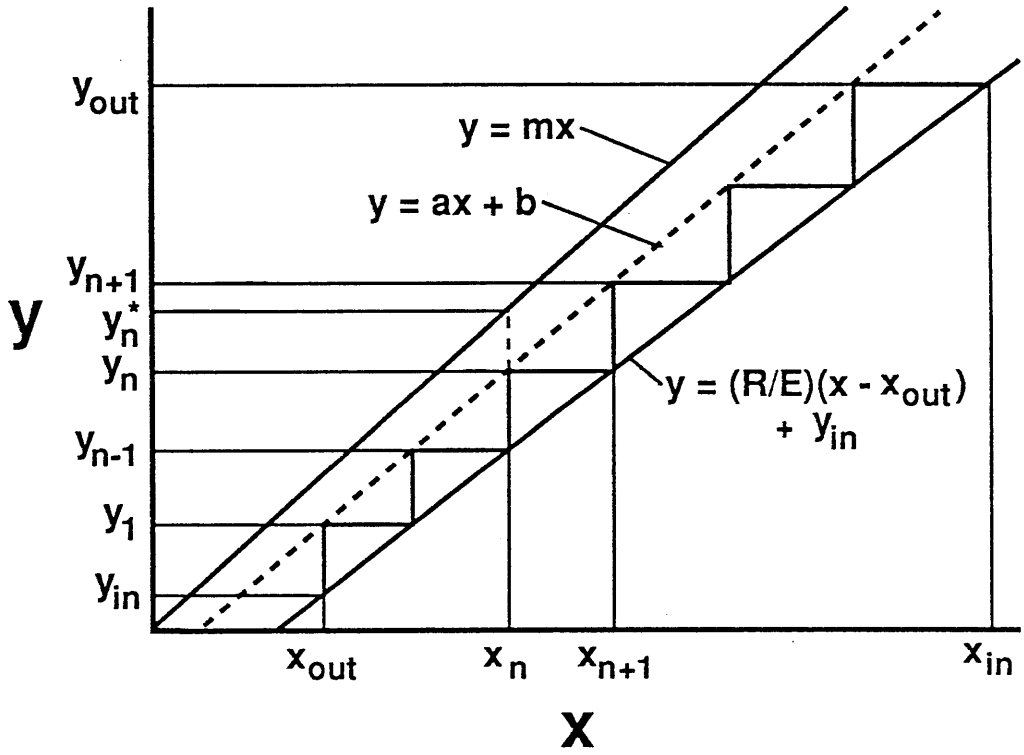

Fig.8.A.1 x-y diagram for countercurrent extraction column.

NOMENCLATURE

E	flow rate of extract phase	[m^3/s]
E_{Ox}	stage efficiency based on aqueous phase concentration	[-]
E_{Oy}	stage efficiency based on organic phase concentration	[-]
H_{Oy}	overall height of a transfer unit	[m]
H_x	height of a transfer unit for aqueous phase [m]	
H_y	height of a transfer unit for organic phase	[m]
N_{Oy}	overall transfer unit	[-]
n	agitation speed	[s^{-1}]
m	distribution ratio of iodine	[-]
R	flow rate of raffinate phase	[m^3/s]
U_O	superficial velocity of organic phase	[m/s]
U_W	superficial velocity of aqueous phase	[m/s]
x	iodine concentration in aqueous phase	[$kmol/m^3$]
y	iodine concentration in organic phase	[$kmol/m^3$]
Z	height of one stage	[m]

Subscripts

in	inlet
n	*n*-th stage
out	outlet

Superscripts

*	equilibrium

REFERENCES

1) Bailes, P.J. and Stitt, E.H.: *Chem. Eng. Res. Des.*, 65, 514 (1987).
2) Gaubinger, W., Husung, G. and Marr, R.: *Ger. Chem. Eng.*, 6, 74 (1983).
3) Gerster, J. A., Colburn, A.P. Bonnet, W.E. and Carmody, T. W.: *Chem. Eng. Progr.*, 45, 716 (1949).
4) Horvath, M. and Hartland, S.: *IEC Process Des. Dev.*, 24, 1220 (1985).
5) Kirou, V. J. and Tavlarides, L. L.: *AIChE J.*, 34, 283 (1988).
6) Scheibel, E.G.: *Chem. Eng. Progr.*, 44, 681 (1948).
7) Steiner, L., E. von Fisher and Hartland, S.: *AIChE Symp. Ser.*, 80, No.238, 230 (1984).

8) Takahashi, K., Nakano, M. and Takeuchi, H.: *Kagaku Kogaku Ronbunnshu*, 13, 256 (1987).
9) Takahashi, K., Nakashima, H., Nii, S. and Takeuchi, H.: *Kagaku Kogaku Ronbunshu*, 19, 440 (1993).
10) Takahashi, K. and Takeuchi, H.: *J. Chem. Eng. Japan*, 23, 12 (1990).
11) Takahashi, K. and Takeuchi, H.: *"Solvent Extraction 1990"*, Elsevier, p.1357-1362 (1992).

SUMMARY

In permabsorption of CO_2 and/or SO_2 using alkali aqueous solutions, the CO_2 and SO_2 flux was predicted by the mass-transfer model based on membrane permeation and gas absorption. For selective removal of SO_2 with respect to CO_2, the high selectivity was attained at both low liquid flow rate and low solute concentration.

Membrane absorption of CO_2 and/or SO_2 could achieve larger flux rather than permabsorption because of low mass-transfer resistance through the membrane. For gas phase mass-transfer coefficient, a semi-empirical correlation was developed. The mass-transfer model which the gas diffusion through the membrane pore was combined with the gas absorption well expressed the CO_2 and SO_2 flux. The selective removal of SO_2 to CO_2 being successfully achieved when both the liquid flow rate and solute concentration were low.

In gas sweeping pervaporation of alcohols from its aqueous solution, the permeation rate of alcohol was illustrated by the solution-diffusion model taken the vapor-liquid equilibrium into account. The model was applicable for the conventional vacuuming pervaporation.

The operation mode of bulk liquid membrane with porous partition membrane could realize a fast separation in comparison with the operation in supported liquid membrane because of a bulk motion of the membrane liquid through the partition. A mass-transfer coefficient for the bulk motion of the membrane liquid was introduced to the transfer model developed for this operation mode. The transfer of the solute was well simulated by the model.

In extraction of lithium by 18-crown-6 as a typical neutral cyclic polyether, the effect of counterion on the distribution ratio of lithium ion was satisfactorily explained with introducing the Jones-Dole parameter.

A multistage extraction column was developed, which could achieve larger throughput at higher agitation rate. The large throughput was produced by the suction pressure with the lifter-turbine impeller, which was ascertained by the pressure measurement in the column. The operation was stabilized in a wide operation range by installing a drop coalescer between the setter and mixer.

The mixer setter column developed here also exhibit both a large stage efficiency and a large throughput. The stage efficiencies decreased with

the ratio of the slope of equilibrium line and that of operating line. The heights of a transfer unit for the two phases were correlated with the agitation speed, and the stage efficiency calculated with these correlation reproduced the experimental value within small error.

LIST OF PAPERS

(1) "Removal of CO_2 by gas absorption across a polymeric membrane." *J. Chem. Eng. Japan*, **25**, No. 1, 67-72(1992).

(2) "Counterion effect on the extraction of lithium by 18-crown-6." *J. Chem. Eng. Japan*, **25**, No. 2, 220-223(1992).

(3) "Maximum throughput in mixer-settler column." *Kagaku Kogaku Ronbunshu*, **19**, No. 3, 440-445(1993).

(4) "Stage efficiency of mixer-settler extraction column." *J. Chem. Eng. Japan*, **26**, No. 6, 715-719(1993).

(5) "Gas absorption with membrane permeation - acid gas temoval from flue gases by a permabsorption method." *Trans. IChemE, Part B Proc. Safety and Env. Prot.*, **72**, No. B2 (1994). (to be published)

(6) "Removal of CO_2 and/or SO_2 from flue gases by membrane absorption." *Gas Separation and Purification*, (1994). (to be published)

(7) "Pervaporation with sweeping gas in polymeric hollow fiber membrane module - separation of alcohols from aqueous solution." *J. Memb. Sci.* (submitted)

(8) "Bulk liquid membrane with porous partition membrane." *J. Chem. Eng. Japan* (submitted)

ACKNOWLEDGMENT

This study has been carried out under the guidance of Drs. Hiroshi Takeuchi and Katsuroku Takahashi, Professors of Nagoya University. I wish to express my sincere gratitude to them for their kind advice, critical reading of the manuscript and warm encouragement.

I am also grateful to Dr. Takeshi Kobayashi , Professor of Nagoya University, for his useful suggestions.

Let me conclude by acknowledging the many people who helped me writing this dissertation. I wish to thank Nobuaki Ito for the advice for simulation work in permabsorption and for the work of membrane absorption, and Makoto Sakamoto, Zhong Gui Mao and Soichiro Kondo who made energetically the PV experiments for a long run time, extraction, and Izumi Haryo for her earnest work of the BLM operation, and A. H. Lissa Nuri who worked hard for Lithium extraction, and Hajime Nakashima who has a craftsmanship for inner parts of mixer-settler column. Finally, I wish to acknowledge all the colleagues in our Diffusional Separation Technology Laboratory. They always give much help and inspired me. I hope the laboratory will become a fruitful big tree.

Susumu Nii